From linking patches to linking theories: Cooperation in metapopulations

A thesis
Submitted towards the partial fulfillment of
BS-MS dual degree programme
by

Kaustubh Vishram Kulkarni

Indian Institute of Science Education and Research Pune
Dr. Homi Bhabha Road,
Pashan, Pune 411008 INDIA.

March, 2025

Supervisor: Dr. Thomas Koffel
Université Claude Bernard Lyon 1, France

Co-supervisor: Dr. Partha Sharathi Dutta
Indian Institute of Technology Ropar, India

Certificate

This is to certify that this dissertation entitled "From linking patches to linking theories: Cooperation in metapopulations" submitted towards the partial fulfillment of the BS-MS degree at the Indian Institute of Science Education and Research, Pune represents original research carried out by Kaustubh Vishram Kulkarni at Laboratoire de Biométrie et Biologie Évolutive, Université Claude Bernard Lyon 1, Villeurbanne, France and Indian Institute of Technology Ropar, Rupnagar, Punjab, India under the supervision of Dr. Thomas Koffel and Dr. Partha Sharathi Dutta during the academic year 2024 – 2025.

Dr. Thomas Koffel
(Supervisor)

Maître de Conférences
Laboratoire de Biométrie et
Biologie Évolutive
Université Claude Bernard Lyon 1
Villeurbanne, France

Date: 25/03/2025

Dr. Partha Sharathi Dutta
(Co-supervisor)

Associate Professor
Department of Mathematics
Indian Institute of Technology
(IIT) Ropar
Rupnagar, Punjab, India

Date: 26/03/2025

Thesis Advisory Committee (TAC):

Dr. Thomas Koffel

Dr. Partha Sharathi Dutta

Prof. Sutirth Dey

Declaration

I, Kaustubh Vishram Kulkarni, hereby declare that the matter embodied in the report titled "From linking patches to linking theories: Cooperation in metapopulations" is the result of the investigations carried out by me at Laboratoire de Biométrie et Biologie Évolutive, Université Claude Bernard Lyon 1, Villeurbanne, France and Indian Institute of Technology (IIT) Ropar, Rupnagar, Punjab, India from the period May 2024 – March 2025 under the supervision of Dr. Thomas Koffel and Dr. Partha Sharathi Dutta and the same has not been submitted elsewhere for any other degree. Wherever others contribute, every effort is made to indicate this clearly, with due reference to the literature and acknowledgement of collaborative research and discussions.

Kaustubh Vishram Kulkarni
Roll No. 202011107
BS-MS
IISER Pune

Date: 25/03/2025

This thesis is dedicated to those who question everything

Acknowledgements

This was a dream project to work on. There is no other way to begin the acknowledgements than to thank my supervisor, Dr. Thomas Koffel, for giving me the opportunity to work on it. He has been a brilliant mentor, and his guidance has been invaluable throughout the course of this project. The ample amount of time he dedicated to having fruitful discussions with me was vital for my progress. His expertise in ecology and evolution and the references he suggested I read enabled me to draw connections between my results and broader concepts in ecology and evolution. His comments on my thesis also significantly enhanced its quality compared with my first draft.

In addition to being a fantastic supervisor, I would also like to thank Thomas for making my time in Lyon more pleasant and enjoyable. From picking me up when I arrived in Lyon and accompanying me to my apartment to helping me open a bank account and assisting me with all the French paperwork, he substantially eased my stay in a foreign country. I also thank all the members of Laboratoire de Biométrie et Biologie Évolutive, especially Emma, Rémi, Rayan, Chloé and Barbara, for their support and help whenever needed.

I express my gratitude to my co-supervisor, Dr. Partha Sharathi Dutta, for his precious guidance and unwavering support. His insightful feedback and encouragement have been pivotal in motivating me to push my boundaries. I also thank the members of his research group, including Ravi, Arindam, Shubham and Smita, for assisting me whenever needed and making my stay in Ropar more comfortable.

I am profoundly grateful to Prof. Christopher A. Klausmeier and Dr. Jonas Wickman for their enlightening advice and actionable remarks that provided helpful directions for my work. Their recommendations were effective in both working through the results and presenting them in the thesis. When it comes to numerical analysis, Jonas is a magician. The methodological ideas he suggested were instrumental in solving technical problems with my code and improving its efficiency. A part of the results in the thesis were obtained using a modified version of the code he wrote.

I thank Prof. Sutirth Dey for his constructive feedback during the evaluation process. His suggestions helped me understand the importance of presenting my results in biological language. The amazing courses he taught at IISER Pune also played a prominent role in helping me better appreciate ecology and evolution.

I am a fellow of the Kishore Vaigyanik Protsahan Yojana (KVPY) fellowship (Reg. no.: SA-1810040). I acknowledge the same for financial support.

Looking back at my five-year journey at IISER Pune, I cannot fail to notice the unforgettable moments with my friends, may it be an evening spent climbing a hill, a barbecue dinner, a group project, a bicycle outing, a surprise birthday party or just some academic discussion. While naming just a few might disappoint others, I would like to take that risk and thank, in no particular order, Manas, Akilan, Ayush, Ameya, Nakul, Vaishakh, Vasudeva, Sumant, Asutosh, Shreya and Mridusmita for the wonderful time I spent with them. Manas was an awesome roommate during my time on the IISER Pune campus (which became apparent to me after sharing a room with another person). The countless late-night musings with him on philosophy, science, history and mythology were intellectually rewarding (We should have recorded them!). I had several discussions on eco-evo with Akilan, Ayush and Nakul. Special

thanks to Ayush, Vasudeva and Mridusmita for touring European cities with me during our thesis projects. And thanks a million to the Afghan stranger in Paris who sprinted with us two kilometres to the Bercy Seine Bus Station at midnight just to ensure we catch the bus we were about to miss due to losing our way.

Finally, I am deeply indebted to my parents, grandparents and extended family for their eternal support and encouragement throughout the years. From persuading a schoolgoing me to focus less on school exams and more on exams like Dr. Homi Bhabha Balvaidnyanik Competition and assisting me through the projects I did for the same— may it be for raising firecracker awareness or studying butterfly diversity in my city— to buying me a telescope as a child and to not questioning my unconventional choices— regarding career or otherwise— my parents have been a constant source of encouragement from my childhood until today. None of this would have been possible without their support.

Contributions

Contributor name	Contributor role
Kaustubh Kulkarni, Thomas Koffel, Christopher Klausmeier	Conceptualization
Kaustubh Kulkarni, Thomas Koffel	Methodology
Kaustubh Kulkarni, Jonas Wickman	Software
Kaustubh Kulkarni, Thomas Koffel	Validation
Kaustubh Kulkarni	Formal analysis
Kaustubh Kulkarni	Investigation
Thomas Koffel	Resources
Kaustubh Kulkarni	Data Curation
Kaustubh Kulkarni	Writing — original draft preparation
Kaustubh Kulkarni, Thomas Koffel, Jonas Wickman	Writing — review and editing
Kaustubh Kulkarni	Visualization
Thomas Koffel, Partha Sharathi Dutta	Supervision
Kaustubh, Kulkarni, Thomas Koffel	Project administration
Thomas Koffel	Funding acquisition

This contributor syntax is based on the Journal of Cell Science CRediT Taxonomy[1]

[1] https://journals.biologists.com/jcs/pages/author-contributions

Abstract

Organisms in nature cooperate with one another, facilitating each other's survival and reproduction. Since cooperators may experience reduced fitness compared to non-cooperators, why cooperation evolves has been an enigmatic question in evolutionary biology. Ecologically, due to a phenomenon called the Allee effect, small populations of cooperators can be particularly vulnerable to extinction. How do cooperators persist despite these seemingly adverse phenomena that threaten their survival on ecological and evolutionary timescales? Spatial structure is known to be one of the factors that can allow cooperation to evolve. However, the links between the ecology of Allee effects and the evolution of cooperation in spatially structured populations remain unexplored. In this thesis, I use a stochastic metapopulation framework to mathematically model the ecology and evolution of cooperation. Using numerical analyses, I reveal that small-scale Allee effects can disappear on larger spatial scales, enabling small populations to colonise spatially structured habitats. Further, I show that a metapopulation structure favours the evolution of cooperation in a situation where cooperation cannot evolve in a well-mixed population. I connect these results to metacommunity concepts, unifying the theories of cooperation and metacommunity ecology. My results suggest a mechanism rooted in metacommunity ecology, to explain the evolution of cooperation. In addition to contributing new paradigms to ecological and evolutionary theory, these findings are also relevant to applied fields such as wildlife conservation and invasion biology.

Contents

Chapter 1

Introduction

> The problem of pattern and scale is the central problem in ecology, unifying population biology and ecosystems science, and marrying basic and applied ecology.
>
> Simon Levin (1992)

Ecology and evolution are complex disciplines that are deeply interconnected. They transcend spatiotemporal scales and levels of biological organisation, producing a large and diverse quantity of biological results through experiments and observation. To make sense of these observations of the natural world, it is essential to have a body of theory that serves as a conceptual framework to explain and predict ecological and evolutionary phenomena. Theoretical work often involves constructing mathematical models of a system and analysing them to obtain insights into its characteristics. Mathematical models also help strip the system of its non-essential parts and focus on what matters biologically (Levins, 1966).

Today, ecology and evolution are among the subdisciplines of biology with the richest theory available. A central concept in both ecology and evolution is *competition*, which has acted as a mainspring of ecological and evolutionary theories. Organisms compete with each other for resources, and this competition negatively impacts their growth. In ecology, prominent models ranging from the logistic model (Verhulst, 1838) to Lotka-Volterra competition models (Lotka, 1932; Volterra, 1926) to Tilman's consumer-resource models (Tilman, 1982) have focused on competition as a driver of population dynamics. In evolution, the idea of a "struggle for existence" (Darwin, 1859) dominated for a long time. Individuals have varied competing abilities, and the best ones survive and reproduce better, increasing in proportion in the population. While competition is indeed the cornerstone of ecology and evolution, an excessive focus on it leaves out another important biological phenomenon: *cooperation*.

As is largely documented, organisms can also cooperate with each other, helping each other's survival and reproduction. Cooperation is known to take place in taxa ranging from bacteria to mammals. Cooperation can occur both among individuals of the same species and among individuals of different species and is now recognised to play an important role alongside competition. Though cooperation has received less attention than competition in theoretical studies,

a large body of literature also exists on the role of cooperation in shaping population dynamics. However, the ecology and evolution of cooperation have largely been treated separately despite the obvious links between the two fields. This thesis is an attempt to bridge the ecology and evolution of cooperation and understand how cooperation interacts with competition on different spatiotemporal scales.

While an idealist mind may be at first delighted to hear about the importance of cooperation in biology, the biological world is not a utopia. As we will see throughout the thesis, cooperation is fragile on both ecological and evolutionary timescales. Nevertheless, cooperation persists in nature in a wide range of taxa. What factors cause cooperation to be fragile and sensitive? What enables cooperation to persist despite its vulnerability to these factors? How do the ecology and the evolution of cooperation influence each other? What scenarios allow cooperators and non-cooperators to coexist? This thesis engages with these questions using the tools of mathematical modelling.

Particularly, we concentrate on two features of biological populations that can allow cooperation to persist on ecological and evolutionary timescales: spatial structure and stochasticity. Populations are distributed in space, which affects who interacts with whom. Additionally, chance phenomena play a major role in biology, making interactions inherently stochastic. The thesis explores how the interplay of these two factors affects cooperation.

Spatial structure and stochasticity point towards a branch of ecology, namely, *metacommunity ecology* (Leibold and Chase, 2017), where the ecological effects of these two facets have been deeply investigated, both theoretically and empirically. However, metacommunity ecology and the evolution of cooperation have remained detached topics (but see Parvinen, 2011, 2013), leaving the links between them unexplored. Here, we ask, can metacommunity theory help us understand the evolution of cooperation? Although our answer is affirmative, the thesis explains in detail the nuanced relationship between metacommunity theory and the evolution of cooperation. Using the tools of metacommunity theory, we situate cooperation in an ecological context. This allows us to investigate the evolutionary ecology of cooperation, revealing deep associations between metacommunity concepts and the theories of cooperation.

Moreover, spatial structure brings one more factor into the picture: *dispersal*, or the movement of organisms throughout their lifespans. We investigate how dispersal affects the ecology and evolution of cooperation and how cooperation, in turn, affects the evolution of dispersal. Finally, we probe the coevolution of cooperation and dispersal.

As we perform mathematical modelling in the thesis, parts of it may seem fraught with equations and mathematical details. Nonetheless, we constantly insist on the biological implications of the results, which we hope makes the thesis accessible to anyone with a background in ecology and evolution. The prerequisites assumed include the basics of ordinary differential equations, linear algebra, dynamical systems and probability theory. The knowledge of stochastic processes, metacommunity theory, and adaptive dynamics is useful but not required, as we elaborate on these topics in the required detail in appropriate places. These methodological prerequisites aside, a knowledge of the fundamentals of ecology and evolution is essential for understanding the results of this thesis and their broader implications.

1.1 Cooperative interactions in nature

Cooperative behaviours and positive interactions are ubiquitous in nature. Organisms cooperate in different contexts, including breeding, resource production or procurement, hunting, defence

from predators, environmental conditioning and several other social interactions. In this section, we provide illustrative examples of different types of cooperation. We use the term cooperation *sensu* Jacobs (1984), i.e., in a wide sense, that refers to any interaction with conspecifics that increases individual fitness.

Cooperation has important consequences for the ecology and evolution of populations. Ecologically, cooperation can lead to Allee effects that have negative consequences for population growth and persistence. Evolutionarily, cooperation is susceptible to invasion by defectors who freeload on the cooperators' efforts, enjoying the benefits without contributing anything on their own. This thesis aims to seek explanations for the ecological and evolutionary persistence of cooperation and connect it to certain ecological theories.

In birds and mammals, cooperation takes numerous forms, including cooperative hunting, cooperative feeding, cooperative breeding alarm calls to signal the presence of predators or cooperative defence from predators through mobbing (Dugatkin, 1997). In these examples, cooperators share the benefits they obtain or put themselves at risk for the sake of other individuals.

In plants, examples of cooperation include creating favourable conditions for other plants, supporting a useful resource, communicating about the presence of herbivores and synchronous seed production or masting (Dudley, 2015).

An example of cooperation in microbial systems is the secretion of siderophores by bacteria. Siderophores are iron-scavenging compounds that aid microbes in iron acquisition (Kramer *et al.*, 2020). Bacteria secrete siderophores in the surroundings, which sequester iron molecules, followed by their uptake. Since these are extracellular compounds, some individuals could defect by not manufacturing them but yet benefit from the siderophores produced by other individuals (Kramer *et al.*, 2020).

A similar situation occurs in yeast, where cells secrete an enzyme called invertase to break down sucrose. Since the enzyme is released into the surroundings, cells can defect by reaping its benefits without producing the enzyme (Greig and Travisano, 2004).

In cases such as these microbial examples, cooperation can be thought to occur through a common good or a public good (Rankin *et al.*, 2007), which is a resource shared among individuals. Individuals contribute to this common good, and the benefits are shared with everyone.

1.2 Allee effects: A consequence of cooperative interactions

Obviously, cooperation requires multiple individuals to be present together. When organisms cooperate, the consequences of such interactions can surface in population dynamics in the form of Allee effects (Odum and Allee, 1954). The facilitatory interactions become dominant over competition in small or sparse populations, with the consequence that increasing abundance leads to an increase in each individual's survival and reproduction and, hence, in the population's per capita growth rate. The effect of increased cooperation is greater than the effect of increased competition at small abundances, due to which increased abundance benefits population growth.

Allee effects can arise through several mechanisms. In addition to cooperative interactions such as cooperative feeding, defence, and breeding, Allee effects also arise through mechanisms

including limited availability of mates or habitat alteration (Kramer *et al.*, 2009). Allee effects have been documented in several species that are important from the point of view of conservation or harvest management or are invasive or pests (Kramer *et al.*, 2009).

Allee effects can be classified into component Allee effects and demographic Allee effects (Stephens *et al.*, 1999). Component Allee effects refer to an increase in a particular component of fitness with increasing abundance, whereas demographic Allee effects refer to an increase in the overall fitness with increasing abundance. In this thesis, we will only be concerned with demographic Allee effects. Another important classification of Allee effects is into strong and weak Allee effects (Courchamp *et al.*, 2008). In the case of strong Allee effects, a population's growth rate is negative below a threshold abundance called the Allee threshold. With a weak Allee effect, the growth rate is positive but increasing at small abundances. In this thesis, we shall only deal with strong Allee effects.

Due to strong Allee effects, a small population has a negative growth rate, making it difficult for it to grow. Even for a large population, perturbations that reduce its size below the Allee threshold can impede its regrowth. Then, how do populations experiencing strong Allee effects persist in nature? How do they establish in newer habitats from small initial abundances? This thesis explores two potential processes that can answer these questions.

First, natural populations are not governed by deterministic rules. Population dynamics are inherently noisy. When stochastic fluctuations play an important role in the population dynamics, the Allee threshold no longer remains a strict barrier. Instead, small populations may be able to increase in abundance if the stochastic dice roll in their favour. However, stochasticity can also undermine the stability of large populations and may cause them to collapse.

Second, if the population in a certain location collapses, recolonising it would require individuals to arrive from outside. Migration from other spatial locations can also prevent a population from going extinct due to Allee effects. To understand this, one needs to take a broader outlook, viewing a patch inhabited by a population as embedded within a collection of multiple such patches, from where immigrants can arrive to recolonise the patch or prevent its extinction. Since the population within this patch faces an Allee effect, one might wonder if the aggregate collection of patches also faces an Allee effect. Put differently, can the entire landscape of patches be colonised by a population that has a small abundance, or is there a threshold abundance required to colonise it? If such a threshold exists, how is it related to the threshold at the level of a single patch?

To explore these questions, we inspect how patterns of Allee effects appear on different spatial scales. We build a mathematical model of cooperation that displays strong Allee effects, where the carrying capacity and the Allee threshold vary with the level of cooperation. Then, we look at cooperators in a metapopulation and investigate whether a patch-scale Allee effect produces a metapopulation-scale Allee effect.

1.3 Evolution of cooperation: A paradox?

As we have seen, cooperators are sensitive to Allee effects, which undermines their propensity to persist and invade new habitats. But how does cooperation evolve in the first place? Cooperation often comes with a cost that affects survival and reproduction. While cooperation may be beneficial if everyone cooperates, a defector who seeks the benefits without paying the cost may fare better than cooperators who suffer from the cost.

As an example, consider a scenario where each individual in the population can contribute to producing a common good. This good can be consumed indifferently by everyone in the population. Producing the good is accompanied by a cost of reduced fitness, while its consumption increases fitness. Suppose all individuals are cooperators, to begin with, and contribute to the common good. Now, due to a mutation or external immigration, a defector enters the population. The defector consumes the common good but does not produce it. It has a higher fitness than the cooperators, because it reaps the benefits of the common good without paying the cost that goes into its production. Thus, the defector survives and reproduces better. Eventually, the defector population increases and the cooperators disappear. In a population full of defectors, the common good is not produced. If the common good is essential for survival, the population will go extinct. This phenomenon, where individuals exploit a common resource and destroy its value, is called the *tragedy of the commons* (Hardin, 1968).

While crude intuition may suggest that a tragedy of the commons should occur wherever cooperation is involved, the biological examples previously discussed show that cooperation clearly persists in nature. This apparent paradox demands an explanation.

There are several reasons that can be responsible for the evolution of cooperation, making it robust against defectors (Nowak, 2006). First, though a tragedy of the commons occurs in the common good example mentioned above, the way cooperation affects fitness may be different in different situations. The payoffs received by individuals in their interactions may not always facilitate defectors (Maynard Smith and Price, 1973). Second, individuals may interact with each other multiple times during their lives, due to which cooperating once can lead to future benefits, directly from the recipient (Trivers, 1971) or indirectly from others (Nowak and Sigmund, 1998). Third, selection on the level of collectives of individuals may favour cooperation if groups of cooperators are fitter than the groups of defectors (Maynard Smith, 1976). This is called multilevel selection (Lion and van Baalen, 2008), an example of which is kin selection (Hamilton, 1963, 1964a,b). According to kin selection, cooperative behaviours that increase the fitness of relatives can be favoured by selection. Fourth, in spatially structured populations, cooperators may be able to huddle together and keep defectors at bay, promoting the evolution of cooperation (Hauert and Doebeli, 2004; Nowak and May, 1992). These and other factors, or their combinations thereof, may play a role in sustaining cooperation in the long term.

Furthermore, cooperators and defectors are not always binary categories. Cooperation can exist on a continuum, where the strategy of an individual lies somewhere between complete cooperation and complete defection (Doebeli and Knowlton, 1998; Doebeli *et al.*, 2004; Killingback and Doebeli, 2002; Wahl and Nowak, 1999). For example, in the common good example described above, the investment into the common good can take continuous rather than discrete values. Then, the population dynamics may depend on the level of cooperation in the population (Lehmann, 2008), due to which the strength of the Allee effect and the equilibrium abundance of the population varies with the level of cooperation. Under this scenario, what happens when populations with different levels of cooperation compete? To what level does cooperation evolve? Can populations with varying levels of cooperation coexist? These questions demand an integration of ecological and evolutionary dynamics in a combined framework.

Though several resolutions to the apparent paradox of cooperation are possible, in this thesis, we focus on the role of spatial structure. Incidentally, it also leads to an interpretation through the angle of multilevel selection. To study the role of spatial structure, we employ a metacommunity framework, which enables us to connect metacommunity theory and both the

ecology of Allee effects and the evolution of cooperation.

1.4 Connecting metacommunity theory, Allee effects and evolution of cooperation and dispersal

A metapopulation is a collection of populations interconnected by dispersal, whereas a metacommunity is a collection of such interconnected communities. Like most metacommunity models, we shall use a model of two scales: local and regional. Throughout the thesis, the term 'local' shall refer to a single population or community in such a collection, present on a single patch of habitat in space. The term 'regional' shall refer to the scale of the entire metapopulation or metacommunity. We use the terms 'local abundance' (or 'patch abundance') and 'regional abundance' to refer to the population sizes on a patch and in the metapopulation, respectively.

Since metacommunity ecology is a key aspect of this thesis, we briefly introduce some pertinent concepts from the field. Particularly, we discuss the four metacommunity archetypes (Leibold and Chase, 2017), which are frameworks that represent metacommunities by highlighting different properties and assuming different premises regarding the nature of metacommunities.

The four metacommunity archetypes are *neutral theory*, *patch dynamics*, *species sorting* and *mass effects*. *Neutral theory* is the simplest of the archetypes, as it assumes that community assembly and species coexistence occur due to stochastic events and dispersal rather than niche differences. A central concept in neutral theory is *ecological drift*, the changes in species abundances due to stochasticity.

The *patch dynamics* archetype assumes that the local abundances vary as a result of repeated colonisations and stochastic extinctions. The habitat is assumed to be homogenous, due to which coexistence can occur when species niches differ sufficiently. The local extinctions also make the role of dispersal important. A central concept in this archetype is *competition-colonisation trade-off*. This trade-off takes place when one species is a better competitor than the other, but the other is better at colonising empty patches (for example, has a higher dispersal rate). Thus, a competition-colonisation trade-off allows regional coexistence of different species, though one of them is locally the superior competitor.

The *species sorting* archetype focuses on habitat heterogeneity and posits that different species get sorted across local habitats according to the niche differences among them. Both local and regional coexistence can be possible, depending on the species niches and the differences in conditions (such as resources) across local patches.

Finally, the *mass effects* archetype assumes high dispersal rates that allow a species to coexist in local habitats with conditions detrimental to its survival. A locally inferior competitor may be able to locally coexist with the superior competitor, if it has a sufficiently high dispersal rate. Mass effects can lead to *source-sink dynamics*, where large abundance patches (*sources*) coexist with small abundance patches (*sinks*).

While these archetypes are distinct ways to look at metacommunities and make different predictions, natural metacommunities are quite kaleidoscopic. They can be better understood by integrating the archetypes and observing which processes have a greater role to play in different types of metacommunities (Leibold and Chase, 2017; Lerch *et al.*, 2023). In this thesis, we apply these metacommunity concepts to cooperation to study its ecology and evolution.

As discussed above, dispersal is a key factor that influences metacommunity patterns and

processes. Therefore, we explore how dispersal affects the evolution of cooperation. Since dispersal is such an important trait, it is also under selection pressure. Naturally, one can flip the argument and ask, how does cooperation affect the evolution of dispersal? We also deal with this question and consider the evolution of dispersal as well as the coevolution of cooperation and dispersal. Thus, we attempt to develop a holistic understanding of cooperation and dispersal in the light of metacommunity ecology.

At various points in the thesis, we will come across patch dynamics, competition-colonisation trade-offs, mass effects and source-sink dynamics. Ecological drift also forms the backbone of several ideas presented throughout the thesis. Hence, this thesis serves to connect the theories of metacommunities and cooperation using mathematical models.

1.5 An outline of the rest of the thesis

Summarising, we couple the tools from metacommunity theory and adaptive dynamics and study how cooperators invade and persist in spatial habitats. Importantly, we view cooperation through the lens of metacommunity concepts and propose a mechanism rooted in metacommunity ecology for the evolution of cooperation. The rest of this thesis is organised into five chapters, whose contents can be briefly sketched out as follows:

- Chapter 2 is a methodological chapter. Different interconnected modelling formalisms are discussed in short, and our choice of framework is expounded in detail.
- Chapter 3 explores cooperation on an ecological scale. The scaling of Allee effects from smaller to larger spatial scales is investigated. Specifically, we study whether a patch-level (local) Allee effect produces a metapopulation-level (regional) Allee effect.
- Chapter 4 is perhaps the most important chapter of the thesis. In this chapter, we capitalise on Chapter 3 and examine the evolution of cooperation in a metapopulation. Specifically, we ask whether cooperation can evolve on the metapopulation (regional) scale, if defectors always win over cooperators on the patch (local) scale. If yes, what conditions favour the evolution of cooperation? We also delve into the coexistence of cooperators and defectors, scrutinising the factors that lead to regional and local coexistence. We propose a metacommunity theory-based mechanism for the evolution of cooperation.
- In Chapter 5, we consider the evolution of dispersal and its coevolution with cooperation.
- Chapter 6 is the Discussion. In this ultimate chapter, we discuss the implications of our results for ecological and evolutionary theory, their relations to the results from other studies and their applications. We conclude by discussing some unanswered questions, the limitations of our work and suggestions for how future studies could overcome them.
- Appendices A, B and D provide supporting analytical and numerical results for Chapter 2 and 3. Appendix E provides supporting results for Chapter 4. Appendix F mentions technical details on numerical calculations and programming.

In a nutshell, this thesis is an attempt to connect metacommunity ecology and the evolution of cooperation. Using a model of linked patches, we link the two theories and reveal elegant explanations for the observed phenomena based on both theories. We hope that the thesis

piques the readers' curiosity in metacommunities and cooperation and motivates a broader integration of concepts in ecology and evolution.

Chapter 2

Modelling stochastic, spatially-structured populations

> Paradoxically, perhaps the major weakness of traditional community ecology, and why it has so conspicuously failed to come up with many patterns, rules and workable contingent theory, is its overwhelming emphasis on localness.
>
> John Lawton (1999)

In nature, it is rare to find a population where an individual is equally likely to interact with every other individual in the population. Location in space is one of the most important factors that influence the likelihood of interaction among individuals. Thus, to develop ecological and evolutionary theory that provides deeper biological insights, it is essential to take space into account.

Lawton (1999) attributed the shortcomings of contemporaneous ecological theory to an excessive focus on local dynamics that overlooks spatial interactions and scaling. Although metacommunity ecology (Leibold *et al.*, 2004; Leibold and Chase, 2017) has remedied several of the drawbacks rooted in an emphasis on local themes, it has also underscored the importance of understanding the scaling of outcomes.

As explained in Chapter 1, our objective is to investigate the evolutionary ecology of cooperation in metapopulations. On an ecological scale, we shall explore how local Allee effects appear at the metapopulation level. On an evolutionary scale, we shall explore how a metapopulation structure allows cooperation to evolve where defecting is the locally dominant strategy. It is essential to choose an appropriate modelling framework that is methodologically simple and elegant but permits sufficient ingredients to model cooperative interactions and Allee effects in a spatial setting. Moreover, since stochasticity plays a key role in metacommunity theory, we need a framework that seamlessly integrates space and stochasticity in a manner that we can use to explore our research questions.

Myriad approaches exist for modelling spatially structured populations, ranging from meth-

ods that characterise individuals by spatial coordinates to those that treat space in a tacit, indirect fashion. In this chapter, we briefly summarise the gist of different modelling methods. Then, we explicate the Lerch *et al.* (2023) framework used throughout this thesis. Starting with a single species nonspatial deterministic model, we add layers of complexity to construct a stochastic metapopulation model. While the simpler models serve to build intuition as well as to focus on local outcomes, the metapopulation model helps us understand the outcomes on a regional scale. Further, we explain how the model extends to two species and the eco-evolutionary methods applied to study invasion dynamics in the model, including adaptive dynamics in the nonspatial model and the use of pairwise invasibility plots (PIPs).

2.1 Methods to model spatially structured populations

Approaches to model spatial population dynamics in ecology and evolution can be broadly classified into spatially explicit and spatially implicit methods (Tilman *et al.*, 1998), though they may also be thought to exist on an explicit-implicit continuum. Spatially explicit models assume that organisms are present and move in a hypothetical space— usually a two-dimensional plane— and certain coordinates can characterise their location. Thus, these models constitute a simplified projection of the actual spatial dynamics.

Examples of spatially explicit modelling frameworks include reaction-diffusion equations (Kierstead and Slobodkin, 1953; Skellam, 1951) and cellular automata models (Hogeweg, 1988). Lattice-based models, such as cellular automata, divide space into a grid of sites where an individual on a site interacts with its neighbours. Dispersal takes place locally, from one site to nearby sites. Often, agent-based simulations are run on such spatial arrays to analyse the dynamics. As the results from these simulations may not be clearly apparent, running repeated simulations is sometimes necessary to obtain interpretable results, amplifying the computational burden of such models.

Adding a layer of simplicity, reaction-diffusion models consider space as a continuous variable with populations as waves in this continuous space. The reaction refers to a population growth function, whereas the diffusion term highlights the spread of the population in space. This class of models offers slightly greater analytical tractability and can be studied better with powerful numerical techniques for partial differential equations. Such models have been successfully applied to a wide range of phenomena and are particularly useful for studying spatial patterning. While these spatially explicit models are useful to capture minute details and may be well applicable to specific systems (DeAngelis and Yurek, 2017), more often than not, they lack analytical tractability or involve running intensive simulations which may not be easy to interpret.

On the other hand, spatially implicit frameworks "incorporate space without taking space into account". Though this may sound paradoxical, spatially implicit models are neither merely illusory nor do they involve some mathematical sorcery. In fact, spatially implicit models have dominated most of the theory of ecology (DeAngelis and Yurek, 2017).

The fundamental idea in spatially implicit models, such as Levins's metapopulation model (Levins, 1969), is to assume that the individuals are distributed within patches. A patch is a local population present within a spatially bounded area. These models assume global dispersal and focus on the proportion of patches harbouring specific population sizes at a given instant. Global dispersal implies that all patches are equally connected to each other, with dispersal occurring at equal rates across them. This kind of dispersal is equivalent to building a disperser

pool that collects individuals from all patches and redistributes them. Thus, there is no notion of distance in these models. Space is considered "implicitly" by allowing for distinct patches but without any equations for spatial coordinates. Following this assumption, one can write equations for the proportions of empty and occupied patches or the proportions of patches with specific population sizes or densities. Importantly, these models are mathematically and computationally simpler to analyse than spatially explicit models and may be preferable for developing general theoretical results (Roughgarden, 2018).

Levins's model, which is a spatial analogue of the logistic model, describes such a population spread across patches. It focuses only on the presence and absence of individuals in patches, ignoring the population size. In this way, Levins's model tracks the proportion of occupied and empty patches in a metapopulation, explaining the conditions for persistence and the equilibrium proportion of occupied sites. In Levins's model, the colonisation rate depends on the proportion of occupied patches, and the occupied patches go extinct at a constant rate. A primary insight from Levins's model is that a species can invade a region when its rate of colonising new patches is greater than the rate at which local populations go extinct. Additionally, even at equilibrium, a certain proportion of the patches remain empty. While Levins's model only considers occupied and empty patches, the abundances of small populations fluctuate due to ecological drift. A recently colonised patch is not equivalent to an established large-abundance patch, as the former is more sensitive to stochastic extinction. Thus, further work has developed frameworks that can account for variation in population size on different patches (Casagrandi and Gatto, 2002; Drechsler and Wissel, 1997; Metz and Gyllenberg, 2001) which may also be used to study the evolution of traits in a metapopulation.

Overall, one may use diverse approaches to investigate the role of spatial structure in ecology and evolution. Spatially implicit models are not only good approximations of well-connected systems, but also have the advantage of tractability and interpretability over explicit models, because of which they may be more beneficial than the latter in exploring spatial scaling and generalising eco-evolutionary phenomena. Thus, in this thesis, we employ a spatially implicit modelling framework developed by Lerch *et al.* (2023) to investigate how populations with Allee effects establish and persist, how local Allee effects scale to the metapopulation level and how cooperation and dispersal evolve in a population spread across space.

2.2 Modelling framework with one species

We build the modelling framework in three steps: First, we take a nonspatial deterministic model and convert it into an open system, i.e., a mainland-island model, by including dispersal into the focal patch from a region with a constant abundance. This allows us to study the influence of the region on a local population. Second, we convert this model into a stochastic model by defining the demographic processes of birth, death, immigration and emigration as stochastic processes occurring at specific rates. This stochastic open system reveals how demographic noise alters the local dynamics within the patch of focus. Last, we take this stochastic open system model and *close it*, obtaining a stochastic closed system model that describes our metapopulation of interest. This metapopulation is assumed to consist of infinitely many equally connected patches. We can now compute metapopulation-level equilibria, their stability and the criteria for invasion into an empty or occupied metapopulation habitat. Since the metapopulation model is a closed system without migration from outside, we can compare it to the nonspatial deterministic model to observe how spatial structure and stochasticity affect

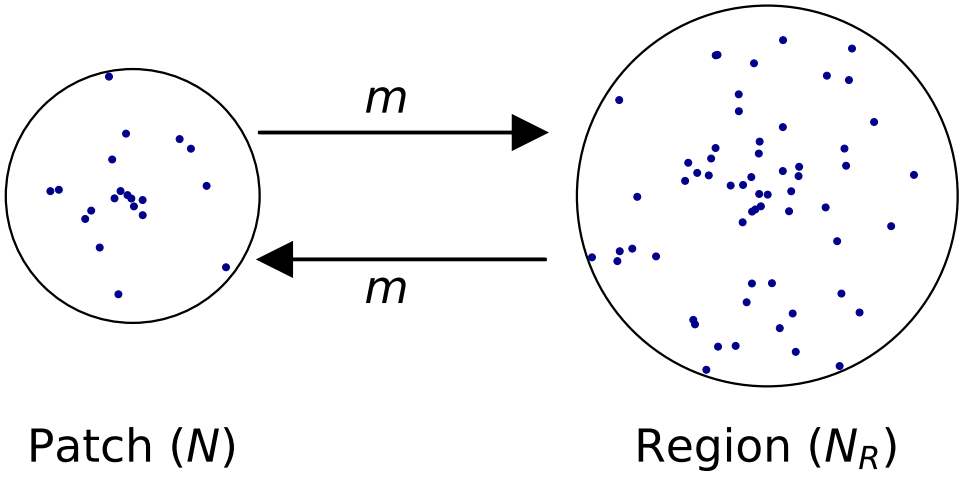

Fig. 2.1. Schematic figure showing the focal patch with variable population size N and the connected region of constant population size N_R in the determinisitic open system model. The arrows represent the transfer of individuals occurring at rate m.

the outcomes. In the following subsections, we elucidate in detail the steps to construct our model and the numerical and analytical methods implemented for the analysis.

2.2.1 Deterministic open system model

To begin with, consider a population in an isolated patch whose per-capita birth rate and per-capita death rate are given by $b(N)$ and $d(N)$ respectively, where N is the population size. The per-capita growth rate is $g(N) = b(N) - d(N)$. The overall birth and death rates in the population are $B(N) = b(N) \cdot N$ and $D(N) = d(N) \cdot N$. The net population growth rate is the difference between the birth and the death rate, i.e., $f(N) = B(N) - D(N)$. Hence, the population dynamics are given by the equation

$$\frac{dN}{dt} = f(N) \tag{2.1}$$

The equilibrium population sizes N_{eq} are the values of N where $f(N) = 0$. An equilibrium is stable if $\frac{df}{dN}|_{N=N_{\text{eq}}} < 0$ and is unstable if $\frac{df}{dN}|_{N=N_{\text{eq}}} > 0$.

The simplest way to incorporate spatial structure in such a deterministic model is to couple this patch to a regional reservoir, making it a mainland-island model (Hanski and Gyllenberg, 1993), where processes occurring on the island do not affect the mainland. Thus, we add constant immigration and emigration to this model by assuming that the population we are modelling is in a patch connected to a region with a constant abundance N_R (Fig. 2.1). Immigration occurs in our patch of focus from this region at a rate given by I, and emigration takes place at the rate $E(N)$. Throughout this thesis, we assume density-independent dispersal, defining

$$I = mN_R \tag{2.2}$$

$$E = mN \tag{2.3}$$

where m is termed as the dispersal rate. Note that the rate of immigration into the patch does not depend on the population size of the patch. Dispersal in nature is often costly or risky and can lead to increased mortality (Gaines and McClenaghan, 1980; Greenwood and Harvey, 1982; Lucas *et al.*, 1994; Yoder *et al.*, 2004), which can be incorporated into our model simply by including a survival factor $0 < \delta < 1$ into the immigration rate, redefining it as

$$I = \delta m N_R \tag{2.4}$$

which assumes that only a fraction δ of the migrants entering the patch survive the dispersal events. Unless mentioned otherwise, we always assume $\delta = 1$, i.e., no dispersal mortality.

Hence, considering all four demographic processes of birth, death, immigration and emigration, the equation for our deterministic open system model becomes

$$\frac{dN}{dt} = f(N) + m(\delta N_R - N) \tag{2.5}$$

We can analyse this equation to explore the influence of dispersal on local population dynamics and abundance.

2.2.2 Stochastic open system model

While deterministic equations may well approximate the dynamics of large populations, the effects of stochasticity cannot be neglected in small populations. Therefore, in the next step, we wish to explore the effects of demographic noise on our model, for which we introduce stochasticity, creating our stochastic open system model. The population on our patch fluctuates in a stochastic fashion, while the population of the connected region stays constant at N_R.

We define the demographic events of birth, death, immigration and emigration as continuous-time stochastic processes (Karlin, 2014) occurring at rates given by $B(N), D(N), I$ and $E(N)$ respectively, as in the deterministic case. We also include catastrophes that cause local extinction at a rate X. The catastrophes represent large disturbances that wipe out the entire population within a patch. Thus, the population on our focal patch increases from N to $N+1$ at the rate $B(N) + I$ and decreases from N to $N-1$ at the rate $D(N) + E(N)$, respectively. Local extinctions take the population on the patch from N to 0 at the rate X. These "rates" of demographic processes are rates in the sense of stochastic processes, i.e., a process with a rate Z takes place in a short time interval δt with the probability $Z\delta t$. The rates are not probabilities of transition between population sizes and thus can take any value in the range $[0, \infty)$.[1]

The patch population size is described by a continuous-time Markov chain whose states are the discrete population sizes $N \in \{0, 1, 2, 3, \dots\}$, and transitions occur across these states at the rates defined above (Fig. 2.2). The probability distribution $P(N, t)$ over these states represents how likely the system is to be in the state N at a given instant of time t. Thus, we

[1] Empirical biologists sometimes use the term "dispersal rate" or "migration rate" to refer to the fraction of individuals that emigrate from a patch, which, being a fraction, lies in the range $[0, 1]$. However, it is important to note that our definitions of "dispersal rate" (m), "immigration rate" (I) and "emigration rate" (E) in this thesis, as defined in (2.2, 2.3) and (2.4) are not fractions and can take any non-negative value. Rather, the rates I and $E(N)$ are the rates at which a patch with N individuals turns into a patch with $N+1$ and $N-1$ individuals solely due to migration, respectively.

can write the master equation for this Markov chain as

$$\begin{aligned}\frac{d}{dt}P(0,t) &= [D(1)+E(1)]P(1) - [B(0)+I+X]P(0) + X \\ \frac{d}{dt}P(N,t) &= [B(N-1)+I]P(N-1) \\ &\quad + [D(N+1)+E(N+1)]P(N+1) \\ &\quad - [B(N)+I+D(N)+E(N)+X]P(N) \text{ for } N \neq 0\end{aligned} \tag{2.6}$$

the equilibrium solution of which returns the stationary distribution of the Markov chain. This stationary distribution $P_{\text{eq}}(N; N_R)$ describes the probability of the patch having population N when there is no knowledge of the preceding time series, thus revealing the behaviour of the system on a long-term.

Since the master equation (2.6) is linear in the probabilities $P(N)$, we can write it in the form $\frac{dP}{dt} = TP$, where T is the transition-rate matrix of our Markov chain and P is the vector whose i^{th} term is the probability $P(i)$.

T is a sparse matrix, which necessarily has a unique zero eigenvalue (Keizer, 1972). The stationary distribution is the eigenvector corresponding to the zero eigenvalue, which can be obtained numerically. For numerical calculations, we need the transition-rate matrix to be finite, and thus to set an upper limit $N_{\max}$ on the population size. Hence, the population states are given by $N \in \{0, 1, ..., N_{\max}\}$. Setting $N_{\max}$ as twice the carrying capacity of the patch suffices to ensure that the numerical analysis well-approximates the dynamics without an upper limit (Lerch *et al.*, 2023). This upper limit changes our master equation to the one given by

$$\begin{aligned}\frac{d}{dt}P(0,t) &= [D(1)+E(1)]P(1) - [B(0)+I+X]P(0) + X \\ \frac{d}{dt}P(N,t) &= [B(N-1)+I]P(N-1) \\ &\quad + [D(N+1)+E(N+1)]P(N+1) \\ &\quad - [B(N)+I+D(N)+E(N)+X]P(N) \text{ for } 0 < N < N_{\max} \\ \frac{d}{dt}P(N_{\max},t) &= [B(N_{\max}-1)+I]P(N_{\max}-1) - [D(N_{\max})+E(N_{\max})+X]P(N_{\max})\end{aligned} \tag{2.7}$$

At this point, it is helpful to explain the behaviour of the system in two different limits: no dispersal ($m = 0$) and high dispersal ($m \to \infty$). With no dispersal, the population always goes extinct since isolated finite populations eventually collapse to zero (MacArthur and Wilson, 1967). Simply put, over a long time, a finite population will necessarily attain a state of zero population size due to random fluctuations. The absence of immigration leaves no room for regrowing this population, causing it to remain extinct forever. Mathematically, since zero is an absorbing state of the Markov chain when $I = 0$ (Karlin, 2014), the population on the patch will go extinct when there is no dispersal. For a simple proof, see Appendix A, Section A.1. However, the time to extinction increases with increasing population sizes and can be large compared to the life spans of individuals (Méléard and Villemonais, 2012). Under such scenarios, the system may settle to a transient distribution called the quasi-stationary distribution (Méléard and Villemonais, 2012). However, we do not perform quasi-stationary analysis in this thesis, since our main focus is on the effects of dispersal and not on closed populations.

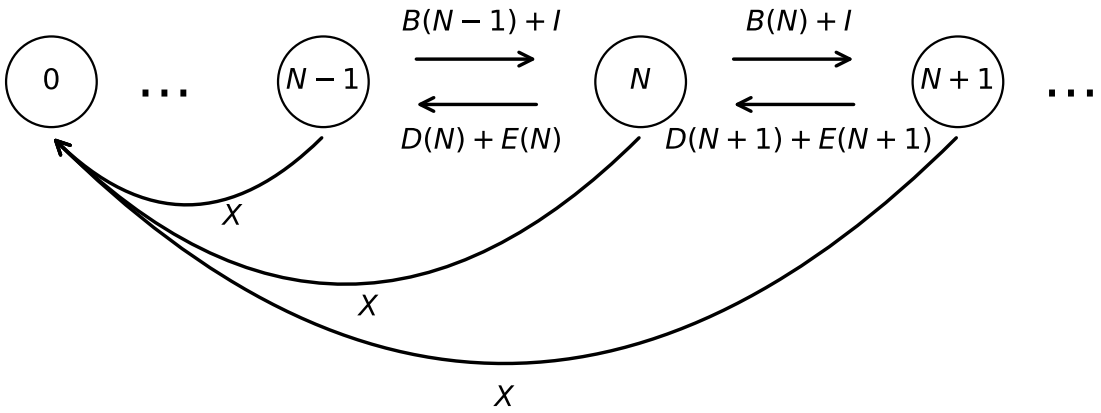

Fig. 2.2. Schematic figure showing the transitions between states of the Markov chain in the stochastic open system model. The arrows represent the transitions across states that take place at the adjacently mentioned rates.

The case of the high dispersal limit is more interesting. Intuitively, one might assume that with increasing dispersal, the patch equilibriates increasingly with the region, its population ultimately reaching the regional abundance N_R as $m \to \infty$. However, the stochastic component of dispersal in the model maintains the fluctuations, and the probability distribution of the patch does not become a sharp peak at N_R. Actually, we show that the probability distribution over the patch population becomes a Poisson distribution with average N_R, which we denote by $\text{Pois}(N; N_R)$. Thus,

$$\lim_{m\to\infty} P_{\text{eq}}(N; N_R) = \text{Pois}(N; N_R) \tag{2.8}$$

where $P_{\text{eq}}(N; N_R)$ is the stationary distribution of the patch. A proof of (2.8) is given in Appendix A, Section A.2. However, a simple way to understand this is to know that it is a consequence of assuming density-independent dispersal (2.2). At very high dispersal rates, the local dynamics are completely dominated by immigration and emigration processes, and the birth and death terms can thus be ignored in (2.7). Since immigration and emigration processes occur at constant per-capita rates, one migration event (immigration or emigration) does not influence the probability of another. Hence, the distribution is determined by events that occur at constant rates and independently of other events, which is the defining characteristic of the Poisson distribution.[2] In the deterministic open system model (2.1), the equilibrium in the high-dispersal limit is N_R, which happens to be the average of the stationary distribution in the stochastic equivalent of the model with high dispersal.

It is worth mentioning that this method of including demographic stochasticity differs from adding a noise term to a deterministic equation (Richter-Dyn and Goel, 1972). Here, the demographic processes are discrete events occurring stochastically at certain rates. Thus, we can use the Gillespie algorithm (Gillespie, 1977) to simulate the dynamics within a patch. By sampling the time to the next event and the type of the event (birth / death / immigration / emigration / local extinction), this algorithm simulates how the population size on the patch varies with time.

[2]If you know some queuing theory, the model becomes an $M/M/\infty$ queue (Guillemin and Simonian, 1995) at high dispersal rates.

In brief, the stochastic open system model considers the population of a single patch coupled to a regional reservoir through constant immigration and describes the pattern of population variation on the patch in terms of a probability distribution.

2.2.3 Metapopulation model

While the open system models elucidate the role of dispersal, mass effects (Loreau and Mouquet, 1999; Shmida and Whittaker, 1981; Shmida and Ellner, 1984; Shmida and Wilson, 1985) and ecological drift (Leibold and Chase, 2017; Vellend, 2010) in establishment and persistence of populations, they are insufficient to obtain insights into the feedback between local (patch-level) and regional (metapopulation-level) processes. After all, the region is itself a collection of smaller patches that the open system models abstract into a single combined region. To explore how local and regional processes interact to produce metapopulation-level patterns, we turn to our metapopulation model, which we obtain by modifying the stochastic open system model.

We consider a spatially implicit model comprising an infinite number of patches equally connected to each other (Fig. 2.3). All patches are identical except for their population sizes, which leads to identical population dynamics on every patch. We consider the probability distribution of the population on a single patch. Ergodicity guarantees that this probability distribution of a single patch through time is the same as the frequency distribution over all the patches at a given instant. In simpler words, if we track the population size on a given patch over time, we will obtain a certain frequency distribution. As all patches are identical, we will get the same distribution for all the patches. Thus, the population size on each of the infinitely many patches is effectively a sample from this distribution. Therefore, the population size at a given instant sampled over all the patches shall recover the same distribution as the one obtained by tracking the population size in a single patch over time. Our goal is to calculate this distribution at equilibrium.

Further, we need to appropriately redefine the regional abundance, as we are no longer dealing with an external regional reservoir. The regional abundance should now be a function of the local probability distribution. However, even at a non-zero equilibrium, the local population sizes will keep fluctuating despite the probability distribution of population sizes staying constant. Due to the assumption of global dispersal and an infinite number of patches, a particular patch can still be thought of as being connected to a regional pool with to-and-fro migration between them. This regional pool is equivalent to the entire metapopulation, as there are infinitely many patches. We define the regional abundance to be the average abundance over all the patches,

$$N_R = \overline{N} \tag{2.9}$$

i.e., as the mean value of the probability distribution given by

$$\overline{N}(t) = \sum_N P(N,t)N \tag{2.10}$$

The average abundance $\overline{N}$ (2.10) also happens to be the average abundance over time on a single patch, as mentioned above. Hence, in a way, a patch in the metapopulation model is connected to a "temporally extended mirror to itself".

To obtain the dynamical equations for our metapopulation model, we thus simply substitute the average local abundance $\overline{N}(t)$ in place of N_R in the immigration terms in the master

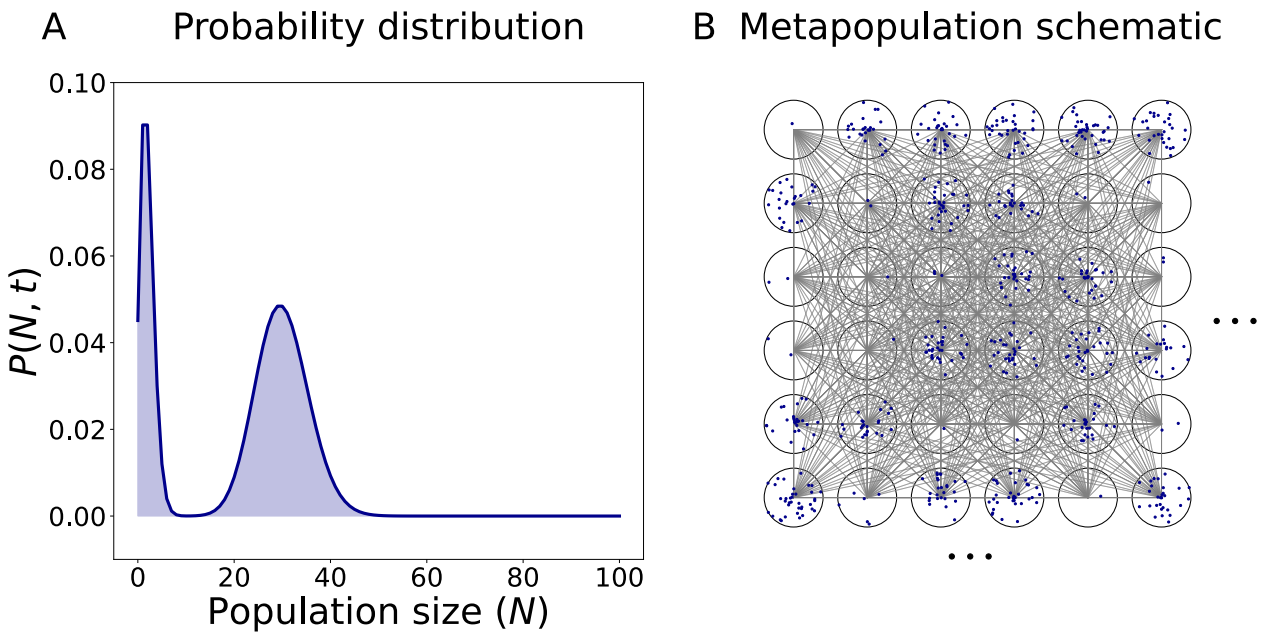

Fig. 2.3. Schematic figure showing a probability distribution at a given instant and the corresponding state of the metapopulation with infinitely many patches in the model. **A** $P(N,t)$ is the distribution at time t that gives the probability of finding N individuals in a patch. **B** The circles represent patches with individuals within them, and the connecting lines represent the strength of coupling. All of the infinitely many patches are equally connected to each other.

equation (2.6, 2.7). Having N_R dependent on the probabilities themselves makes our master equation nonlinear, but we can obtain stable equilibria for the model by numerically integrating it.

Alternatively, we can use what we call the LMAO (local mean abundance output) function[3] to compute both stable and unstable equilibria. This approach employs the stochastic open system to calculate the average local abundance on a patch for a given regional abundance. In the metapopulation model, the average local abundance on a patch equals the regional abundance due to the aforementioned equivalence of distributions. Thus, the regional abundance values in the stochastic open system that output identical average local abundance values of stationary distributions correspond to the metapopulation model equilibria. The LMAO function is given by

$$f_{\text{LMAO}}(N_R) = \sum_N P_{\text{eq}}(N; N_R) N \tag{2.11}$$

where $P_{\text{eq}}(N; N_R)$ is the stationary distribution in the stochastic open system model for a regional abundance of N_R.

As described above, the LMAO function takes in a value of regional abundance and returns the open system average local abundance of the stationary distribution. In other words, it calculates the open system transition matrix, its eigenvector corresponding to the zero eigenvalue and returns the weighted average of the eigenvector. We can apply a root-finding algorithm to this function to find its fixed point, and thus find out the metapopulation equilibria. Thus, we obtain the average local abundance (which is also the regional abundance) in the metapopula-

[3] In Lerch *et al.* (2023), this function is referred to as the "black-box function".

tion at equilibrium. However, it is important to note that the dynamics of this metapopulation is an $N_{\max}$-dimensional system of equations (2.7, 2.9), whose steady states are probability distributions given by vectors in an $N_{\max}$-dimensional space. On the other hand, the fixed points from the LMAO function are the average values of these equilibrium distributions. Since the distributions cannot be entirely characterised by their average values, the overall equilibrium distributions may remain an informative component of the model. We shall return to this question in Chapter 3 (see also Appendix D, Section D.2) when we define metapopulation-level Allee thresholds.

Once we know the equilibria, we can calculate their stability. The most straightforward way is to compute the $N_{\max}$-dimensional Jacobian matrix at the equilibrium (see Appendix B) and extract its eigenvalues. If all the eigenvalues are negative, the equilibrium is stable; otherwise, it is unstable. However, a more straightforward heuristic method is to exploit the LMAO function again, using its slope at the equilibrium instead. If the slope $\frac{d}{dN_R} f_{\text{LMAO}} < 1$, the equilibrium is stable; otherwise, it is unstable. While we do not present proof of the previous statement, this result based on intuition was systematically compared to the Jacobian-based matrix mentioned above and never resulted, to our knowledge, in any discrepancy.

Interestingly, the nonlinear nature of the metapopulation dynamics results in the existence of multiple fixed point solutions, such as a (trivial) extinction equilibrium and potentially several persistence equilibria. The extinction equilibrium always exists, and it may be stable or unstable. If it is stable, there may be either no other equilibria or a non-zero stable equilibrium and a non-zero unstable equilibrium. If it is unstable, there exists only a non-zero stable equilibrium. We define the *regional carrying capacity* as the equilibrium average local (regional) abundance, which is the largest among the averages of all stable equilibria, denoted by K_R. If there is an unstable equilibrium present in the metapopulation dynamics, we call it the *regional quasi-Allee threshold*, denoted by A_R. We will describe the details of these emergent parameters in Chapter 3.

It is worth noting that the results in the two limits of the dispersal rate mentioned in the stochastic open system model (Subsection 2.2.2) continue to be valid even for the metapopulation model. As we can remove one patch from the infinitely many patches without changing anything, the metapopulation model is equivalent to the stochastic open system model, except for the regional abundance being a function of the probability distribution. As the regional abundance is constant at equilibrium, the results from the stochastic open system apply to the equilibrium metapopulation. Thus, in the absence of dispersal, the metapopulation goes extinct, implying that zero is an equilibrium point of the system. Extinction occurs as each of the disconnected populations eventually collapses. The zero equilibrium is not specific to the limiting case of no dispersal, as it exists for all dispersal rates. For high dispersal, the metapopulation equilibrium distribution P_{eq} approaches a Poisson distribution with the average local abundance $\overline{N}_{\text{eq}}$ as the mean.

$$\lim_{m\to\infty} P_{\text{eq}}(N) = \text{Pois}(N; \overline{N}_{\text{eq}}) \tag{2.12}$$

Moreover, it is possible to write an equation for the average local abundance $\overline{N}$ itself, in terms of the birth-death function $f(N)$ (2.1).

$$\frac{d\overline{N}}{dt} = \sum_N f(N)P(N,t) - [X + m(1-\delta)]\overline{N} \tag{2.13}$$

We derive this equation in Appendix A, Section A.3. While (2.13) is not a closed-form equation but depends on the probability distribution $P(N,t)$, it is advantageous to explore the model equilibria in the high-dispersal limit. Since we know that the equilibria in the high-dispersal limit are Poisson distributions, their average local abundances are obtained by solving

$$\sum_N f(N)\text{Pois}(N;\overline{N}_{\text{eq}}) - [X + m(1-\delta)]\overline{N} = 0 \tag{2.14}$$

For example, consider a birth-death function given by the logistic equation (i.e., $f(N) = rN(1-N/K)$) in the absence of any catastrophes or dispersal mortality. In the high dispersal limit, the equilibrium average local abundance is given by $\overline{N}_{\text{eq}} = K - 1$ (Appendix A, Section A.4).

If our birth-death function of interest $f(N)$ is more complicated than the logistic model, an analytical solution for $\overline{N}_{\text{eq}}$ like the one shown above may not be possible. In such a case, one can compute $\overline{N}_{\text{eq}}$ by applying a numerical root-finding equilibrium to (2.14).

As the dispersal rate increases, one might intuitively expect the metapopulation model to homogenise, behave like a single well-mixed patch and approach the deterministic nonspatial model given by $f(N)$. However, as shown above, that is not the case, and the equilibria in the deterministic nonspatial model and the stochastic metapopulation model may be unequal.

Notably, in the high dispersal limit, the regional carrying capacity is always smaller than the local carrying capacity,

$$\lim_{m\to\infty} K_R < K \tag{2.15}$$

as in the above example where $\lim_{m\to\infty} K_R = K - 1$. In loose words, the whole is smaller than the part. The regional quasi-Allee threshold in the high dispersal limit may be smaller or larger than its local counterpart, depending upon the latter's magnitude. This difference between the deterministic and the average stochastic equilibria is well-known to occur in both spatial (Chesson, 1981; Klok and De Roos, 1998; Nachman, 2000) and nonspatial (Chesson, 1991) stochastic models. Mathematically, it can be interpreted as a consequence of nonlinearities in $f(N)$ that alter the behaviour of the averaged function. Biologically, it may be understood as a result of stochastic fluctuations in demography that maintain some heterogeneity despite the patches almost fusing with high migration. We provide analytical justifications based on Jensen's inequality for this local-to-regional difference in Appendix A, Section A.4, Subsection A.4.1.

Thus, we conclude the description of the one-species framework. This model provides insights into the interactions between local and regional processes and the role played by stochasticity. In Chapter 3, we use this model to study the spatial dynamics of Allee effects. Going step by step from the deterministic nonspatial to the stochastic metapopulation model, we weave a thread through questions related to the establishment and persistence of stochastic, spatially-structured populations experiencing local Allee effects. Employing this model reveals how the metacommunity archetypes of patch dynamics and mass effects explain the dynamics of single species as well. In the following section, we extend the model to two species and elaborate on the methods to study invasion dynamics and the evolutionary fate of populations.

2.3 Invasion dynamics and evolution

Hitherto, we have dealt with a spatial model of a single species. Naturally, one may ask what happens when multiple kinds of species characterised by different demographic parameters are

both present and compete in this spatial landscape of patches. The framework can easily ascend one level of organisation, going from a metapopulation to a metacommunity (Lerch *et al.*, 2023). In a similar vein to the one-species model, we can take steps that start with a deterministic nonspatial model and culminate into a stochastic metacommunity model. Due to its generality, this extension can represent either two different species or two morphs within the same species.

If two species are present in the habitat, they can influence each other's birth and death rates. We assume that one species does not affect the immigration and emigration rates of the other species. The birth and death rates of species 1 and 2 in the deterministic nonspatial model are denoted by $B_1(N_1, N_2), B_2(N_1, N_2), D_1(N_1, N_2), D_2(N_1, N_2)$, respectively. The associated deterministic net growth rates are $f_1(N_1, N_2) = g_1(N_1, N_2)N_1 = B_1(N_1, N_2) - D_1(N_1, N_2)$ and $f_2(N_1, N_2) = g_2(N_1, N_2)N_2 = B_2(N_1, N_2) - D_2(N_1, N_2)$, where g_1, g_2 are the per capita growth rates. We can now connect this local patch to a region of constant abundances $N_{R,1}, N_{R,2}$ of species 1 and 2, respectively. The immigration and emigration rates are given by

$$\begin{aligned} I_1 &= \delta m_1 N_{R,1} \\ I_2 &= \delta m_2 N_{R,2} \\ E_1 &= m N_1 \\ E_2 &= m N_2 \end{aligned} \tag{2.16}$$

where m_1, m_2 are the dispersal rates and δ is the survival probability during dispersal. The deterministic open system model with two species is given by

$$\frac{dN_1}{dt} = B_1(N_1, N_2) - D_1(N_1, N_2) + m(\delta N_{R,1} - N_1) \tag{2.17}$$

$$\frac{dN_2}{dt} = B_2(N_1, N_2) - D_2(N_1, N_2) + m(\delta N_{R,2} - N_2) \tag{2.18}$$

Next, similar to the one-species model, we can convert this model into a stochastic open system model with a linear master equation

$$\frac{dP(N_1, N_2)}{dt} = TP(N_1, N_2) \tag{2.19}$$

and obtain a two-dimensional stationary distribution $P_{\text{eq}}(N_1, N_2)$ that describes the long-term local population dynamics. In the stochastic open system model, the regional abundances are fixed values $N_{R,1}$ and $N_{R,2}$.

Finally, to obtain the stochastic closed system model, we redefine the regional abundance of species i as the average over the probability distribution, i.e.,

$$N_{R,i} = \overline{N}_i \tag{2.20}$$

where

$$\overline{N}_i = \sum_{(N_1,N_2)} N_i P(N_1, N_2) \tag{2.21}$$

to obtain the metacommunity model.

2.3.1 Adaptive dynamics in the nonspatial case

We use adaptive dynamics (Dieckmann and Law, 1996; Geritz *et al.*, 1997, 1998; Metz *et al.*, 1992, 1995; see Brännström *et al.*, 2013; Klausmeier *et al.*, 2020 for reviews) to study how evolution proceeds in the deterministic nonspatial model. Then, we develop the tools to do the same for our stochastic metapopulation model, which allows us to compare the results from the two models.

The core idea of adaptive dynamics is to first assume that the resident is at its demographic equilibrium, with no invader present. Then, we assume that an invading species has arrived but has a small population size ε. We calculate the per-capita growth rate of the invader population in the environment created by the resident, also called the invasion fitness (Brännström *et al.*, 2013). Here, the crucial assumption is that since the invader is rare, it does not influence the population dynamics of the resident. If the rare invader has a positive growth rate when the resident is at equilibrium, its abundance increases, due to which we say that the invasion is successful.

Now, suppose that we initially have a single resident (say, species 1) with a trait $\gamma = \gamma_1$. Its equilibrium population size is K_1. Then, due to a mutation, a small population ε_m of mutants (species 2) with trait γ_m arises. The per-capita growth rate of this mutant given by

$$g_2(K_1(\gamma_1), 0)$$

is called the invasion fitness. The derivative of the invasion fitness w.r.t. γ_m evaluated at $\gamma_m = \gamma_1$ is called the selection gradient. The selection gradient describes evolution with small mutations (γ_m close to γ_1). If the selection gradient is positive, γ evolves to higher values, and if it is negative, γ evolves to lower values. We assume that mutations are rare so that if a mutant invades, it reaches its own equilibrium before another mutation takes place. The values of γ for which the selection gradient is zero are called evolutionarily singular strategies.

A singular strategy can be either evolutionarily stable (uninvasible by nearby mutants) or evolutionarily unstable (invasible by nearby mutants). Additionally, the strategy may be convergence stable (evolution leads towards that strategy) or convergence unstable (evolution does not lead towards that strategy). Thus, the singular strategies can be classified into four types:

- *Continuously stable strategy* (CSS; Fig. 2.4 A): Evolutionarily stable and convergence stable. Such a strategy is an evolutionary endpoint.
- *Evolutionary branching point* (Fig. 2.4 B): Evolutionarily unstable but convergence stable. Such a strategy is attained through evolution but is invaded by nearby mutants on either side, leading to a dimorphic population.
- "*Garden of Eden*" (Fig. 2.4 C; Hofbauer and Sigmund, 1990; Nowak, 1990): Evolutionarily stable but convergence unstable. Such a strategy will never be attained, although it would have been an endpoint had it been attained.
- *Evolutionary repeller* (Fig. 2.4 D): Evolutionarily unstable and convergence unstable. It potentially indicates the presence of another CSS.

Note that it is also possible to have an evolutionarily stable and convergence stable strategy on the trait space boundary. While the criterion with nearby mutants defines local evolutionary

stability, a global evolutionarily stable strategy is one that cannot be invaded by any other strategy in the trait space. For the purpose of this thesis, the distinction between local and global stability does not matter.

The methods to classify a singular strategy (that use the second derivatives of invasion fitness) are not particularly relevant to this thesis, so we avoid discussing them here. Instead, we describe how we can visually interpret the convergence and evolutionary stability of a singular strategy using pairwise invasibility plots (PIPs) (Brännström *et al.*, 2013; Geritz *et al.*, 1998; Kisdi and Meszena, 1995).

PIPs are a tool to visualise the invasion dynamics. For each value of the resident trait γ_{res}, a PIP shows whether an invader with a trait γ_{inv} can invade (coloured region marked with $+$) or not (white region marked with -). In a PIP, a singular strategy (γ^*) is the point where the boundary of the coloured and the white region intersects the diagonal. If the region directly above and below a singular strategy point is white (marked with $-$), it is evolutionarily stable, i.e., nearby mutants cannot invade it. If the region above and below is coloured (marked with $+$), the strategy is evolutionarily unstable. If the region above the diagonal for γ slightly smaller than γ^* and the region below the diagonal for γ slightly larger than γ^* are both coloured (marked with $+$), the strategy is convergent stable, i.e., the population evolves towards that strategy value. If these regions are white (marked with $-$), it is convergence unstable. With these criteria, one can classify a singular strategy into the four types mentioned above. For a finer classification of the singular strategies, see Geritz *et al.* (1998). Note that it is possible for γ to evolve to ever lower (Fig. 2.5 A) or ever higher (Fig. 2.5 B) values, or evolve to the trait space boundary if the trait values are bounded within a range.

Fortunately (because it makes the analysis and interpretation easier) or unfortunately (because we don't observe richer dynamics), in this thesis, we come across only three possibilities for the evolution of a trait: a continuously stable strategy (Fig. 2.4 A) and evolution to lower (Fig. 2.5 A) or higher (Fig. 2.5 B) values of the strategy. The PIPs we use to portray our results contain a couple of more details than the PIPs shown in this chapter. However, we shall explain them further only in Chapter 4.

2.3.2 Adaptive dynamics in the metapopulation model

Since stochastic metapopulation models can be challenging to study analytically, one may be unable to directly use the concepts of invasion fitness and selection gradient explained above. One option to study invasion dynamics is to calculate the Jacobian of the two-species master equation at the resident equilibrium and use its eigenvalues to infer the stability of the resident equilibrium, which determines whether an invader can invade or not. Another way to perform adaptive dynamics in metapopulations is to use the invasion criterion R_m developed by Metz and Gyllenberg (2001) (see also Casagrandi and Gatto, 2002) and proven by Massol *et al.* (2009). This criterion calculates the average number of dispersers produced by a colony founded by a newborn disperser.

However, as the calculations of R_m or the Jacobian matrix can involve tedious computations, we use the methodologically simpler numerical invasion criteria defined by Lerch *et al.* (2023) based on the LMAO function. Coupled with concepts from adaptive dynamics, the LMAO approach allows us to study evolution in the metapopulation. The two-species LMAO function is defined as

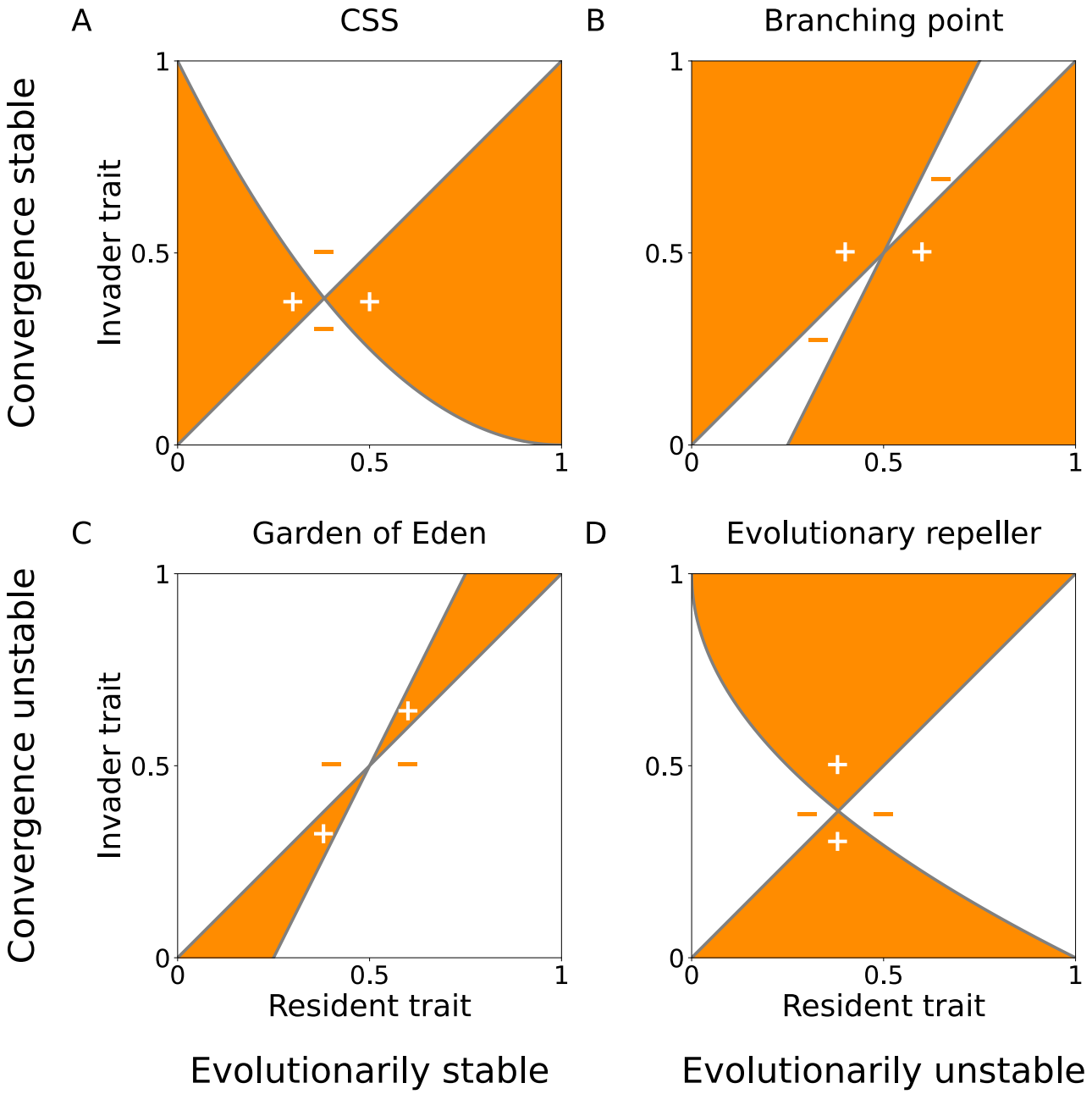

Fig. 2.4. Pairwise invasibility plots (PIPs) showing different possibilities for singular strategies: **A** Continuously stable strategy, **B** Branching point, **C** Garden of Eden and **D** Evolutionary repeller. The coloured regions indicate the strategy combinations for which a resident can be invaded by an invader with a given strategy, and the white regions indicate the strategy combinations where the resident cannot be invaded.

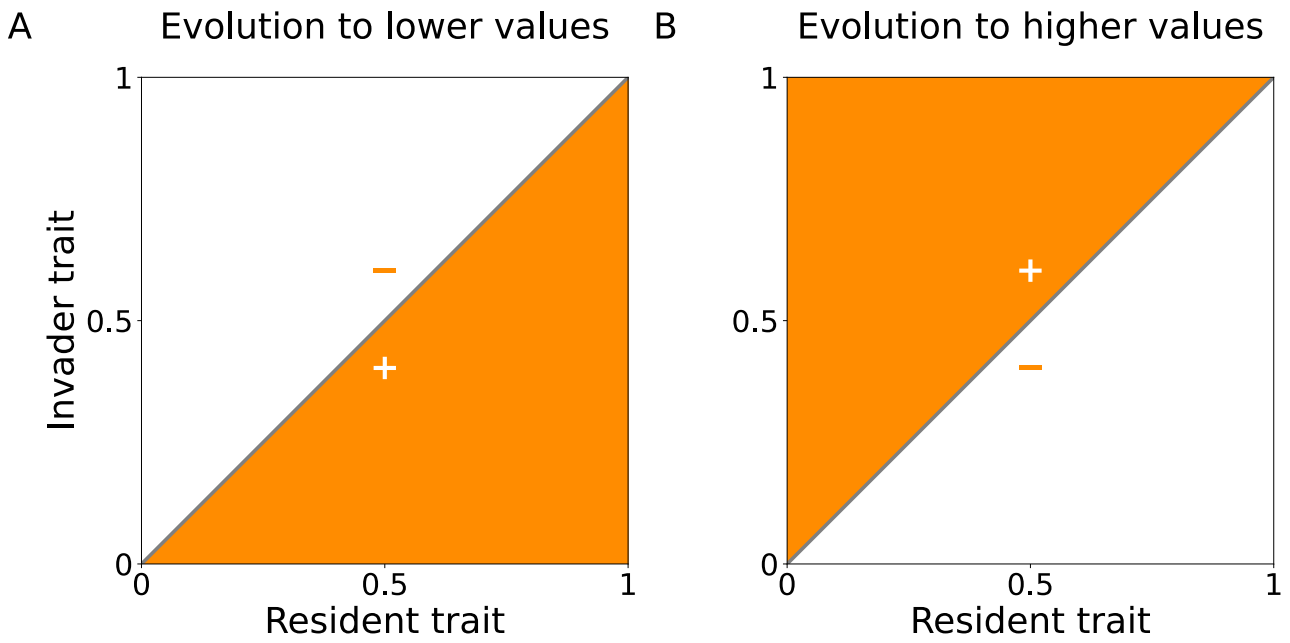

Fig. 2.5. Pairwise invasibility plots (PIPs) showing singular strategies on the trait space boundary. **A** Evolution to lower values. If the trait space is bounded below at 0, the singular strategy is at the trait value of 0. **B** Evolution to higher values of the trait. if the trait space is bounded at 1, the singular strategy is at the trait value of 1. If the trait space is not bounded above, runaway evolution to higher values occurs. The coloured regions indicate the strategy combinations for which a resident can be invaded by an invader with a given strategy, and the white regions indicate the strategy combinations where the resident cannot be invaded.

$$\mathbf{f}_{\mathrm{LMAO}}(N_{R,1}, N_{R,2}) = \left[\sum_{(N_1,N_2)} P_{\mathrm{eq}}(N_1, N_2; N_{R,1}, N_{R,2}) N_1, \sum_{(N_1,N_2)} P_{\mathrm{eq}}(N_1, N_2; N_{R,1}, N_{R,2}) N_2 \right] \tag{2.22}$$

where $P_{\mathrm{eq}}(N_1, N_2; N_{R,1}, N_{R,2})$ is the stationary distribution in the stochastic open system model obtained with $N_{R,1}, N_{R,2}$ as the regional abundances of species 1 and 2.

If $N_{R,\mathrm{eq}}$ is the resident monoculture equilibrium, $(N_{R,\mathrm{eq}}, 0)$ is an equilibrium point of $\mathbf{f}_{\mathrm{LMAO}}$. To identify whether an invader can invade with a small initial abundance, we check whether it grows when its regional abundance is a small positive number ε. If $\mathbf{f}_{\mathrm{LMAO}}(N_{R,\mathrm{eq}}, \varepsilon)[2] > \varepsilon$, we call it a successful invasion, where $\mathbf{f}_{\mathrm{LMAO}}(N_{R,\mathrm{eq}}, \varepsilon)[2]$ is the second component of the vector given by $\mathbf{f}_{\mathrm{LMAO}}(N_{R,\mathrm{eq}}, \varepsilon)$. Otherwise, the invasion fails. In other words, $\ln(\mathbf{f}_{\mathrm{LMAO}}(N_{R,\mathrm{eq}}, \varepsilon)[2]/\varepsilon)$ serves as a stand-in for invasion fitness, whose sign indicates whether invasion is possible or not.

We use this method to construct PIPs by performing pairwise calculations for different resident and invader traits, thus obtaining the singular strategy for a given set of parameters. Then, we can use the visual criteria (or, more rigorously, invasibility calculations for nearby residents and mutants) to determine the evolutionary and convergence stability of the singular strategy. Conceptually, the LMAO invasion criterion is related to R_m (Metz and Gyllenberg, 2001) in the sense that both criteria envision fitness in terms of the output number of individuals produced by a specific input number of individuals in the system.

Does invasion imply replacement?

What happens if two strategies can invade each other? Then, we have coexistence between the two strategies. If neither of the two strategies invades each other, it is said to be a case of founder control, where an initially present strategy prevails.

If we want our PIPs to inform us about the evolutionary trajectory of a population (with small, rare mutations), it is essential that a nearby mutant that can invade also entirely replaces the resident. We need this condition because if the resident and the mutant coexist, the simple tools based on pairwise comparisons are insufficient to determine the fitness of another mutant that would arise in this co-inhabited landscape. While one might be able to extend the model to three species to do so, that would likely make it computationally too heavy and slow. Fortunately, a sign switch at the diagonal is enough to conclude that a protected coexistence between a resident and a similar invading mutant (Poulsen, 1979; Prout, 1968), i.e., a situation where both the resident and the invader are protected from extinction due to mutual invasibility, is not possible. Simply put, if a resident γ_{res} can be invaded by a nearby rare mutant γ_{mut}, but if the vice versa is not true, then there is no possibility of a protected coexistence between γ_{res} and γ_{mut}. However, strictly speaking, the possibility of an unprotected coexistence, where a coexistence equilibrium exists without mutual invasibility (Poulsen, 1979) cannot be ruled out.

Several attempts have been made to characterise the conditions where invasion implies replacement. An example is the Tube theorem that shows that a similar mutant always "inherits the resident attractor" when it replaces it in the absence of a nearby bifurcation point (Geritz *et al.*, 2002; see also Gyllenberg *et al.*, 2002). While conditions that prevent unprotected coexistence have also been characterised (Geritz, 2005), applying them to metapopulations like ours can be difficult. One possible way to confirm the absence of unprotected coexistence between nearby strategies might be to numerically integrate the two-species master equation (2.19) with a non-constant regional abundance, i.e., in conjunction with (2.20). Alternatively, one may consider exploring the high-dimensional phase space or a projected version of it (see Appendix E, Section E.4). If nearby strategies cannot coexist, we can be confident that evolution with small and rare mutations will cause our population to evolve to the singular strategy.

However, if mutations are large, coexistence may indeed be possible. Such cases where different strategies coexist with each other are discussed in Chapter 4.

This marks the end of this methodological chapter. We have explained our modelling framework in detail, along with some interesting results that emerge from it. In a similar metapopulation model, Metz and Gyllenberg (2001) surmised "that it is possible to obtain bistability by incorporating a sufficiently strong Allee-type effect". In the subsequent chapter, we embark precisely in this direction and investigate how local Allee effects scale to the metapopulation level using our single-species model.

Chapter 3

Scaling up Allee effects

> Investigators in the topic [of Allee effects] have an Allee effect of their own, so to speak.
>
> Brian Dennis (2002)

Allee effects arise in a population when mechanisms like resource cooperation, cooperative defence, or mate limitation necessitate cooperative interactions among individuals and influence their survival and reproduction. Due to these intraspecific positive interactions, the per capita growth rate of the population increases with increasing abundance when the abundance is small.

The Allee effect is called *weak* if the per capita growth rate is positive and increasing at small population sizes (Fig. 3.1 A). On the other hand, an Allee effect is said to be *strong* when there is a minimum abundance level, called the Allee threshold (denoted A), below which its per capita growth is negative (Fig. 3.1 B). Therefore, populations with initial abundance smaller than A tend to go extinct, and those with larger abundances tend to establish themselves and reach their carrying capacity (denoted K). Thus, strong Allee effects epitomise bistability: there are two stable equilibria at $N = 0$ and $N = K$, separated by the unstable equilibrium at $N = A$, where N is the population abundance.

The bistability resulting from strong Allee effects (henceforth, Allee effects) amplifies the risk of extinction due to perturbations that may reduce the abundance below the Allee threshold. Additionally, Allee effects impede a population's propensity to invade new habitats and expand its range. These two factors raise the question of how populations experiencing Allee effects persist and how they establish themselves in the first place.

3.1 Allee effects, space and stochasticity

Ecological theory hints at least two factors that can potentially mitigate the fragility of populations engendered by Allee effects: stochasticity and space. First, small populations may be able to invade if stochastic fluctuations occasionally favour them, allowing them to leap over the Allee barrier. Second, migrants from other spatial locations can recolonise extinct habitat patches or rescue dying patches.

For instance, consider Levins's (1969) metapopulation model, which explains the regional

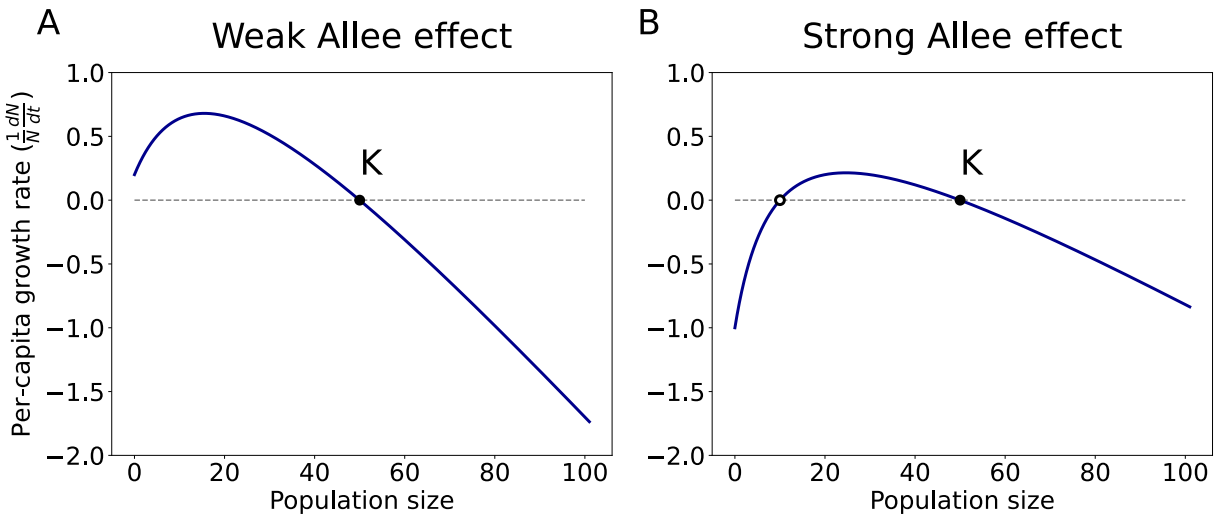

Fig. 3.1. Per-capita growth rates as a function of the population abundance (N) that characterise Allee effects. **A** Weak Allee effect. **B** Strong Allee effect. Strong Allee effects are characterised by an Allee threshold (A), below which the per-capita growth rate is negative. K is the carrying capacity.

dynamics as a consequence of local extinctions and recolonisations. If local Allee effects are present within patches, recolonising extinct patches may require either chance events or mass effects from the region to overcome the threshold. Indeed, spatial models show that Allee effects tend to restrain the ability of populations to invade novel habitats (Kanarek and Webb, 2010; Lewis and Kareiva, 1993; South and Kenward, 2001) and turn dispersal into a double edged-sword that facilitates or hampers population growth, depending on other parameters (South and Kenward, 2001; Kanarek *et al.*, 2013). Restrained by Allee effects, some patches in the spatial habitat may exist as low-abundance sinks maintained by an inflow of immigrants from high-abundance source patches, enhancing spatial heterogeneity (Ackleh *et al.*, 2007; Amarasekare, 1998b; Crespo-Miguel *et al.*, 2022; Ferdy and Molofsky, 2002; Gruntfest *et al.*, 1997; Gyllenberg *et al.*, 1999; Kang and Lanchier, 2011; Kang and Yakubu, 2011; Vortkamp *et al.*, 2020).

Though stochasticity allows some local populations to jump over the Allee threshold and grow to large abundances, it often intensifies the chance of large populations going extinct, due to which a threshold-like behaviour appears in the probabilistic population dynamics (Allen *et al.*, 2005; Dennis, 1989, 2002; Dennis *et al.*, 2016; Hui and Li, 2004; Liebhold and Bascompte, 2003; Surendran *et al.*, 2020). In this chapter, our goal is to understand how the interplay of stochasticity and spatial structure with local Allee effects materialises at the metapopulation level.

Extending Levins's model, Amarasekare (1998a) considers such a metapopulation-level "Allee-like extinction threshold" formally imposed on the proportion of occupied patches. The metapopulation goes extinct if it initially occupies a smaller fraction of patches. This threshold can prevent a population from establishing itself even in suitable habitats. Here, our aim is to link a higher-scale Allee threshold of this kind to a lower-scale Allee threshold.

Some models suggest that a lower-scale Allee effect may or may not manifest at a higher scale, being negated by aggregation of individuals (Jorge and Martinez-Garcia, 2024), pack formation in social animals (Lerch *et al.*, 2018) or spatial configuration of populations (Sato, 2009). However, characterising how a patch-level Allee effect translates into a metapopulation-

level Allee effect in the presence of stochasticity remains a standing question that warrants further exploration.

In this chapter, we develop a general theory of spatial scaling of Allee effects from the local to the regional level using the modelling framework explained in Chapter 2. First, we describe our baseline deterministic nonspatial model. Then, we use deterministic and stochastic mainland-island models to study the influence of migration and demographic stochasticity on local populations with Allee effects. Next, we analyse the scaling of Allee thresholds from patches to a metapopulation. Lastly, we interpret our results in the light of concepts such as ecological drift and mass effects.

3.2 Modelling Allee effects

We begin with the model of Allee effects given by Jacobs (1984) and further studied by Dennis (1989, 2002). In this model, the per-capita birth rate given by $b(N) = \frac{\rho N}{a+N}$ increases with N and saturates at ρ (Fig. 3.2 A). a is the population size at which the per-capita birth rate reaches half its maximum value. Such an increasing birth rate can arise in a population when individuals cooperate to produce or procure a common good or a public good that can be indifferently utilised by the members of the population (see Appendix C). A part of the per-capita death rate $d(N) = c + \alpha N$ is the constant per-capita death rate c. Additionally, death also occurs due to intraspecific competition captured by the competition coefficient α (Fig. 3.2 B). Thus, the overall birth and death rates in this model are given by

$$B(N) = \frac{\rho N^2}{a+N} \tag{3.1}$$

$$D(N) = cN + \alpha N^2 \tag{3.2}$$

yielding an overall growth rate $g(N)$ given by

$$\frac{dN}{dt} = \frac{\rho N^2}{a+N} - cN - \alpha N^2 \tag{3.3}$$

For $c > 0, a > 0$, this model shows strong Allee effects (Fig. 3.2 C,D). For $a = 0$, this model is equivalent to the logistic model.

While the birth and death rates in this model make it a natural extension of the logistic model to Allee effects, viewing the equation in terms of its equilibria helps analyse the model and compare local and regional equilibria. Hence, we rewrite (3.3) in terms of a carrying capacity (K) and an Allee threshold (A) (Fig. 3.2 D; see Appendix C), obtaining the growth rate given by

$$\frac{dN}{dt} = \frac{rN}{\frac{N}{a}+1}\left(1 - \frac{N}{K}\right)\left(\frac{N}{A} - 1\right) \tag{3.4}$$

For a fixed A and K in (3.4), taking the limit $a \to \infty$ recovers the usual quadratic per-capita growth function used to model Allee effects. This deterministic model has three equilibria: two stable equilibria at 0 and K and an unstable equilibrium at A. Thus, a population smaller than A goes extinct, and one larger than A establishes itself by reaching the carrying capacity (Fig. 3.2 D).

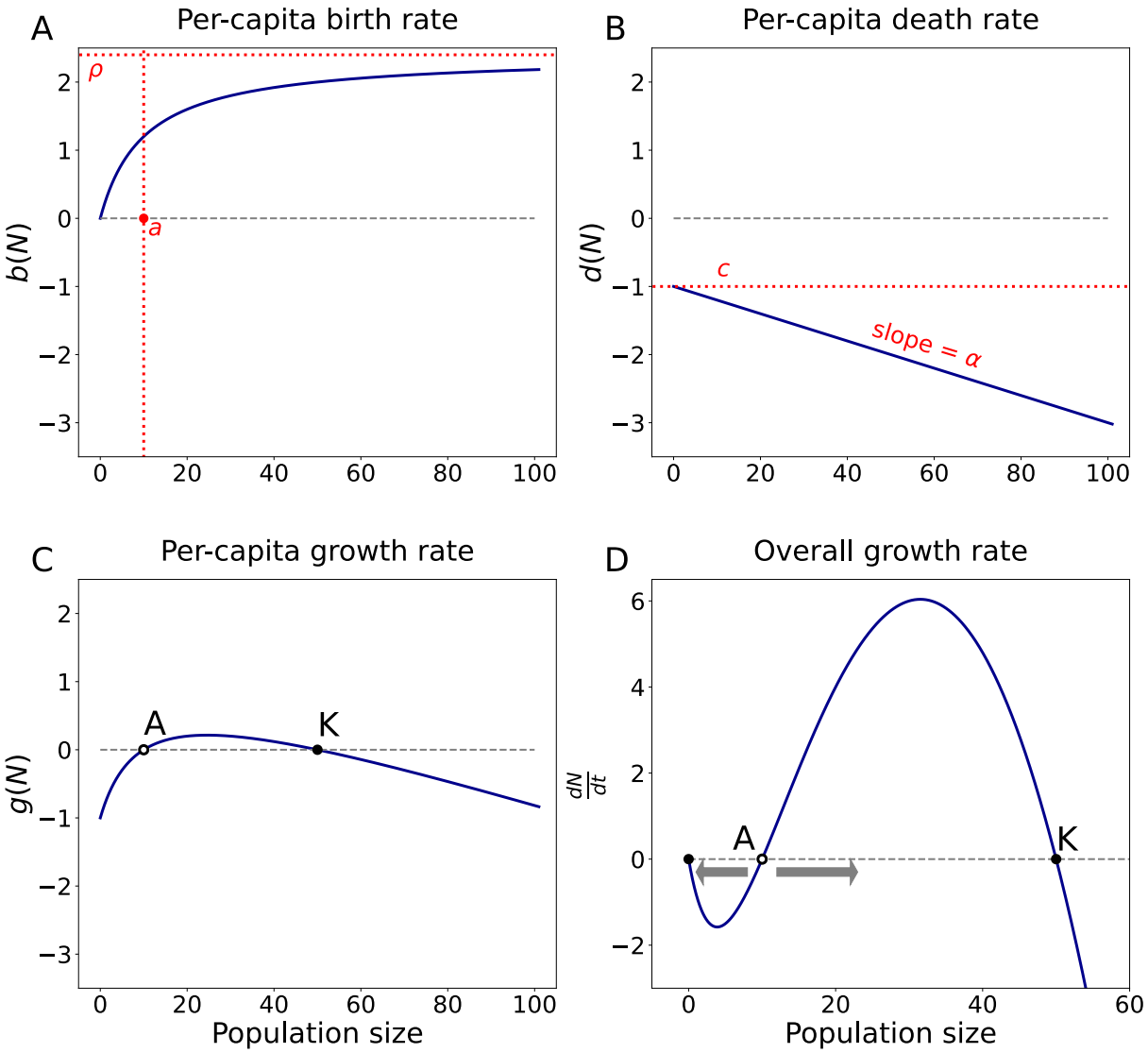

Fig. 3.2. Growth rates as a function of the population abundance (N) in the deterministic model. **A** Per-capita birth rate, **B** Per-capita death rate, **C** Per-capita growth rate and **D** Population growth rate. A is the Allee threshold (open circle) and K is the carrying capacity (closed circle). Other parameters ρ, a, c and α are marked in subfigures **A** and **B**.

3.3 Mass effects and stochastic source-sink dynamics

In spatially extended systems, the flux of individuals can locally reduce the minimum population size required for persistence. To explore this phenomenon, we connect our focal patch to a region with a constant abundance N_R. This converts (3.4) into a deterministic open system model (i.e., a mainland-island model; Chapter 2, Section 2.2, Subsection 2.2.1). Thus, we introduce density-independent immigration and emigration at rates $I = mN_R$ and $E = mN$, respectively, where m is the dispersal rate.

$$\frac{dN}{dt} = \frac{rN}{\frac{N}{a}+1}\left(1-\frac{N}{K}\right)\left(\frac{N}{A}-1\right) + m(N_R - N) \tag{3.5}$$

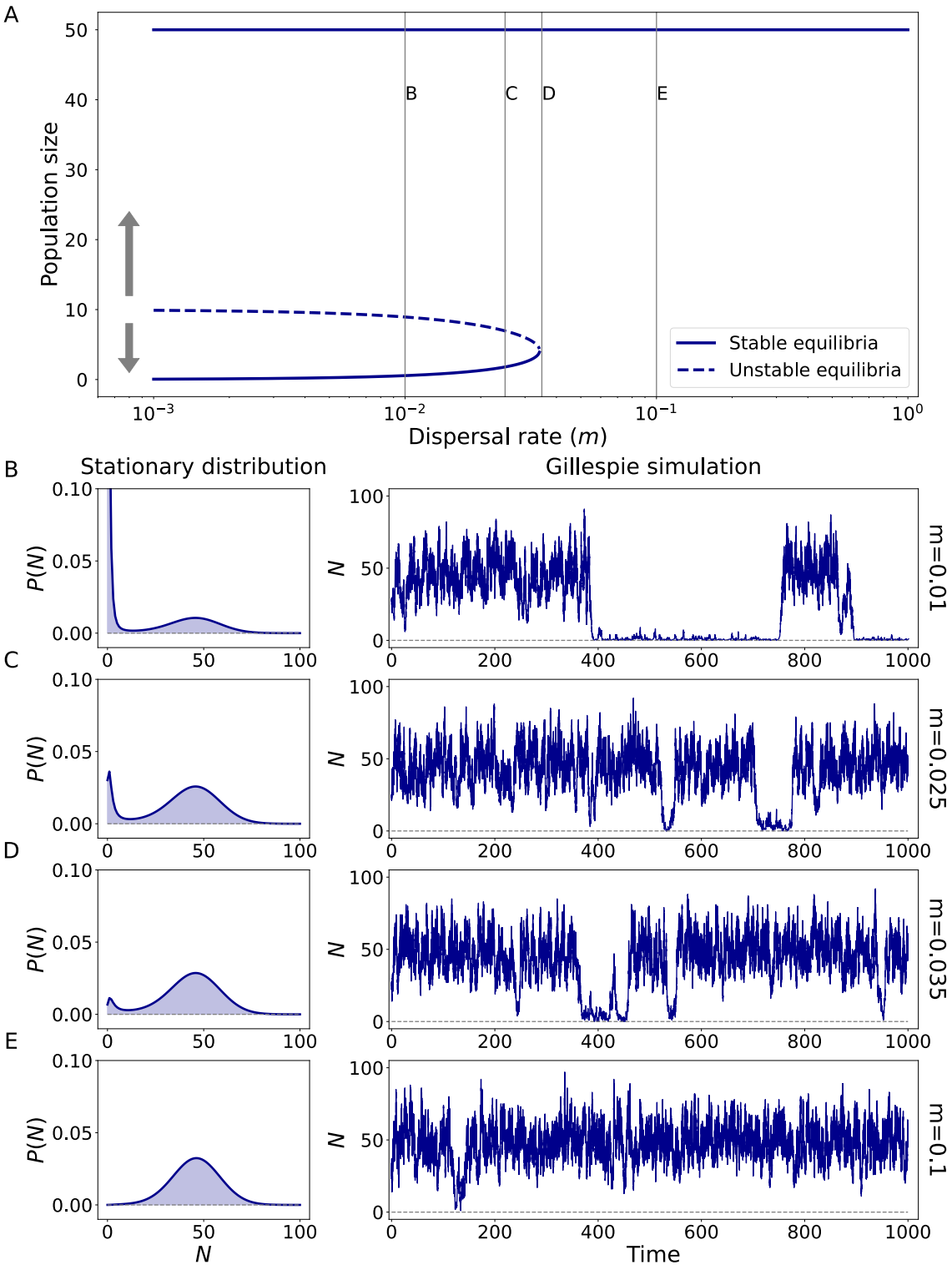

Fig. 3.3. Migration can cause source-sink dynamics and nullify Allee effects. **A** Bifurcation diagram for the deterministic open system model w.r.t. the dispersal rate (m). The vertical lines mark the dispersal rate values in subfigures B—E. **B, C, D, E** Stationary distributions in the stochastic open system model and corresponding representative time series obtained using the Gillespie algorithm for $m = 0.01$, 0.025, 0.035 and 0.1 respectively. Parameters: $A = 10$, $r = 1$, $K = 50$, $a = 10$, $X = 0$, $N_R = 50$.

The bifurcation diagram for this model w.r.t. the dispersal rate m is shown in Fig. 3.3 A. For low dispersal rates, there are two stable equilibria, where the population either persists in a high or a low abundance state. The low abundance state is now non-zero, where the population persists but without any growth. As the dispersal rate increases, the unstable equilibrium decreases, and the lower stable equilibrium increases in magnitude. Thus, for small initial population sizes, the patch stays in a low-abundance *sink* state, with the region acting as a high-abundance *source*. With increasing dispersal rates, the Allee threshold vanishes at a critical point. The source-sink dynamics no longer occur, and the population attains the high stable equilibrium for any initial abundance. This qualitative shift in the dynamics occurs through a saddle-node bifurcation (Strogatz, 2018), where the lower stable equilibrium merges with the unstable equilibrium. The system is not bistable anymore.

Therefore, with excess dispersal rates, mass effects from the region overcome the Allee effect and allow the population to fully establish in the patch where it would otherwise remain at a low or zero abundance. As immigrants pour in from the region, mass effects effectively subdue the Allee threshold. This result implies that for strong enough dispersal, immigration can overcome the Allee threshold, and the patch can be colonised irrespective of its initial abundance. A change in the dispersal rate does not affect the higher stable equilibrium in Fig. 3.3 A, because we choose the regional abundance to be equal to the carrying capacity of the patch ($N_R = K$). Otherwise, the higher stable equilibrium would also approach N_R with very high dispersal rates (Appendix D, Fig. D.1).

The source-sink dynamics become more interesting when stochasticity is introduced, as low-abundance sinks can cross the Allee threshold due to stochastic events, and vice-versa. We convert the mainland-island model into a stochastic model and obtain a stationary probability distribution that describes the long-term population dynamics in the patch (Chapter 2, Section 2.2, Subsection 2.2.2). Alongside this distribution, we simulate the time series of the patch population using the Gillespie algorithm (Gillespie, 1977).

Fig. 3.3 B—E shows the stationary distributions and single representative stochastic time series obtained using the Gillespie algorithm. For low dispersal rates, the probability distribution is bimodal with a high peak at $N = 0$ and a short peak near $N = K$ (Fig. 3.3 B). Thus, the population predominantly remains in the extinct state with intermittent leaps to high population sizes. As the dispersal rate increases, the low-abundance peak becomes shorter and shifts to a small non-zero value. Thus, there is now a sink state where the population is small but non-zero. In contrast, the high-abundance peak becomes larger in height (Fig. 3.3 C,D). The patch alternates between high- and low-abundance states in this bimodal regime. Beyond a critical dispersal rate, the distribution becomes unimodal with a single peak close to $N = K$ (Fig. 3.3 E). Thus, for high dispersal rates, the population stops alternating between two different states as mass effects take over the dynamics of the patch. Notably, the value of the dispersal rate for which alternative stable states disappear in the deterministic open system does not correspond to that for which bimodality disappears in the stochastic open system. At $m \approx 0.035$, there are no alternative stable states in the deterministic model (Fig. 3.3 A), but the small abundance mode continues to persist in the stochastic model for that (Fig. 3.3 D) and a range of higher values (see also Appendix D, Section D.1). This difference occurs because, unlike the deterministic model, stochasticity can cause populations with high abundances to go extinct and require higher dispersal rates to compensate for these chance extinctions.

The stochastic model shows that chance events can also allow small populations to invade and persist at high or low abundances in a patch. Small populations may get lucky and

cross the Allee threshold and reach high population sizes where a deterministic system would predict them to stay as a sink. The modes in the stochastic model approximately follow the deterministic equilibria, but the fluctuations around them create a possibility of stochastic switching from one mode to another.

3.4 Metapopulation-level Allee thresholds

We have seen that migration and stochastic drift can alleviate Allee effects in local patches, enabling populations to invade and persist despite the Allee threshold. The key ingredient in both the above models was migration from the region, which we assumed to have a constant abundance. But what about the Allee effects faced by the region itself? Knowing that the region itself consists of different patches, each with its own Allee effect, we return to the question we asked at the beginning of this chapter: How do local Allee effects scale up to the level of the region?

Following the Lerch *et al.* (2023) methodology, we construct our metapopulation model with infinitely many patches, all equally coupled to each other (Chapter 2, Section 2.2, Subsection 2.2.3). The metapopulation model describes the region in terms of a probability distribution over the population abundance N, which may be considered to be the distribution of individuals over all patches at a given instant of time, or the distribution within a given patch over time. The regional abundance is defined as the average patch abundance ($\overline{N}$), i.e., the average over the probability distribution (2.20, 2.21). We compute the equilibrium distributions and the corresponding regional abundances.

As it turns out, the metapopulation model always has a zero equilibrium point corresponding to population extinction. What about the other equilibria? Does the metapopulation mimic the local dynamics, producing an unstable Allee threshold and a stable carrying capacity? In some cases, the answer is yes.

Fig. 3.4 shows the simplest possible scenario in the metapopulation model. The extinction equilibrium is always stable. Interestingly, there is a minimum dispersal rate required for persistence ($m_{\min}$), below which the population always goes extinct. This is similar to the minimum colonisation rate required in Levins's (1969) model. When $m > m_{\min}$, the nature of the equilibria resembles the local dynamics: besides the stable zero equilibrium, there is a stable equilibrium at a higher value. The average abundance at this higher stable equilibrium is called the *regional carrying capacity* (K_R), as defined in Chapter 2. These two stable equilibria are

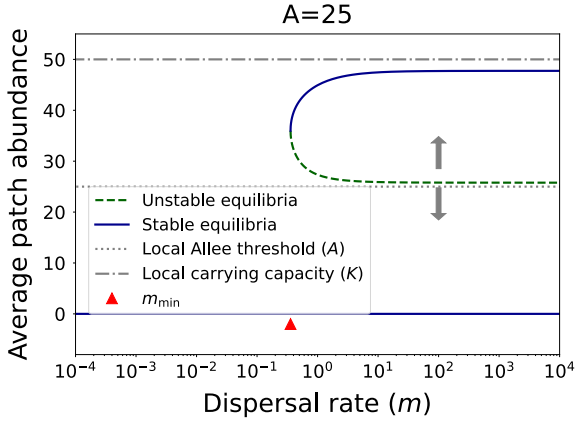

Fig. 3.4. Bifurcation diagram in the metapopulation model as a function of the dispersal rate (m) for a particular value of the local Allee threshold. The solid lines indicate the stable equilibria and the dashed lines indicate the unstable equilibria. The arrows highlight that the equilibria shown by the dashed line are unstable. Parameters: $A = 25$, $r = 1$, $K = 50$, $a = 10$, $X = 0$.

separated by an unstable equilibrium, whose average abundance is called the *regional quasi-Allee threshold* (A_R). At $m = m_{\min}$, a sharp transition occurs through a saddle-node bifurcation, where the equilibria K_R and A_R emerge. With increasing dispersal rate, K_R increases and A_R decreases.

Recall that we began with the question of how a local Allee threshold scales up to the metapopulation level. Fig. 3.4 shows that for a sufficient dispersal rate, the metapopulation dynamics are qualitatively identical to the local dynamics. But is this always the case? Meticulous readers would have noticed the choice of the local Allee threshold in Fig. 3.4 may be considered relatively high ($A = 25$) when one looks at the local carrying capacity chosen ($K = 50$). What happens if the local Allee threshold is lower? Indeed, the situation becomes more complicated.

Fig. 3.5 shows how the equilibria and their stability change with the dispersal rate for smaller Allee thresholds. As with the previous case, a minimum dispersal rate ($m_{\min}$) is always necessary for persistence. However, for $A = 5$ (Fig. 3.5 A), the zero equilibrium becomes unstable ($A_R = 0$) at $m = m_{\min}$. For a range of dispersal rates, it remains unstable. This implies that there is a range of dispersal rates where there is no regional Allee effect! A population can invade the region irrespective of its initial abundance. However, as the dispersal rate increases further, a regional Allee threshold reappears, and the extinction equilibrium becomes stable. The qualitative transitions, in this case, take place through transcritical bifurcations.

For intermediate Allee thresholds (Fig. 3.5 B,C), the transition at $m = m_{\min}$ is sharp, but

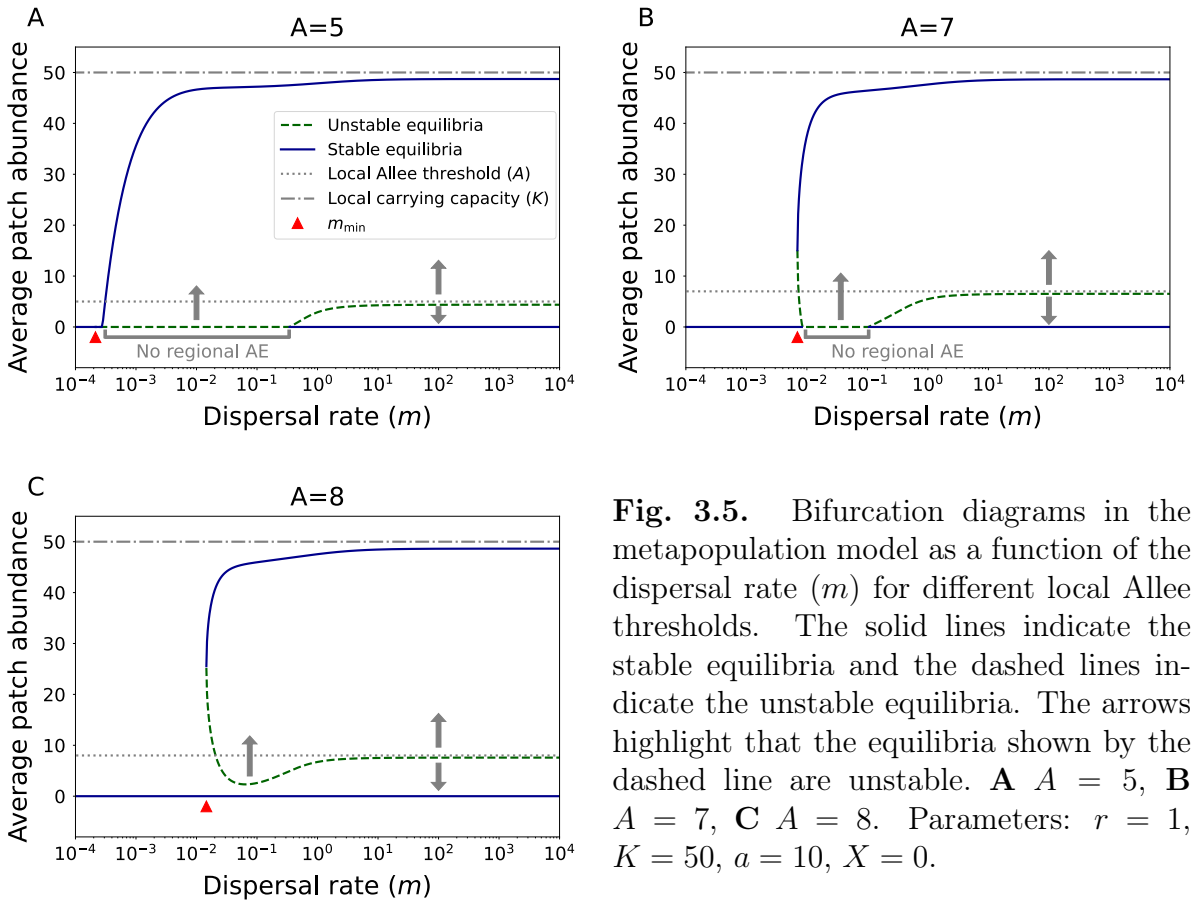

Fig. 3.5. Bifurcation diagrams in the metapopulation model as a function of the dispersal rate (m) for different local Allee thresholds. The solid lines indicate the stable equilibria and the dashed lines indicate the unstable equilibria. The arrows highlight that the equilibria shown by the dashed line are unstable. **A** $A = 5$, **B** $A = 7$, **C** $A = 8$. Parameters: $r = 1$, $K = 50$, $a = 10$, $X = 0$.

with increasing dispersal rate, A_R decreases, reaches a minimum, and then increases again. The minimum value may fall to zero (Fig. 3.5 B), producing an intermediate range of dispersal rates where invasion from small abundances is possible.

Further, the pattern in the limit of high-dispersal rates ($m \to \infty$) deserves a mention. The regional carrying capacity (K_R) always saturates at a value smaller than the local carrying capacity (K). On the other hand, the regional quasi-Allee threshold (A_R) saturates at a value smaller or larger than its local counterpart (A). This pattern can be analytically explained, and we can recover the deterministic nonspatial model with increasing carrying capacity (see Appendix A, Section A.4).

Thus, the primary result of our model is that local Allee effects can disappear when one zooms out from the level of a single patch to that of the metapopulation. Essentially, the presence of local Allee effects does not imply that the metapopulation also faces strong Allee effects. For certain parameters, $A_R = 0$, signifying that the zero equilibrium is unstable and a population can invade irrespective of its initial regional abundance. In other cases, we also see a positive A_R, implying that the population requires a positive, non-infinitesimal regional abundance to invade.

To highlight the combined effect of the two main parameters in our metapopulation model—local Alle threshold (A) and dispersal rate (m)— we depict two-dimensional bifurcation diagrams that exhibit the averages of metapopulation equilibria as a function of both A and m (Fig. 3.6). We can discern three different regimes in the parameter space of m and A: the extinction regime, the invasion regime, and the bistability regime. In the extinction regime,

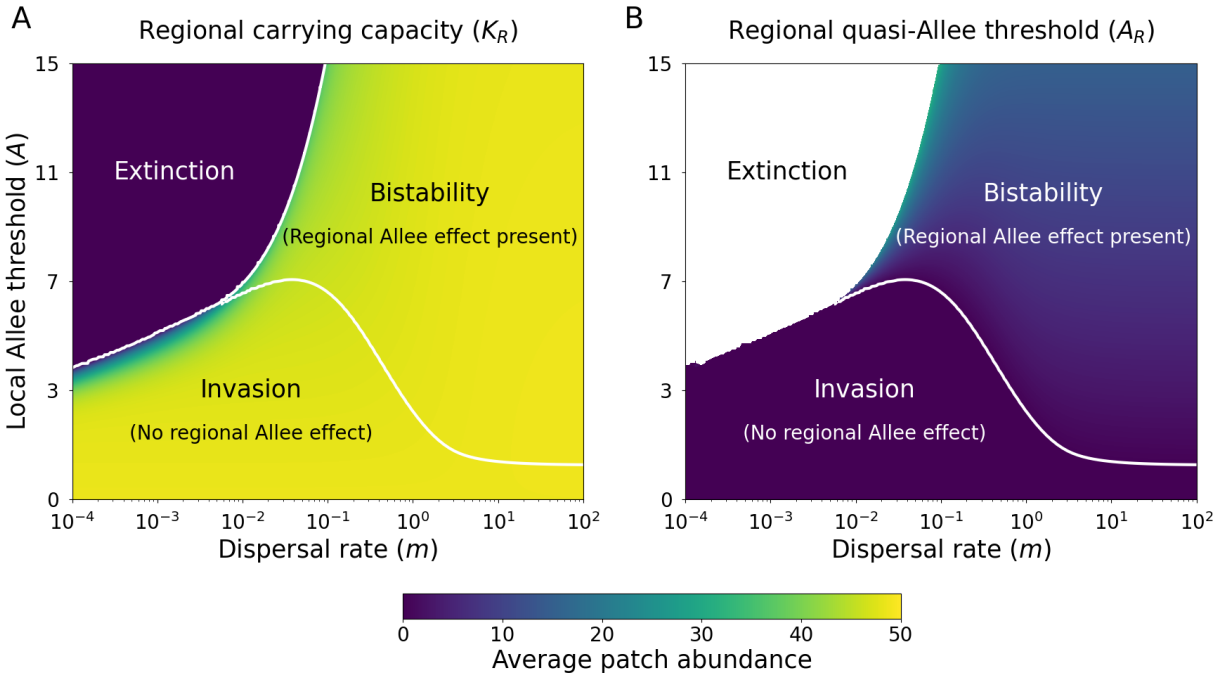

Fig. 3.6. Three different outcomes in the metapopulation model. **A** The regional carrying capacity (K_R) as a function of the dispersal rate (m) and the local Allee threshold (A). **B** The regional quasi-Allee threshold (A_R) as a function of m and A. Three distinct regimes corresponding to a guaranteed extinction, invasion from small abundances and bistability are observed. Parameters: $r = 1$, $K = 50$, $a = 10$, $X = 0$.

the population can never persist, no matter how large its initial abundance is. In the invasion regime, the population can always invade, no matter how small its initial abundance is (as long as it is positive): there is no regional strong Allee effect. In the bistability regime, the population can invade if it has a certain threshold abundance: a regional Allee effect does emerge from local Allee effects.

The extinction regime boundary in Fig. 3.6 shows that higher local Allee thresholds require higher minimum dispersal rates (m_{min}) for persistence. For small A, K_R gradually rises from zero (transcritical bifurcation) at $m = m_{\text{min}}$, whereas its transitions discontinuously (saddle-node bifurcation) for a larger A (Fig. 3.6 A). In Fig. 3.6 B, the invasion regime corresponds to $A_R = 0$. For small A, A_R increases continuously from 0 with increasing m, leading to the bistability regime. For intermediate A, there is no invasion regime separating extinction and bistability, but A_R is the minimum for an intermediate value of m. For high A, A_R decreases with increasing m. We discuss potential causes for this pattern in Section 3.5.

In the invasion regime, it is possible to estimate the rate at which a small population invades the habitat, using the Jacobian matrix (see Appendix B) of the metapopulation master equation (2.6, 2.9). This rate is maximum for an intermediate value of m and decreases with increasing A (Appendix B, Fig. B.1).

Further, we point out that even when the metapopulation is at its carrying capacity, some patches may persist at sub-Allee threshold levels, i.e., as sinks, while other patches with higher abundances act as sources. This source-sink dynamics occurs where m is close to m_{min} (see Appendix D, Fig. D.2). To emphasise this aspect of our results, we further characterise the regional carrying capacity (K_R) using square-pie charts (Lerch *et al.*, 2023).

Fig. 3.7 shows square-pie charts concentrating on the part of parameters space where the dispersal rate is close to m_{min}. Each square in the grid represents a combination of m and A. A square is divided into two parts, whose area depicts the probability mass below and above the local Allee threshold (A) in the stable equilibrium distribution (corresponding to K_R). The colour of the parts stands for the average abundance below and above A, respectively. The average local abundance is calculated on the condition that the patch is a source (average greater than A) or a sink (average smaller than A). For m below m_{min}, the population is always zero. For the values of m close to m_{min}, source-sink dynamics are observed within the patches. The probability mass below A decreases, and that above A increases with increasing m. The population in the high-abundance sources is higher for higher m and lower A. For high dispersal rates, the distribution is unimodal with no sinks and a negligibly small probability mass below the local Allee threshold. This transition takes place at higher dispersal rates for higher Allee thresholds.

Until now, we have mostly overlooked a particular detail in the metapopulation model. Since our framework is stochastic, the metapopulation equilibria are probability distributions. The "equilibria" shown in Figs. 3.4, 3.5 are the averages of these probability distributions. We elaborate on this attribute of our model in Appendix D, Section D.2 and discuss why it has little consequences for our main conclusions.

Metapopulations can be affected by local catastrophes that occur stochastically, wiping off an entire patch. Such a patch requires immigration in order to be recolonised, emboldening the patch dynamics where the equilibrium is maintained as a result of local extinctions and recolonisations. The effect of catastrophes on metapopulation dynamics is similar to increasing the local Allee threshold (see Appendix D, Section D.3).

Along with the sporadic catastrophes, a species can also fail to take over potentially colonis-

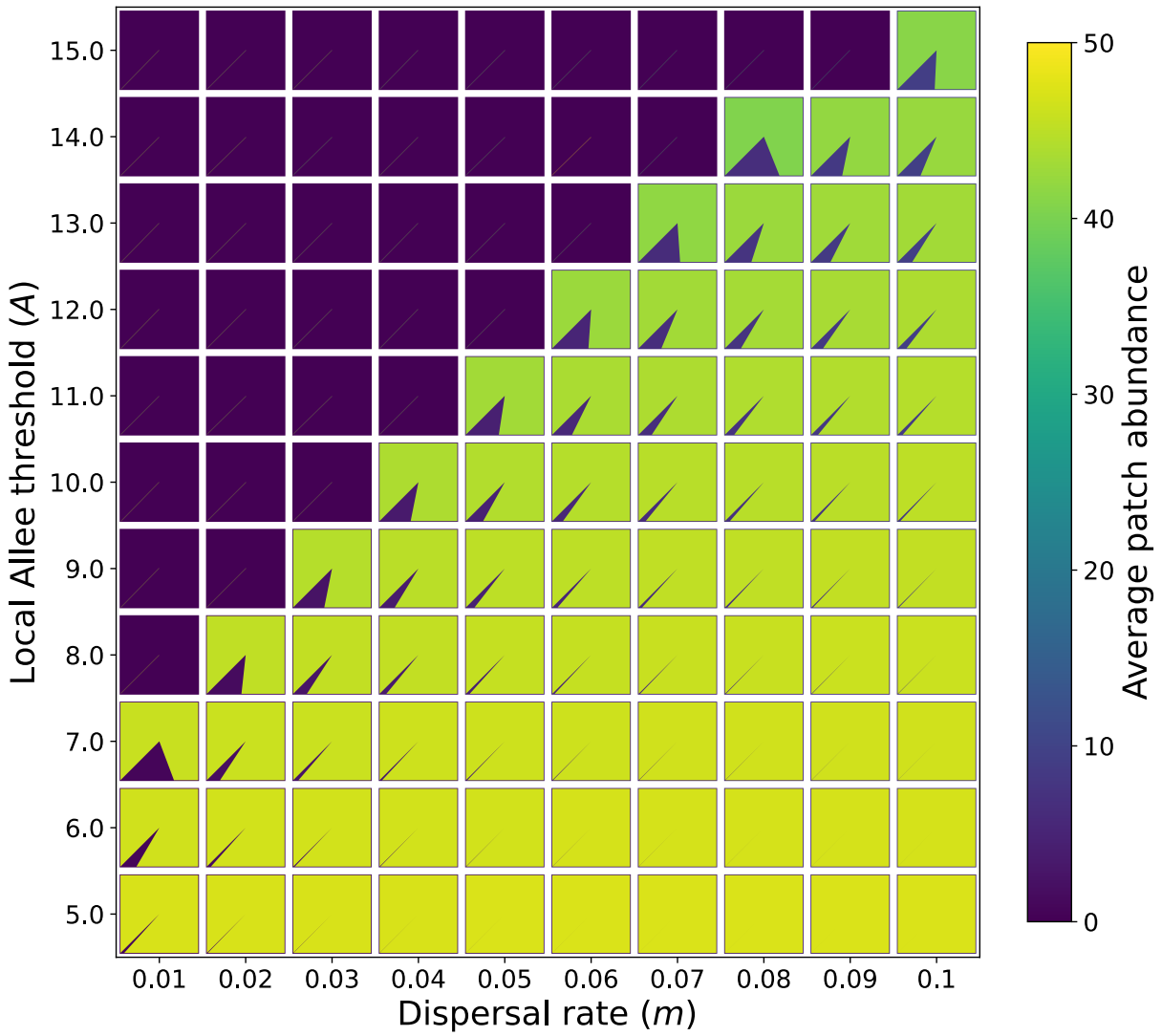

Fig. 3.7. Source-sink dynamics in the metapopulation model. The square pie-charts show probability mass (area within the square) and the average abundance (as the colour) on patches given that their abundance is above A (sources) and given that it is below A (sinks). Parameters: $r = 1$, $K = 50$, $a = 10$, $X = 0$.

able patches due to mortality during the dispersal process. Here, dispersal mortality only makes high dispersal detrimental (see Appendix D, Section D.3), but later (in Chapter 4 and 5) we will find that it has important consequences on evolutionary dynamics.

3.5 Ecological drift-driven establishment of populations

We have seen that demographic stochasticity and spatial structure are potential answers to the question of how populations with Allee effects establish and persist in nature. Here, we present a plausible explanation for the phenomena exhibited by our model. It is possible to break down our model into three salient factors: birth-death processes, migration and stochastic ecological drift. The interactions between these three forces produce the rich dynamics observed in our

results. The effect of birth-death processes depends on the local population abundance. If it is smaller than the local Allee threshold (A) or larger than the local carrying capacity (K), they reduce the abundance. If it is between A and K, the birth-death processes increase it. On the other hand, the net effect of migration depends on the difference between the local and the regional abundances. If the local population is smaller than the regional average, immigration exceeds emigration, and the overall effect is an increase in the local abundance. Ecological drift can push the abundance in either direction, as it acts neutrally. However, the effects of drift are more relevant for small rather than large populations as deterministic processes are more dominant in the latter case (Leibold and Chase, 2017).

Consider our deterministic nonspatial model of Allee effects (3.4). The only processes involved here are birth and death. Hence, whether a population establishes or goes extinct is solely determined by whether its initial abundance is above or below A (Fig. 3.2 D). However, when we add dispersal from a region with a larger abundance, the net effect of migration enables the population to persist in a sink state (Fig. 3.3 A) with a small but non-zero abundance. With increasing dispersal rate, the mass effects dominate, and the population no longer faces an Allee effect. Thus, high dispersal can rescue populations with Allee effects and allow them to persist.

Including demographic stochasticity adds a third force, due to which a small population can cross the Allee threshold and reach high local abundances (Fig. 3.3 B—E). However, drift can also push a large population to a smaller value, because of which eliminating alternative modes takes a higher dispersal rate in the stochastic model than eliminating alternative stable states in the deterministic model (Fig. 3.3 A,D; Appendix D, Section D.1).

In the metapopulation model, all these factors converge to create the three different regimes of extinction, invasion and bistability (Fig. 3.6). Ecological drift and mass effects can explain the observed pattern. For a given A, a minimum dispersal rate ($m_{\min}$, Figs. 3.4, 3.5) is required for persistence because if immigrants are too rare, every population eventually goes extinct due to ecological drift. This threshold dispersal rate gives rise to the extinction regime.

With a sufficient dispersal rate, stochasticity acts as a mechanism for establishing small populations. First, let us explain the case of small local Allee thresholds (Fig. 3.5 A). Consider an invading population with a small regional abundance. If A is small, the effect of birth-death processes on reducing the population of sub-Allee threshold patches is compensated by drift, causing some of them to grow above A and establish locally. Additionally, a population can be regionally small but locally abundant to begin with. Emigrants from the newly created or pre-existing source patches enter the empty patches. Again, drift causes some of these patches to grow, allowing the population to spread in the spatial habitat. Thus, we get the region of invasion where there is no regional Allee threshold. However, if the dispersal rate is too high, individuals in the growing sinks tend to leave it midway, preventing the population from expanding. In such a case, mass effects produced by a non-infinitesimal regional abundance and the high dispersal rate are necessary to compensate for the individuals that leave the growing sinks. Such compensation could occur through migration into sinks that some individuals have abandoned or simply by producing more and more sinks, increasing the likelihood that some of them reach high population sizes. This process generates the bistability region for small A. The minimum regional abundance needed behaves effectively as an Allee threshold on the entire metapopulation, which we term the regional quasi-Allee threshold (A_R). A_R increases with increased dispersal (Fig. 3.5 A) due to a greater loss of individuals from rising sinks.

Now, let us consider the case of intermediate and high Allee thresholds (Figs. 3.4, 3.5 B,C).

For small dispersal rates, drift alone falls short of helping patches grow above the larger local Allee thresholds. The probability of a sink turning into a source is smaller for larger A values, causing small populations to go regionally extinct. But when a sufficient regional abundance is present, mass effects pump enough individuals into patches to allow some of them to overcome the local Allee threshold. This may occur by rescuing dying sinks or creating enough sinks so that some of them are established locally due to drift. Increasing dispersal rate enhances mass effects and sink creation or rescue, decreasing the required threshold regional abundance A_R (Figs. 3.4 B.C, 3.5). This decrease may produce an invasion regime (Fig. 3.5 B) for an intermediate range of dispersal rates. For intermediate A, very high dispersal turns counterproductive for the same reason discussed for low A: the growth of sinks is arrested due to emigration. Hence, A_R reaches a minimum and increases again (Fig. 3.5 B,C). For high dispersal rates, a minimum like this is not observed because the chance of a sink turning into a source is so small that the advantage of creating newer sinks exceeds the disadvantage caused by the loss of individuals from existing sinks (Fig. 3.4).

Summarising, ecological drift and dispersal can unfetter cooperating populations from their strong Allee effects. In a situation where bistability is the only outcome on a smaller spatial scale, a larger spatial scale may show different possibilities of extinction, invasion and bistability. A local Allee effect does not necessarily scale up to produce a regional Allee effect. Thus, we reiterate that to understand ecological phenomena, one must look at the "big picture" and think beyond the local dynamics. These results have intriguing implications for ecological theory and its applications, which we discuss in Chapter 6. They also serve as a fundamental basis for the next chapter.

While stochasticity and dispersal may tender some respite to cooperating populations, they continually face another threat: invasion by cheaters who free-ride on the efforts of cooperators. Cheaters who put little effort into local interactions can arise due to mutations and breach a cooperator fortress, causing the cooperator population to collapse. In the next chapter, we shift our attention to this problem and propose a mechanism rooted in metacommunity theory to explain the persistence of cooperation on an evolutionary timescale.

Chapter 4

Evolutionary ecology of cooperation

> Today, Gause is most closely associated with ecology, but before the Second World War it is clear that ecological competition and natural selection were synonyms.
>
> James Mallet (2012)

Cooperation is observed in nature in a wide range of taxa. Cooperating can involve increasing others' fitness at the cost of one's own. Since it may seem logical that defectors would be able to exploit cooperators and grow at their expense, why cooperation evolves is an important question. Spatial structure can promote the evolution of cooperation by restricting the benefits of cooperation within a group of cooperators (Akçay, 2020). Here, our goal is to understand whether a metapopulation structure can favour the evolution of cooperation and explore possible mechanisms behind it.

To do so, we slightly modify the model dealt with in the previous chapter to view it with a focus on cooperation. We extend it to two strategies and show that cooperation cannot evolve in a well-mixed population in this model. Then, we employ our stochastic metapopulation framework with the same model to observe whether cooperation can evolve. We analyse the role of different factors and explore the possibility of the coexistence of cooperators and defectors. We conclude by proposing a metacommunity theory-based mechanism that can explain the evolution of cooperation.

4.1 Evolutionary suicide in a well-mixed population

We begin by studying how cooperation evolves in a well-mixed system with a deterministic model. This first step sets a baseline to compare with, as we later switch to our stochastic metapopulation framework and observe the differences in the results.

To study the evolution of cooperation, we include a term γ in (3.3), which can be obtained by rescaling the parameter a from the model in the previous chapter (3.3). We refer to γ as a "cooperation", as this trait captures the investment of an individual in a cooperative interaction. Such an investment could take the form of a contribution towards producing or

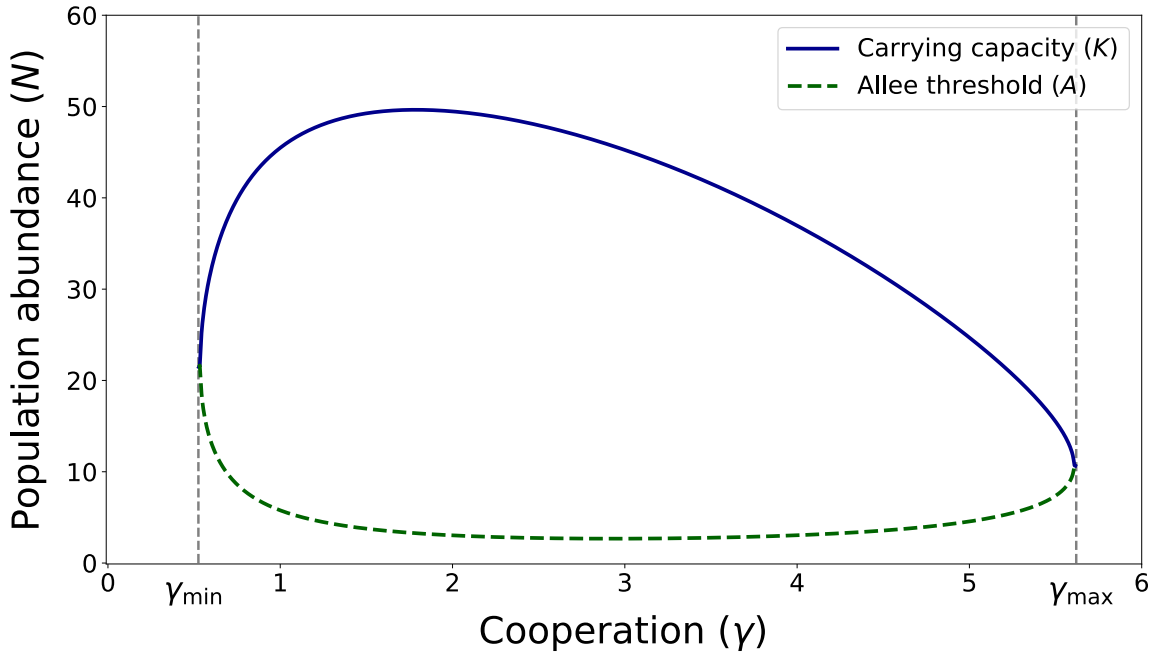

Fig. 4.1. The monomorphic population equilibria equilibria in the deterministic nonspatial model (4.1) as a function of cooperation trait (γ). The population can persist when $\gamma \in (\gamma_{\min}, \gamma_{\max})$. Parameters: $\rho = 3.5$, $a = 10$, $c = 1$, $\alpha = 0.04$, $b = 0.05$, $\theta = 2$.

securing a common good that can be utilised indifferently by all the members present on a patch. This common good is implicit in our model, as we do not include a term that measures its abundance. However, it is possible to arrive at our model starting with a more mechanistic model that involves the common good (see Appendix C).

We assume that the per-capita birth rate increases with increasing cooperation and saturates at ρ so that it takes the form $b(N) = \frac{\rho\gamma N}{a+\gamma N}$. Cooperation also comes at a cost given by $b\gamma^\theta$, which increases the death rate. We mostly assume quadratic costs ($\theta = 2$), which implies that the cost increases faster with increasing cooperation. In Appendix E, Section E.2, we also explore the effect of linearly rising costs. Including these new terms, the growth rate a of population where all individuals have the trait γ is given by

$$\frac{dN}{dt} = \frac{\rho\gamma N^2}{a+\gamma N} - cN - \alpha N^2 - b\gamma^\theta N \tag{4.1}$$

Note that apart from the cost term, this model is the same as Jacobs's model of Allee effects (3.3) that we studied in Chapter 3 (for $\gamma = 1$). Thus, the modified model also contains a local Allee threshold implicit in (4.1). Introducing the explicit cooperation term γ produces upper and lower limits on γ, $\gamma_{\max}$ and $\gamma_{\min}$, below and above which a population fails to persist (Fig. 4.1). Hence, a population with the strategy γ has a non-zero stable equilibrium only if $\gamma \in (\gamma_{\min}, \gamma_{\max})$. This implies that a population goes extinct if it cooperates too much or too little. In the viable range of cooperation, the carrying capacity is the maximum and the Allee threshold is the minimum for an intermediate level of cooperation (Fig. 4.1).

Now, we extend this model to a situation with two morphs, 1 and 2, characterised by the strategies γ_1 and γ_2, with abundances N_1 and N_2, respectively. We call the morph with a larger γ as the cooperator and the morph with a smaller γ as the defector. Note that "cooperator"

and "defector" are relative terms, without an absolute distinction between them. When the population is closed (no migration) and well-mixed, the birth and death rates of the two morphs are given by

$$\begin{aligned} B_1(N_1, N_2) &= \frac{\rho(\gamma_1 N_1 + \gamma_2 N_2) N_1}{a + \gamma_1 N_1 + \gamma_2 N_2} \\ D_1(N_1, N_2) &= cN_1 + \alpha(N_1 + N_2)N_1 + b\gamma_1^\theta N_1 \\ D_2(N_1, N_2) &= cN_2 + \alpha(N_1 + N_2)N_2 + b\gamma_2^\theta N_2 \end{aligned} \tag{4.2}$$

where B_i, D_i are respectively the birth and death rates of the morph i. Thus, the presence of one morph increases the birth rates of another morph. This implies that the implicit common good is beneficial to both the morphs. However, each morph bears the cost of its own cooperation, which increases its death rate. The overall death rate is the sum of a constant death rate cN_i, the death due to competition $\alpha(N_1 + N_2)N_i$ and the death due to cooperative investments $b\gamma^\theta N_i$.

Therefore, in the deterministic model, the growth rates of the two morphs are given by

$$\begin{aligned} \frac{dN_1}{dt} &= \left[\frac{\rho(\gamma_1 N_1 + \gamma_2 N_2)}{a + \gamma_1 N_1 + \gamma_2 N_2} - c - \alpha(N_1 + N_2) - b\gamma_1^\theta\right] N_1 \\ \frac{dN_2}{dt} &= \left[\frac{\rho(\gamma_1 N_1 + \gamma_2 N_2)}{a + \gamma_1 N_1 + \gamma_2 N_2} - c - \alpha(N_1 + N_2) - b\gamma_2^\theta\right] N_2 \end{aligned} \tag{4.3}$$

Now, we analyse this deterministic model using adaptive dynamics (Chapter 2, Section 2.3, Subsection 2.3.1) to study the evolution of the cooperation trait γ. Here, we are focused on the dynamics of two morphs within a single patch. First, we assume that there is only a single morph with trait γ_1 present at its carrying capacity given by $K_1(\gamma_1)$. Now, we consider a new morph with a small abundance, $N_2 = \varepsilon_2$. The per-capita growth rate of this invader (morph 2) in the environment set by the resident (morph 1), denoted g_2, is called the invasion fitness. The invader grows if the invasion fitness is positive, and it goes extinct if the invasion fitness is negative. Here, the invasion fitness is given by (see Appendix E, Section E.1 for a derivation)

$$g_2 = b(\gamma_1^\theta - \gamma_2^\theta) \tag{4.4}$$

which is positive when $\gamma_2 < \gamma_1$ and negative when $\gamma_2 > \gamma_1$. Thus, a more cooperating strategy will always be invaded by a less cooperating mutant. This mutant will eliminate the resident and take over the population. The process continues, decreasing the level of cooperation in the population.

As we have seen, there are upper and lower limits on γ for persistence. If a mutant that invades is not viable on its own ($\gamma_2 < \gamma_{\min}$), the invasion leads to the extinction of both the morphs. This phenomenon, whereby a population evolves to its own extinction, is called evolutionary suicide (Parvinen, 2005) or Darwinian extinction (Webb, 2003).

We draw a pairwise invasibility plot (PIP) that portrays this phenomenon (Fig. 4.2A). In the PIP, the coloured region marked with a "+" represents the resident-invader trait combinations where invasion is possible, and the white region marked with a "−" represents the trait combinations where invasion is not possible. The black region indicates the trait values for which a resident cannot persist (the values outside the range $(\gamma_{\min}, \gamma_{\max})$). The upper boundary $\gamma_{\max}$ is not shown in Fig. 4.2 A because it is too high. Additionally, we include a bar on

the right side that indicates whether an invader with a trait value γ_{inv} can invade the empty habitat (coloured part with "+") or not (white part with "−"). The colour in the bar is black with a "−" if the morph cannot persist. Invasion into an empty habitat is not possible in the local deterministic case due to the strong Allee effect in our model. However, note that a small mutant population need not face an Allee effect when a resident is already present at a high abundance.

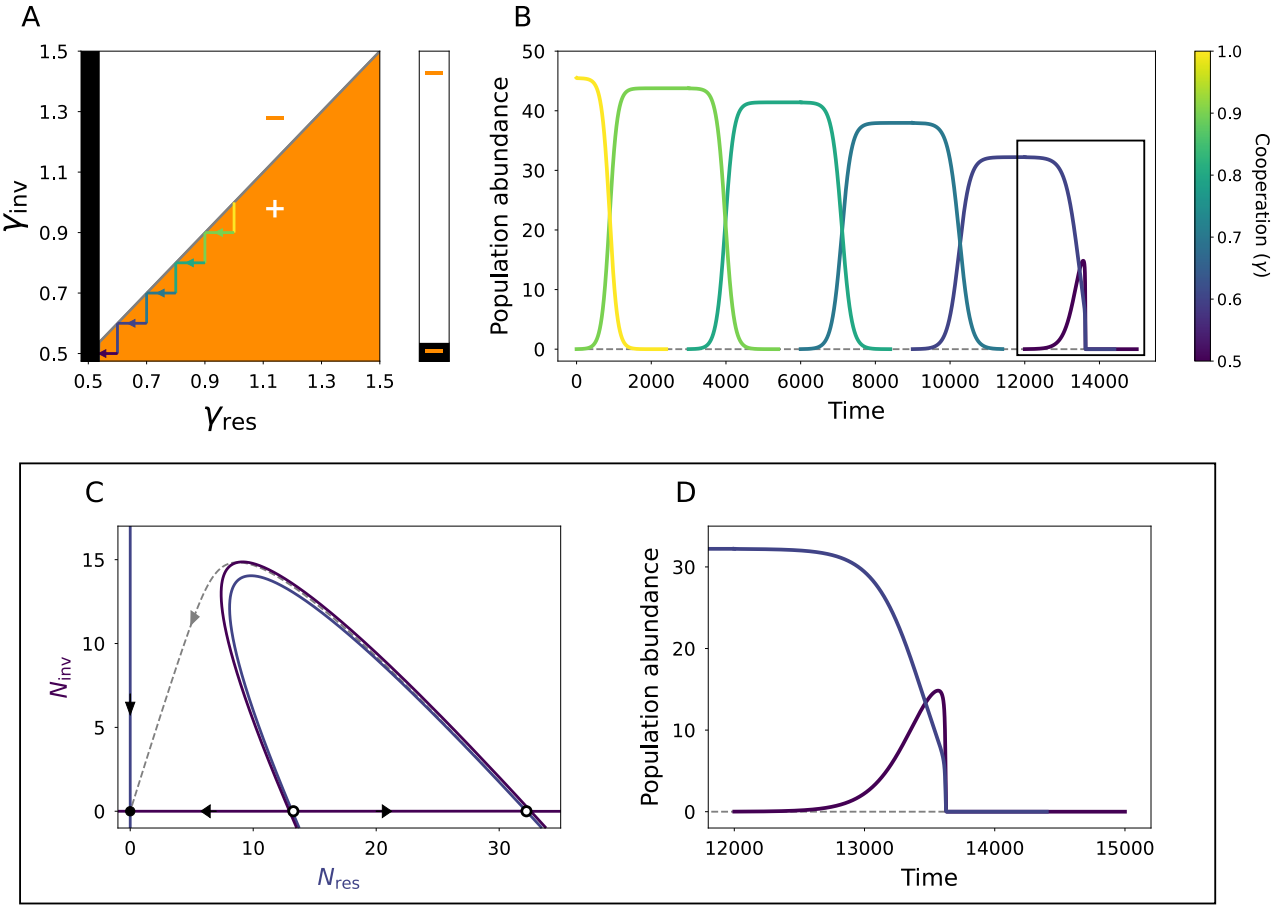

Fig. 4.2. Evolutionary suicide in a single patch (the deterministic nonspatial model, 4.3). **A** Pairwise invasibility plot (PIP). In the square, the coloured (+) and white (−) portions indicate the resident-invader strategy combinations for which invasion occurs. The black portion shows the strategies for which a resident cannot persist. In the sidebar, the coloured (+), white (−) and black (−) parts correspond to the strategy values that can invade an empty system, can persist but cannot invade an empty system and cannot persist, respectively. A sequence of successive invasions and replacements corresponding to panel B is plotted on the PIP. **B** Successive invasions by less cooperating strategies lead to a reduction in population size and, ultimately, evolutionary suicide. The box corresponds to the suicidal trajectory further explained in panels C and D. **C** Nullclines for the last invasion trajectory. The colours correspond to those in panel B. The grey dashed line shows the invasion trajectory through time. Closed circles are stable equilibria and open circles are unstable equilibria. **D** A zoomed-in view of the last invasion trajectory in panel B. Parameters: $\rho = 3.5$, $a = 10$, $c = 1$, $\alpha = 0.04$, $b = 0.05$, $\theta = 2$.

As the PIP reveals, every possible resident trait γ_{res} can be invaded by a mutant with a

lesser level of cooperation γ_{inv}, i.e., when $\gamma_{\text{inv}} < \gamma_{\text{res}}$. A mutant that cooperates more, on the other hand, can never invade a less cooperating population. Thus, selection favours lesser and lesser values of cooperation until the trait value in the population falls below the limit for persistence, and the population goes extinct. The bar on the right side (Fig. 4.2 A) has only black and white parts, as the Allee effects prevent a small population from invading an empty habitat for any value of the cooperation trait (Fig. 4.1).

Fig. 4.2 B shows successive invasions by less cooperating strategies and the fall in the population size until extinction occurs. When a less cooperating strategy invades a more cooperating resident, the resident goes extinct and is replaced by the invader. However, in the last invasion trajectory (Fig. 4.2 D), the invader cannot persist on its own. Initially, the invader population rises and the resident population falls. When the resident population falls below a certain point, the invader population reaches a maximum and decreases sharply. After this, both populations decrease and go extinct. Fig. 4.2 C show the nullclines for the last trajectory. The resident has a non-zero carrying capacity and an Allee threshold, whereas the invader has no non-zero equilibrium point. The extinction of both strategies is the only stable equilibrium.

Hence, although cooperating less harms the population in the long term, the short-term gains on the ecological timescale provide an advantage to defectors who make smaller cooperative investments. This outcome is called a *tragedy of the commons*, where a focus on individual benefit engenders a disaster on the population scale. Evolutionary suicide of this kind is an extreme example of the tragedy of the commons, in which these short-term advantages inevitably lead to extinction.

4.2 Cooperation in a stochastic metapopulation

To explore whether a metapopulation structure allows cooperation to evolve, we convert our model into a stochastic metapopulation model along the same lines as we did in Chapter 3. The demographic processes of birth, death, immigration, emigration and catastrophes are defined to be stochastic processes (Chapter 2, Section 2.3). The birth and death rates are given by (4.2), and the immigration and emigration rates by (2.16). The local population dynamics over time are now described by a probability distribution, which is equivalent to the distribution over all the patches at a given instant. Using the LMAO function (Chapter 2, Section 2.3, Subsection 2.3.2), we construct PIPs and study invasion dynamics in this model.

A metapopulation structure averts the tragedy of the commons and allows cooperation to evolve. Fig. 4.3 shows PIPs for different dispersal rates. The value of cooperation (γ) at the intersection point of the invasion boundary with the diagonal is the singular strategy. In all the cases that we observe, there is only one singular strategy. As the strategy can invade its nearby strategies, it is convergence stable. With evolution, the population will eventually attain this strategy. As it cannot be invaded by nearby strategies, it is evolutionarily stable. Hence, it is a continuously stable strategy (CSS) that will be an evolutionary endpoint. We denote the CSS of the cooperation strategy by γ^*. As the PIPs show, γ^* decreases with increasing dispersal rate. Additionally, the minimum value of the cooperation trait γ_{min} required for persistence also decreases with increasing dispersal rate. High dispersal rates allow persistence for a larger range of cooperation strategies but also decrease the CSS values. Besides, the bars adjacent to the PIPs show that the range of cooperation strategies which can colonise an empty habitat also changes with the dispersal rate. For high dispersal rates, no strategy can colonise an empty habitat starting with a small abundance as regional Allee thresholds that disappear for

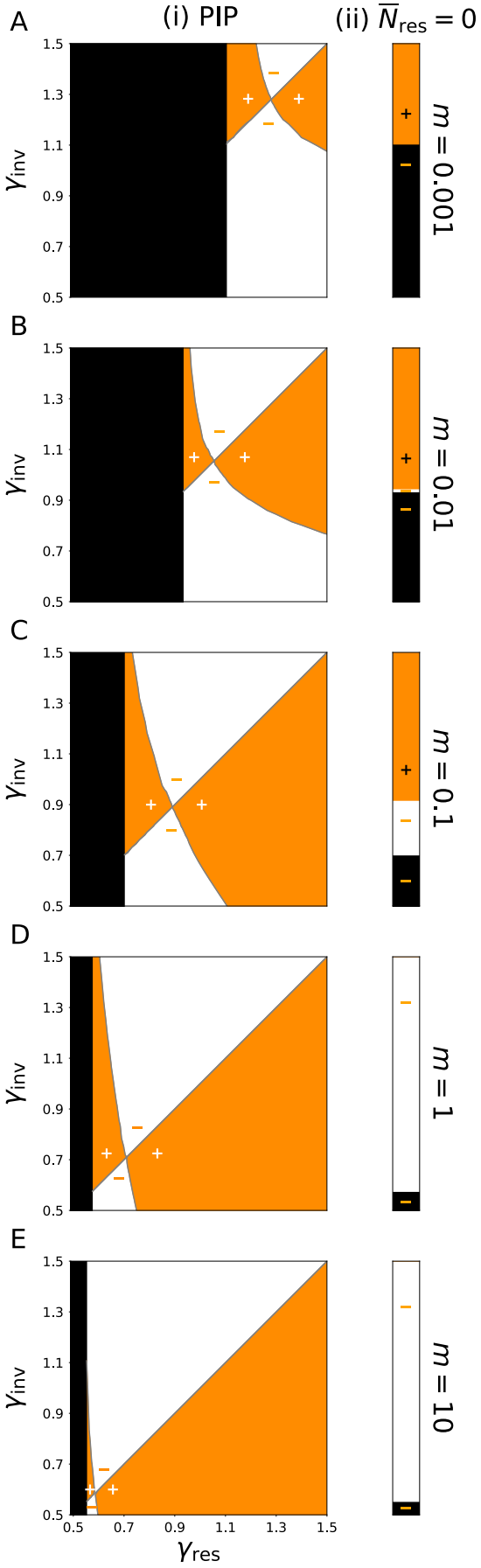

Fig. 4.3. Pairwise invasibility plots w.r.t. cooperation (γ) in the stochastic metapopulation model for different dispersal rates (m). **A** $m = 0.001$ **B** $m = 0.01$ **C** $m = 0.1$ **D** $m = 1$ **E** $m = 10$. The resident strategies are shown on the x-axis and the invade strategies on the y-axis. The black portion shows the strategies for which a resident cannot persist. In the square (Column i), the coloured (+) and white (−) portions indicate the resident-invader strategy combinations for which invasion occurs. The point where the invasion boundary intersects the diagonal is the singular strategy (γ^*). In all these cases, the singular strategy is a continuously stable strategy (CSS). Unlike the deterministic non-spatial model (Fig. 4.2), cooperation now evolves in the population and a tragedy of the commons is averted. The value of γ^* is smaller for higher dispersal rates, meaning that the extent of cooperation in the population decreases with increasing dispersal rates. Further, the range of permissible strategy values increases with increasing dispersal rates. In the sidebar (Column ii), the coloured (+), white (−) and black (−) parts correspond to the strategy values that can invade an unoccupied habitat, can persist but cannot invade an unoccupied habitat and cannot persist, respectively. Invasion into an unoccupied habitat with a small initial abundance can be possible in the metapopulation model, as a population may not face a regional Allee effect despite the presence of the local Allee effect (Chapter 3). The minimum γ need for invasion (sidebar) does not always coincide with the minimum γ needed for persistence (PIP), highlighting the differences caused by the presence and absence of regional Allee thresholds. Parameters: $\rho = 3.5$, $a = 10$, $c = 1$, $\alpha = 0.04$, $b = 0.05$, $\theta = 2$, $X = 0$, $\delta = 1$.

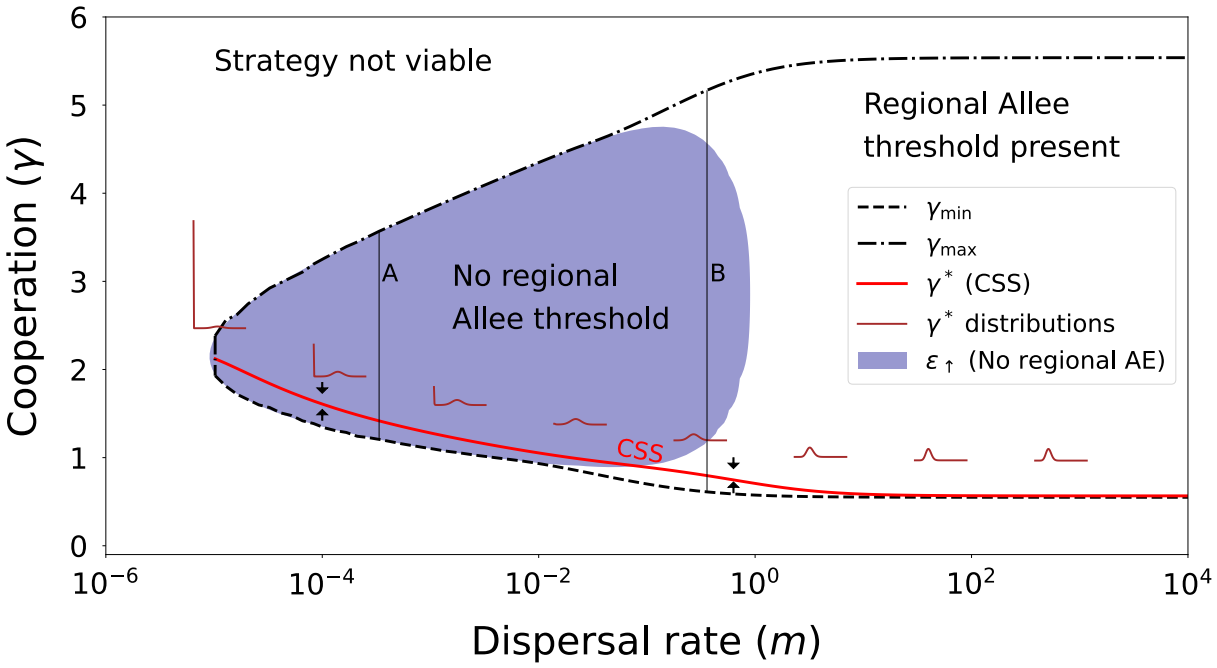

Fig. 4.4. CSS for cooperation (γ^*) as a function of dispersal rate (m). γ^* decreases with increasing m, but evolutionary suicide does not occur. The upper and lower limits $\gamma_{\min}$ and $\gamma_{\max}$ decrease and increase with increasing m, respectively, and saturate as $m \to \infty$. The purple area ($\varepsilon_\uparrow$) is the part of the parameter space where invasion into an unoccupied habitat with a small initial abundance is possible, i.e., where there is no regional Allee effect. Equilibrium population distributions at CSS are depicted for certain values of m. **A** Competitive exclusion of defectors. **B** Successive evolution to a strategy that cannot invade from rarity. Parameters: $\rho = 3.5$, $a = 10$, $c = 1$, $\alpha = 0.04$, $b = 0.05$, $\theta = 2$, $X = 0$, $\delta = 1$.

intermediate dispersal rates appear again for high dispersal (see Chapter 3).

Interplay of cooperation and dispersal rate

Fig. 4.4 captures the essence of these results and displays various outcomes as a function of the dispersal rate (m). First, there is a minimum value of m below which no strategy can persist, consistent with the results we saw in Chapter 3. Second, the maximum permissible value of cooperation, $\gamma_{\max}$, increases with increasing m and saturates at a certain value. Third, the minimum permissible value of cooperation, $\gamma_{\min}$, decreases with increasing m and saturates at a certain value. Fourth, invasion into unoccupied habitats is possible within a part of the parameter space, where there is no regional Allee threshold. We mark these combinations of γ and m as $\varepsilon_\uparrow$.

Importantly, consider how CSS γ^* varies with m. Though γ^* decreases with increasing m, it saturates at a certain point for very high m values. This implies that, in this case, a CSS exists even for high dispersal rates, completely averting evolutionary suicide! Although γ^* is close to $\gamma_{\min}$ for high m, the population does not go extinct with evolution. In Chapter 3, we saw that the metapopulation equilibria differ from the local equilibria even for very high dispersal rates, suggesting that stochasticity plays a key role even though high dispersal fuses the metapopulation into a single aggregate patch. The outcome here reflects the same phenomenon,

where stochasticity enables evolutionary persistence by maintaining heterogeneity, disallowing a complete melding of the patches at high dispersal rates. Nevertheless, it is noteworthy that for some of the other parameter values we will encounter further in the chapter, evolutionary suicide indeed occurs for high dispersal rates.

In addition, Fig. 4.4 also plots the stable equilibrium distributions $P(N)$ (with N on a hidden x-axis) at the strategy γ^* for different m. The distributions are bimodal for low m, and the probability mass associated with the non-zero peak increases with increasing m. However, since the local carrying capacity for γ^* decreases with decreasing γ^* (at least in the values taken by γ^*, Fig. 4.1), the non-zero peak shifts to smaller values of population abundance. For high m, the distribution is a Poisson distribution, as shown in Appendix A.

A careful thought reveals some intriguing properties presented by Fig. 4.4. First, for low dispersal rates, the zone in the trait space corresponding to the colonisation of empty habitat ($\varepsilon_\uparrow$) extends below the γ^* curve. Thus, for these dispersal rates (for example, the vertical line marked A), a small population with a γ smaller than γ^* can invade an empty system. But the same population fails to invade when there is a resident with the strategy γ^*. Hence, a small defector population that would have grown in abundance in the absence of a resident fails to invade a resident cooperator population. This implies that the defector can be competitively excluded by the cooperator. This completely contrasts the local deterministic outcome, where a defector is always a superior competitor and excludes a cooperator. In Section 4.3 and 4.4, we further look into this phenomenon.

Second, consider intermediate dispersal rates in Fig. 4.4 where a population at the CSS experiences a regional Allee effect, but strategies that cooperate more do not face it (for example, the vertical line marked B). Here, an empty habitat can be colonised by a small population that assumes a strategy in the $\varepsilon_\uparrow$ zone. However, evolution will push the population strategy to lower and lower values until it reaches γ^*. In this way, the metapopulation will ultimately consist of individuals with a strategy that could not have invaded in the first place. This phenomenon is akin to ecological succession (Koffel *et al.*, 2018), where a pioneer community modifies the environment in a manner that enables other species to invade, finally producing a climax community with an entirely different composition, which may not consist of the pioneering species. Along similar lines, our metapopulation may begin with a pioneer strategy that invades an empty habitat and secures the common good such that a relatively defecting population can invade. The subsequent replacement of populations would lead to the CSS. Now, if a large-scale disturbance wipes out the entire metapopulation at CSS, recolonising would require either a large abundance or beginning with a cooperator population that can invade with a small initial abundance.

We further explore these connections and potential mechanisms for our results in detail in Section 4.4. Here, we discuss the impact of the evolution of cooperation on two ecological parameters: carrying capacity and Allee threshold, both at the local and regional scales. Recall that unlike in Chapter 3, the local carrying capacity K and the local Allee threshold A are not fixed parameters of the model but vary as a function of γ. Also, recall from Chapter 3 that the regional carrying capacity K_R and the regional quasi-Allee threshold A_R depend on the dispersal rate m. We plot these local and regional equilibria values at the cooperation CSS as a function of the migration rate m in Fig. 4.5. We denote the local carrying capacity, local Allee threshold, regional carrying capacity and regional quasi-Allee threshold at the CSS as $K(\gamma^*)$, $A(\gamma^*)$, $K_R(\gamma^*)$ and $A_R(\gamma^*)$, respectively.

For low dispersal rates, the CSS strategy produces a high $K(\gamma^*)$ but a low $K_R(\gamma^*)$. This

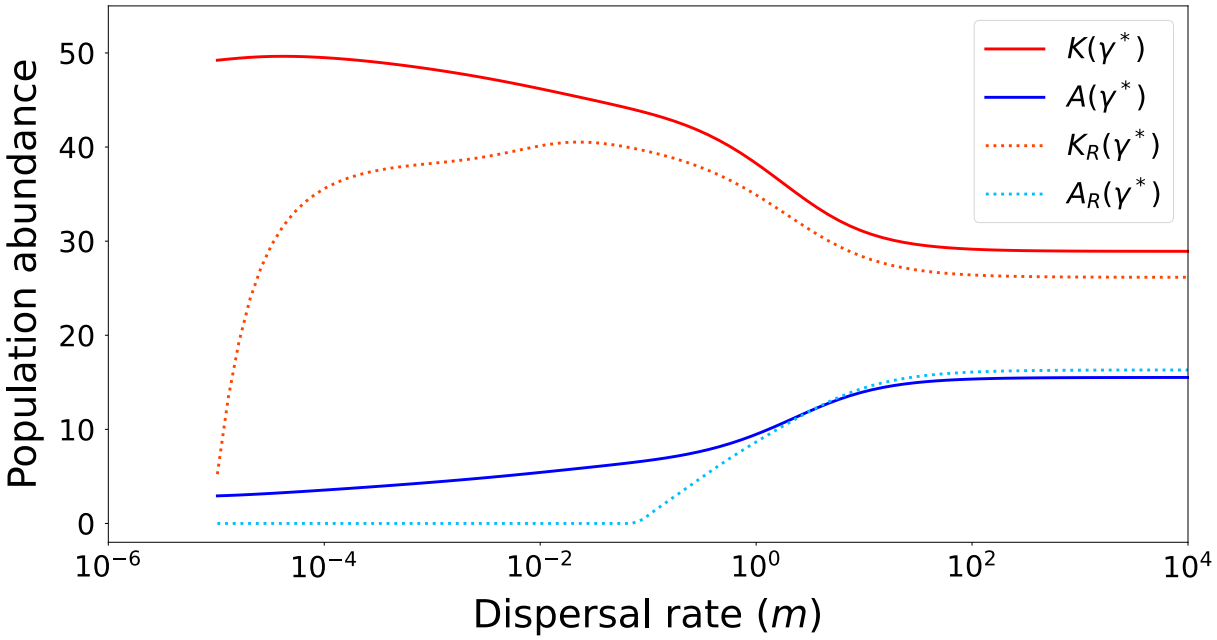

Fig. 4.5. Local and regional ecological parameters at the CSS as a function of dispersal rate (m). Local carrying capacity, regional carrying capacity, local Allee threshold and regional Allee threshold at the CSS are denoted by are denoted by $K(\gamma^*)$, $K_R(\gamma^*)$, $A(\gamma^*)$, $A_R(\gamma^*)$, respectively. Parameters: $\rho = 3.5$, $a = 10$, $c = 1$, $\alpha = 0.04$, $b = 0.05$, $\theta = 2$, $X = 0$, $\delta = 1$.

implies that most of the patches are empty, but the few occupied patches have a high abundance. This scenario corresponds to the bimodal distributions in Fig. 4.4. With increasing m, $K(\gamma^*)$ shows a small initial increase and then decreases, ultimately saturating at a value for high dispersal rates. $K_R(\gamma^*)$ is the maximum for an intermediate dispersal rate and saturates below $K(\gamma^*)$. $A(\gamma^*)$ increases with increasing dispersal rates. $A_R(\gamma^*)$, on the other hand, is zero for small dispersal rates, corresponding to the $\varepsilon_\uparrow$ zone in Fig. 4.4. Beyond this invasion zone, $A_R(\gamma^*)$ rises from zero and saturates at value larger than $A(\gamma^*)$. All these parameters show saturating behaviour at high dispersal rates because γ^* saturates, as shown in Fig. 4.4.

Examples of evolutionary suicide in the metapopulation

The constant death term c is a key life history parameter in our model that determines the natural death rate of individuals in the absence of competition and cooperation. The effect of such life history traits on the evolution of cooperation depends on how they affect population dynamics (Lion and Gandon, 2010). Increasing c amounts to pushing the per-capita growth rate curve downwards (see Chapter 3, Fig. 3.2), increasing the local Allee threshold and decreasing the local carrying capacity. Moreover, changing c also alters $\gamma_{\min}$ and $\gamma_{\max}$.

Increasing the constant death rate promotes the evolution of greater cooperation but can cause evolutionary suicide (Fig. 4.6). For a higher value of c (Fig. 4.6 A,B), evolutionary suicide occurs for high m. High dispersal rates lead to loss of spatial heterogeneity and the metapopulation behaving similarly to a single patch, recovering the deterministic nonspatial result (Fig. 4.2). Interestingly, evolutionary suicide can also take place when the dispersal rates are too low (Fig. 4.6). In such a case, persistence on an evolutionary scale is possible for a range of intermediate dispersal rates. Extreme dispersal rates cause extinction. Evolutionary

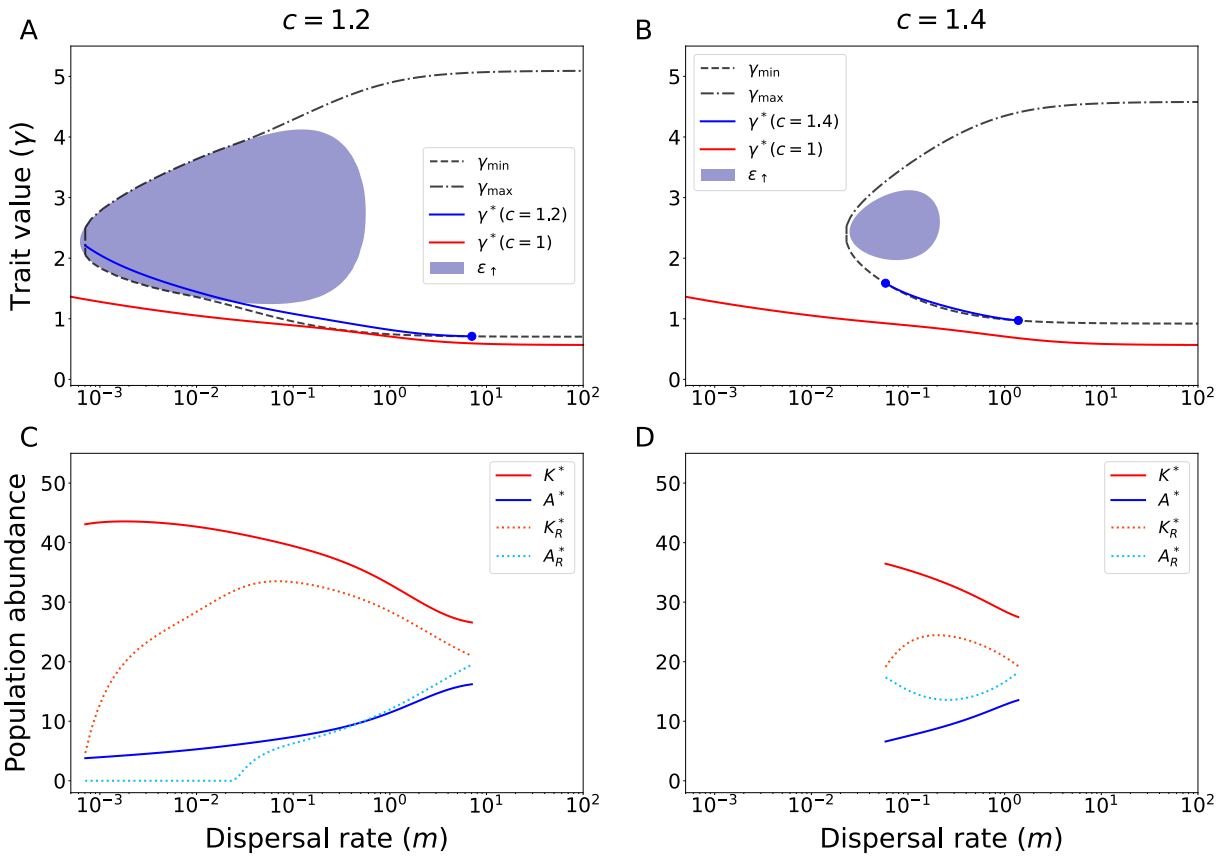

Fig. 4.6. CSS (γ^*) as a function of dispersal rate (m) for **A** $c = 1.2$ and **B** $c = 1.4$. The CSS for $c = 1$ is also shown for comparison. Local and regional ecological parameters at the CSS as a function of dispersal rate (m) for **C** $c = 1.2$, **D** $c = 1.4$. Local carrying capacity, regional carrying capacity, local Allee threshold and regional Allee threshold at the CSS are denoted by are denoted by K^*, K^*_R, A^*, A^*_R, respectively. The terminal dots in **A** and **B** indicate evolutionary suicide. Parameters: $\rho = 3.5$, $a = 10$, $\alpha = 0.04$, $b = 0.05$, $\theta = 2$, $X = 0$, $\delta = 1$.

suicide with low dispersal rates can also be interpreted as a loss of spatial heterogeneity because each patch functions independently on its own. As cheaters dominate cooperators locally, every patch is prone to invasion by cheaters, leading to evolutionary suicide.

From a dynamical systems point of view, a connection between evolutionary suicide and the regional ecological parameters is worth mentioning. Gyllenberg *et al.* (2002) proved that a discontinuous transition to extinction is a necessary condition for evolutionary suicide. In other words, evolutionary suicide cannot occur if the population abundance is a continuous function of the evolving parameter. Our results are consistent with Gyllenberg *et al.*'s theorem (2002). For example, in Figs. 4.4, 4.6 A,B, evolutionary suicide cannot take place in the purple-shaded part of the parameter space, where there is no regional Allee effect. A barrier such as an Allee effect is essential for evolutionary suicide. In Fig. 4.6 A, evolutionary suicide does not occur in a situation where $A^*_R = 0$, i.e., when there is no regional Allee effect. But with increasing m, as A_R becomes non-zero, evolutionary suicide is observed. It takes place on both ends in Fig. 4.6 B, as A_R the parameter zone with no regional Allee effects does not touch the $\gamma_{\min}$ extinction boundary and the transition is always discontinuous. Note that the converse of the Gyllenberg *et al.*'s theorem (2002) is not true, and evolutionary suicide, in general, may not

occur despite a discontinuous transition like an Allee effect (as with Fig. 4.4).

Effect of other factors

In addition to the constant death rate, we also look at the effect of catastrophes, dispersal mortality and the cost of cooperation its evolution. Interestingly, we find that catastrophes and dispersal mortality promote the evolution of cooperation, and that the nature of cost has a nuanced effect. While being somewhat subsidiary, these results serve to support the explanation we propose in Section 4.4. The details of these results are explained in Appendix E, Section E.2.

We have seen that a metapopulation structure allows cooperation to evolve in a situation where defection is the locally dominant strategy. Starting with a monomorphic population, the metapopulation will evolve to a CSS if mutations are small and rare and if strategies close to each other cannot stably coexist. This concept of the non-coexistence of almost identical strategies is related to the concept of limiting similarity (Meszéna *et al.*, 2006) and Gause's competitive exclusion principle (Molles Jr and Sher, 2019).

On the other hand, if mutations are sufficiently large, it is possible that two strategies coexist and produce interesting metacommunity dynamics. However, we surmise that such a coexistence would be temporary on the evolutionary scale. With invasions by a third mutant, coexisting dimorphic metapopulations would likely converge to the CSS (Diekmann *et al.*, 2004), if the third mutant that invades also replaces either or both the coexisting strategies. Our model is computationally burdensome with even two coexisting strategies, making it difficult to rigorously assess this phenomenon.

Nevertheless, although temporary, studying the coexistence of different strategies enables us to determine what transient states can occur on the evolutionary trajectory. Thus, in the following section, we explore the coexistence of cooperators and defectors and connect it to concepts from metacommunity theory.

4.3 Ecological co-existence of cooperators and defectors

While the coexistence of different strategies, i.e., cooperators and defectors, may not last on an evolutionary timescale, the very possibility of coexistence motivates us to look into the ecological nature of this phenomenon. As the coexistence state would probably be transient during evolution, it is important to investigate which strategies can coexist and how large mutations are required for coexistence. Since we are working with a metapopulation model, the possibility of coexistence raises further questions: When two strategies coexist in the metapopulation (regional coexistence), are they segregated into separate patches (absence of local coexistence)? Or do they coexist on a single patch (local coexistence)? What role does the metapopulation-level Allee effect play? Can we relate the coexistence to metacommunity theory? To probe these questions, we dig deeper into different ways cooperators and defectors coexist in our model.

We first tackle the question of whether the strategies coexist locally or on separate patches. We find that the dispersal rate determines whether local coexistence is possible or not, and that we can identify three different categories of coexistence (Fig. 4.7):

- *Segregated coexistence*: For low dispersal rates, the two morphs can coexist regionally, but they are segregated into different patches (Fig. 4.7 A). The equilibrium distribution

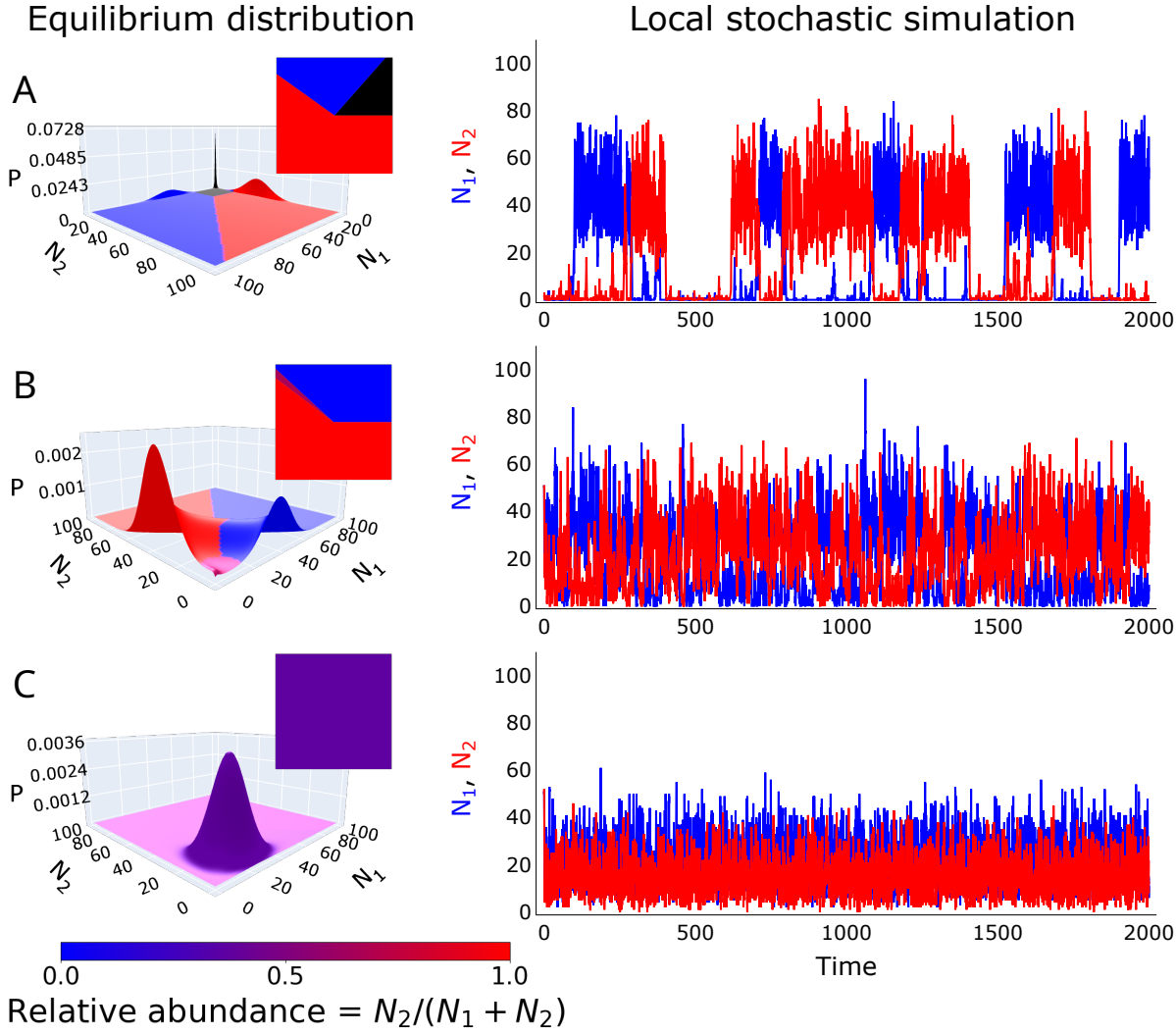

Fig. 4.7. Examples of coexistence of cooperators and defectors. **A** Segregated coexistence. $\gamma_1 = 1.25$, $\gamma_2 = 0.95$, $m = 0.01$. **B** Sink coexistence. $\gamma_1 = 1.0$, $\gamma_2 = 0.8$, $m = 0.1$. **C** Local coexistence. $\gamma_1 = 0.75$, $\gamma_2 = 0.65$, $m = 1$. The left column shows equilibrium probability distributions (the proportion of patches in a given state (N_1, N_2). The distributions are divided into the basins of attraction of different peaks and are coloured according to the relative abundance at the peak. The black peak corresponds to the extinction of both morphs. The square pie-charts adjacent to each graph summarise the distribution: Each part represents the probability mass under a given peak, and its colour represents the relative abundance of morph 2 $(N_2/(N_1 + N_2))$ at the peak. When the peak occurs where $N_1 \neq 0$ and $N_2 \neq 0$ (intermediate colour), the coexistence is local. If either $N_1 = 0$ or $N_2 = 0$ (either red or blue peak), there is no local coexistence. The right column shows a single instance of a stochastic simulation run using the Gillespie algorithm, which depicts how the abundance of a patch varies at equilibrium. In all three subfigures, morph 1 (blue) is chosen as the cooperator and morph 2 (red) as the defector. Parameters: $\rho = 3.5$, $a = 10$, $c = 1$, $\alpha = 0.04$, $b = 0.05$, $\theta = 2$, $X = 0$, $\delta = 1$.

shows three peaks located on the boundaries of the state space, thus corresponding to the presence of morph 1 only (the cooperator), morph 2 only (the defector) and the extinction of both. We interpret this as an example of patch dynamics: regional coexistence is maintained through local extinction and recolonisation. The time series of abundances in a given patch of the metacommunity obtained using the Gillespie algorithm illustrates this: a given patch harbours either only one of the morphs at a given instant or none of them. When the patch is empty, the cooperator (blue) colonises them more often. However, the defector (red) takes over the cooperator patches more often than the other way round. Thus, the cooperator is a better coloniser and the defector is a better competitor. Coexistence occurs due to a competition-colonisation trade-off.

- *Sink coexistence*: For intermediate dispersal rates, source-sink dynamics driven by local Allee effects are observed. In this case, the two morphs can coexist locally, but only within a sink, where each of them has a low abundance. We call this situation as *sink coexistence*. The equilibrium distributions show three peaks, one corresponding to each of the morphs and one corresponding to the sink. Fig. 4.7 B shows an example of this type of distribution. The local time series obtained using the Gillespie algorithm shows that a given patch harbours either of the morphs or a low abundance of both of them at a given instant.

- *Local coexistence*: For high (but not very high) dispersal rates, mass effects drive the local coexistence of different morphs. The equilibrium distribution is unimodal, and the peak corresponds to the coexistence of both the morphs (Fig. 4.7 C). Within a given patch, both morphs exist simultaneously with possibly different abundances.

For very high dispersal rates (see Fig. 4.10 E), the coexistence is lost due to reduced spatial heterogeneity that makes the model approach its nonspatial limit (Leibold and Miller, 2004).

In the cases we considered above, both strategies were also viable on their own. They could invade each other at equilibrium, meaning that the coexistence took place through mutual invasibility. This type of coexistence is protected, as a morph can invade the other when it is rare and the other is abundant. However, what if a resident strategy is invaded by a strategy that can't persist on its own? Is coexistence still possible? It turns out that the answer is yes.

To illustrate this scenario, consider the following example: morph 1 (say, the cooperator) can persist on its own, whereas morph 2 (say, the defector) cannot. However, when morph 1 is present in the system, morph 2 can invade it and then coexist with morph 1. Since a necessary condition for this coexistence is the presence of morph 1 when morph 2 invades, we call this *conditional coexistence*. This concept is similar to obligate parasitism, as the defector needs the cooperator to be present in order to survive. If the cooperator does not have a regional Allee effect, the coexistence is protected from extinction. If the cooperator has a regional Allee effect, the coexistence is unprotected, i.e., both the morphs go extinct if the cooperator becomes rare. Conditional coexistence can also be classified into three different types:

- *Segregated coexistence* (Fig. 4.8 A): This is an extreme example of patch dynamics. When the defector invades a cooperator patch, the cooperator population collapses. The defector cannot persist in the patch on its own for long and collapses as well. Now, the cooperator can again colonise the patch and establish, continuing the cycle of extinction and recolonisation. In other words, the defector is the superior competitor but an inferior coloniser.

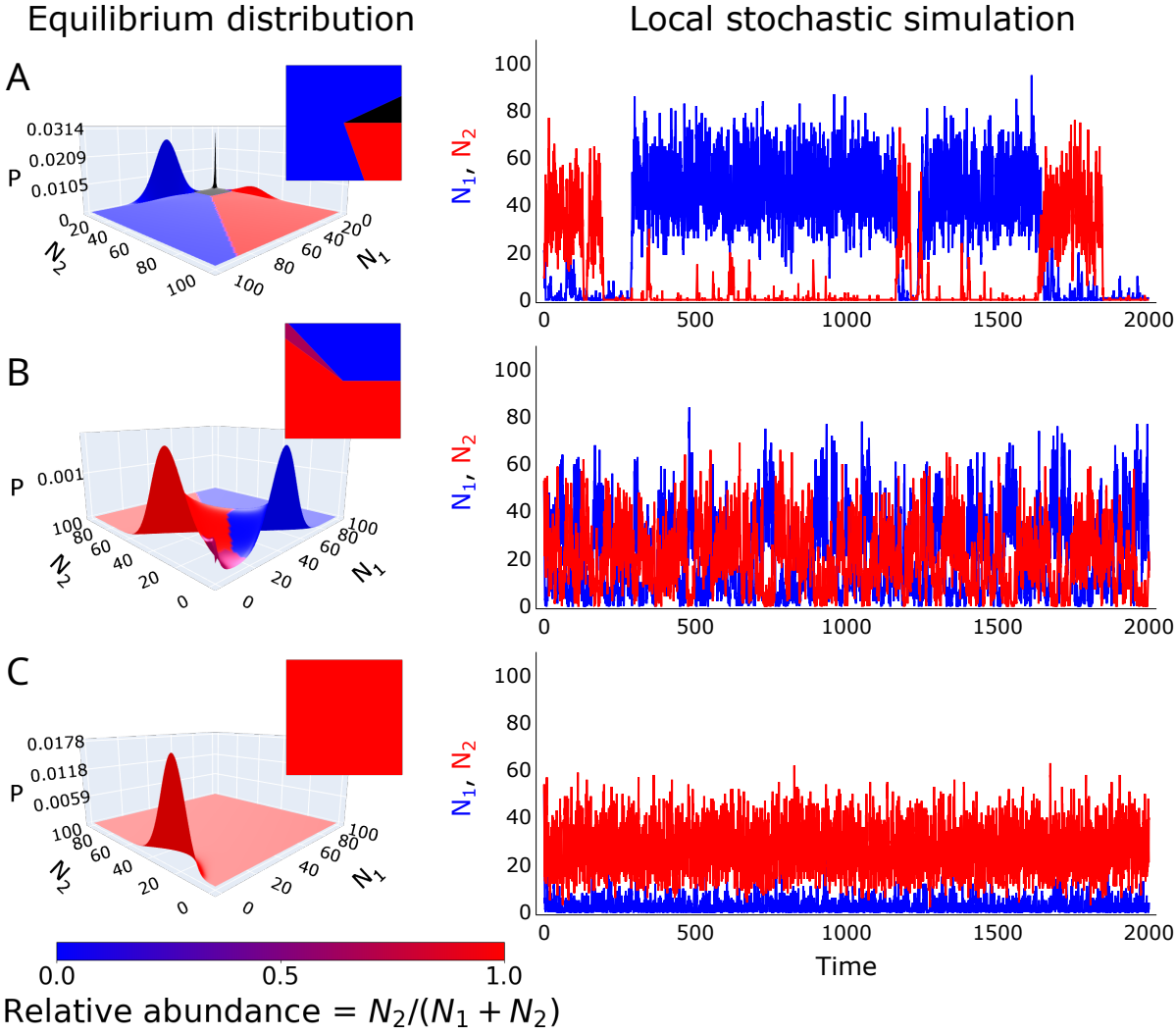

Fig. 4.8. Examples of conditional coexistence. **A** Segregated coexistence. $\gamma_1 = 1.5$, $\gamma_2 = 0.8$, $m = 0.01$. **B** Sink coexistence. $\gamma_1 = 1.3$, $\gamma_2 = 0.6$, $m = 0.1$. **C** Local coexistence. $\gamma_1 = 1.5$, $\gamma_2 = 0.55$, $m = 1$. The left column shows equilibrium probability distributions(the proportion of patches in a given state (N_1, N_2). The distributions are divided into the basins of attraction of different peaks and are coloured according to the relative abundance at the peak. The black peak corresponds to the extinction of both morphs. The square pie-charts adjacent to each graph summarise the distribution: Each part represents the probability mass under a given peak, and its colour represents the relative abundance of morph 2 $(N_2/(N_1 + N_2))$ at the peak. When the peak occurs where $N_1 \neq 0$ and $N_2 \neq 0$ (intermediate colour), the coexistence is local. If either $N_1 = 0$ or $N_2 = 0$ (either red or blue peak), there is no local coexistence. The right column shows a single instance of a stochastic simulation run using the Gillespie algorithm, which depicts how the abundance of a patch varies at equilibrium. In all three subfigures, morph 1 (blue) is chosen as the cooperator and morph 2 (red) as the defector. Parameters: $\rho = 3.5$, $a = 10$, $c = 1$, $\alpha = 0.04$, $b = 0.05$, $\theta = 2$, $X = 0$, $\delta = 1$.

- *Sink coexistence*: For intermediate dispersal rates, the two morphs may coexist within a sink (Fig. 4.8 B).
- *Local coexistence*: For high dispersal rates, the cooperator and the defector may coexist within a patch since mass effects maintain their local abundances. In such a situation, it is possible that the cooperator has a very low regional and local abundance, but it supports a much larger defector population (Fig. 4.8 C).

Thus, we have seen that coexistence can take multiple forms, and that the regional Allee effect determines whether conditional coexistence is protected or not. Next, we engage with the question of which strategies can coexist or conditionally coexist.

One can visualise the combinations of strategies that can coexist using mutual invasibility plots (MIPs). A MIP is constructed by overlaying a pairwise invasibility plot (PIP) with its flipped version. A mutual invasibility plot shows three different regions in the strategy space: two corresponding to each of the species being excluded and one corresponding to coexistence. However, because of the metapopulation structure, Allee effects and conditional coexistence in our model, exploring coexistence necessitates us to dive deeper than what a MIP can show. Thus, we depict our results using a version of MIPs that we call "regional coexistence plots" (RCPs) (Figs. 4.9, 4.10).

Similar to MIPs, we obtain an RCP by overlaying a PIP with its transpose. For different values of the strategies γ_1 and γ_2, an RCP shows whether they coexist or not. In an RCP, the black portion shows the strategies for which extinction is the only stable equilibrium. The black dashed line is the persistence line, i.e. the value of $\gamma_{\min}$. The white dashed line is the invasion line, i.e., the minimum value of γ needed for a single morph to colonise an empty habitat with a small population. The blue portion marked with $+,-$ shows the strategy combinations where morph 1 (x-axis) excludes morph 2, and the red portion marked with $-,+$ shows the vice versa. The purple portion marked with $+,+$ shows the combinations where both morphs can invade each other and thus coexist. The meanings of the remaining combinations of colours and signs can be found in Table 4.1. Briefly, it suffices to know the first sign in each pair indicates whether morph 1 can invade morph 2 when the latter is at its carrying capacity (which may be zero), and the second sign indicates vice versa. In the cases where $\gamma_i < \gamma_{\min}$ so that the carrying capacity of morph i is zero, a 0 is added in the subscript to the i^{th} sign in the pair.

Fig. 4.9 shows an RCP along with example outcomes for specific γ_1, γ_2 combinations. The upper panels subfigures A—L in Fig. 4.9 show the nullclines for different γ_1, γ_2 combinations. These nullclines are the projections of the actual high-dimensional nullclines in the $P(N_1, N_2)$ space onto a two-dimensional plane spanned by the vectors $\overline{N}_1$ and $\overline{N}_2$. The details on how these nullclines were obtained can be found in Appendix E, Section E.4. The lower panels show the time series of invasion, assuming that morph is initially at its (possibly zero) regional carrying capacity and morph 2 has a small initial regional abundance [1].

Further, we use square-pie charts (Lerch *et al.*, 2023) to summarise the equilibrium distributions for various γ_1, γ_2 combinations. Each square represents a particular γ_1, γ_2 combination. Within a square, each distinctly coloured wedge stands for a peak in the equilibrium distribution. The colour of the wedge represents the relative abundance of morph 2 at the peak. The area of the wedge represents the probability mass within the basin of attraction of that peak.

Fig. 4.10 shows RCPs (Column i) and square-pie charts (Column ii) for different dispersal rates. For $m = 0.001$ (Fig. 4.10 A), the invasion and persistence lines coincide (Column i).

[1] The time series figures were obtained using a modified version code originally written by Dr. Jonas Wickman.

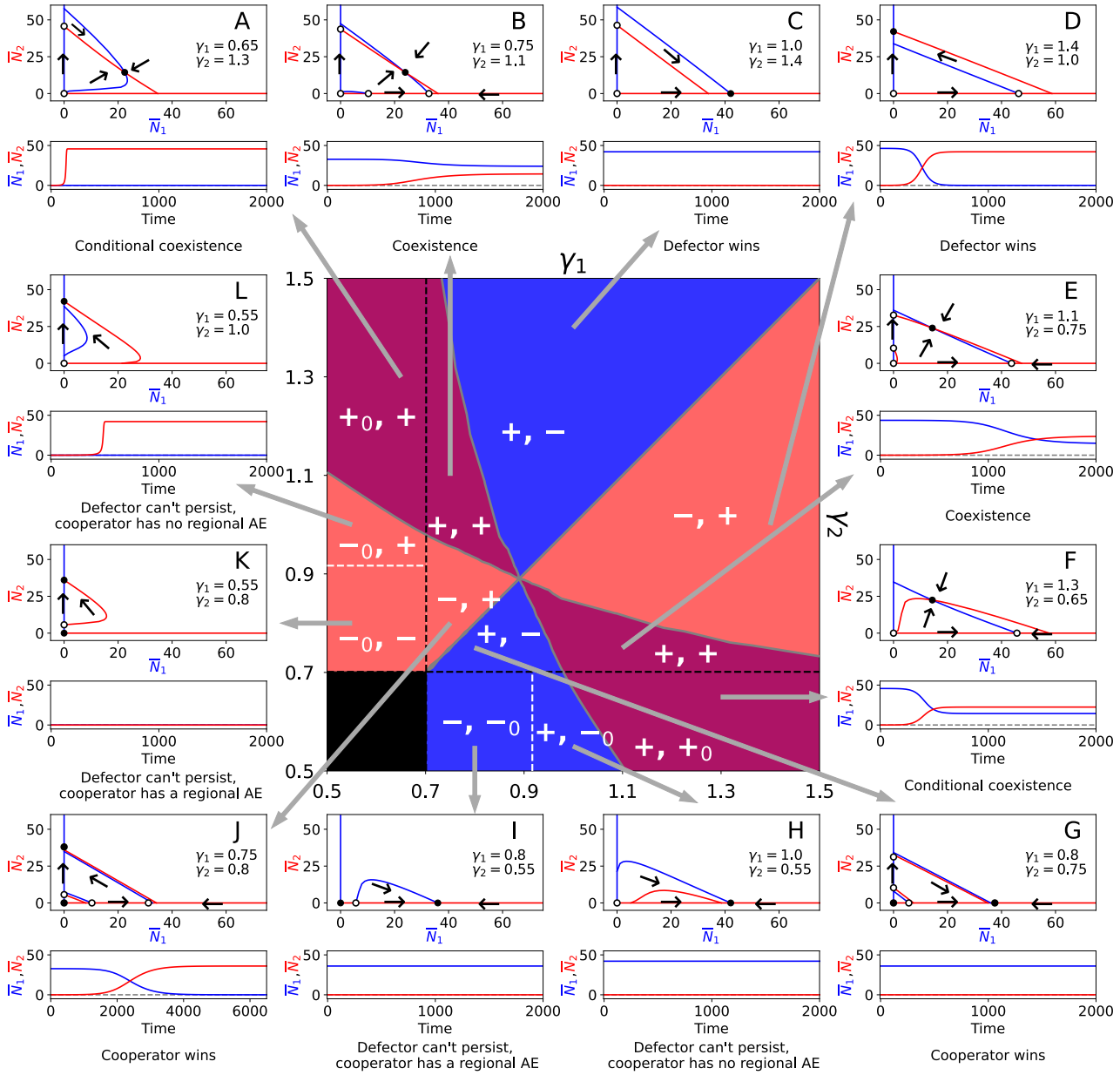

Fig. 4.9. A regional coexistence plot (RCP) showing different outcomes that can occur when two strategies interact. The guidelines for interpreting different combinations of signs and colours are given in Table 4.1. The dashed black line is the persistence boundary, i.e. $\gamma_{\min}$. The dashed white line is the invasion boundary for an unoccupied habitat, i.e., the minimum value of γ needed for invading an empty habitat from a small initial abundance (the sidebar in Fig. 4.3 C). In the subfigures A—L, the upper panels show the projections of the nullclines into a two-dimensional space spanned by $\overline{N}_1$ and $\overline{N}_2$. The lower panels in subfigures A—L show time series assuming that morph 1 is at its regional carrying capacity (which may be zero) and morph 2 is invading with a small regional abundance. Parameters: $m = 0.1$, $\rho = 3.5$, $a = 10$, $c = 1$, $\alpha = 0.04$, $b = 0.05$, $\theta = 2$, $X = 0$, $\delta = 1$.

.

Signs	Colour	Can morph 1 persist on its own?	If yes, can morph 2 invade morph 1? If no, can morph 2 invade the empty system?	What is the final outcome?
$+, -$	Blue	Yes	No	Morph 1 wins
$-, +$	Red	Yes	No	Morph 2 wins
$+, +$	Purple	Yes	Yes	Coexistence
$+, +_0$	Purple	Yes	Yes	Conditional coexistence (coexistence if morph 1 is present when morph 2 invades)
$+_0, +$	Purple	No	Yes	Conditional coexistence (coexistence if morph 2 is present when morph 1 invades)
$+, -_0$	Blue	Yes	No	Morph 1 wins
$-_0, +$	Red	No	Yes	Morph 2 wins
$-, -_0$	Blue	Yes	No	Morph 1 wins but can't invade with a small initial abundance
$-_0, -$	Red	No	No	Morph 2 wins but can't invade with a small initial abundance
$-, +_0$	Purple	Yes	Yes	Conditional coexistence (coexistence if morph 1 is present at high abundance when morph 2 invades)
$+_0, -$	Purple	No	No	Conditional coexistence (coexistence if morph 2 is present at high abundance when morph 1 invades)
$-, +_0$	Black	Yes	Yes	Extinction of both morphs when morph 2 invades morph 1
$+_0, -$	Black	No	No	Extinction of both morphs when morph 1 invades morph 2

Table 4.1: Meanings of different combinations of signs and colours in Figs. 4.9 and 4.10.

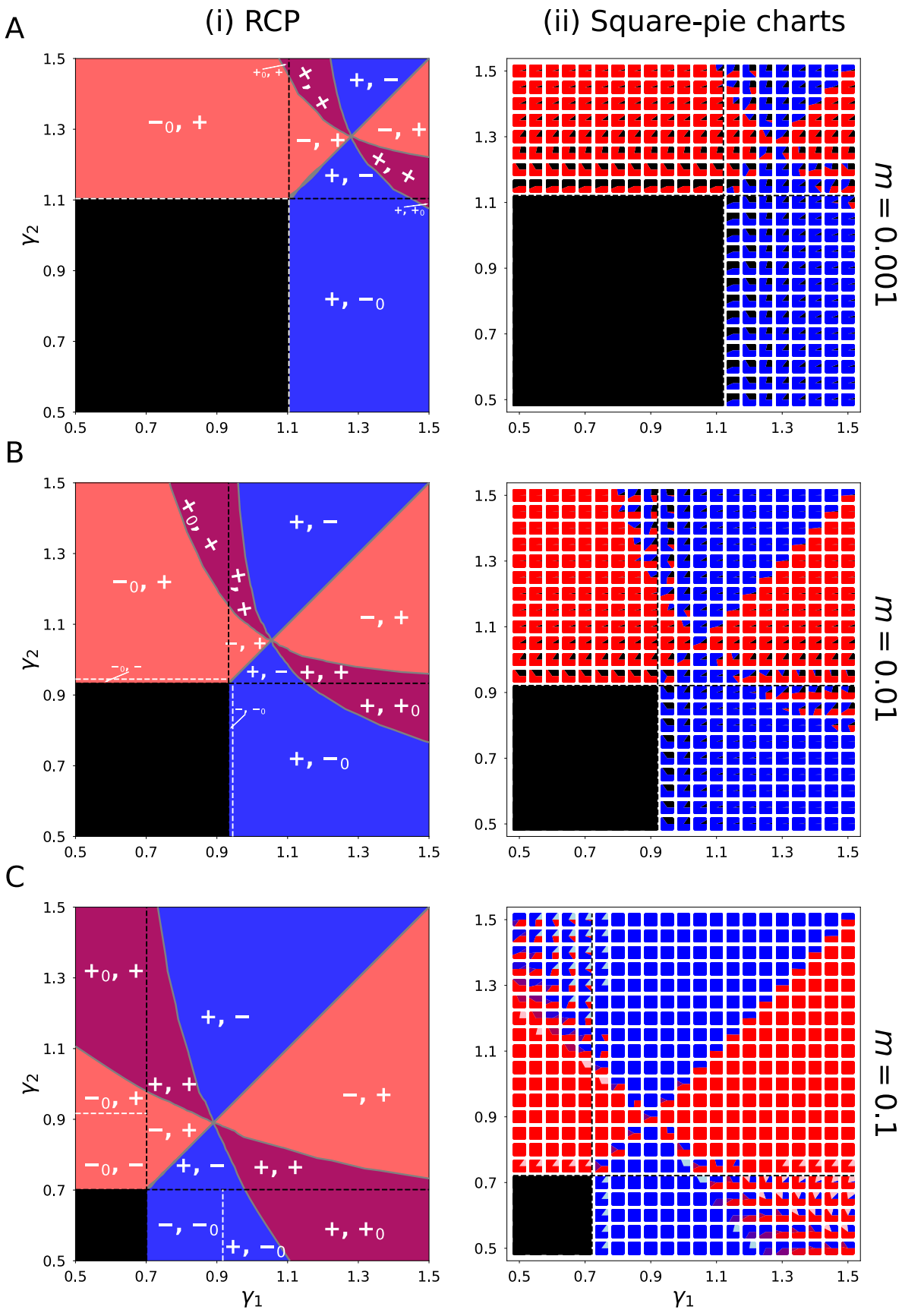

Figure continued on the next page.

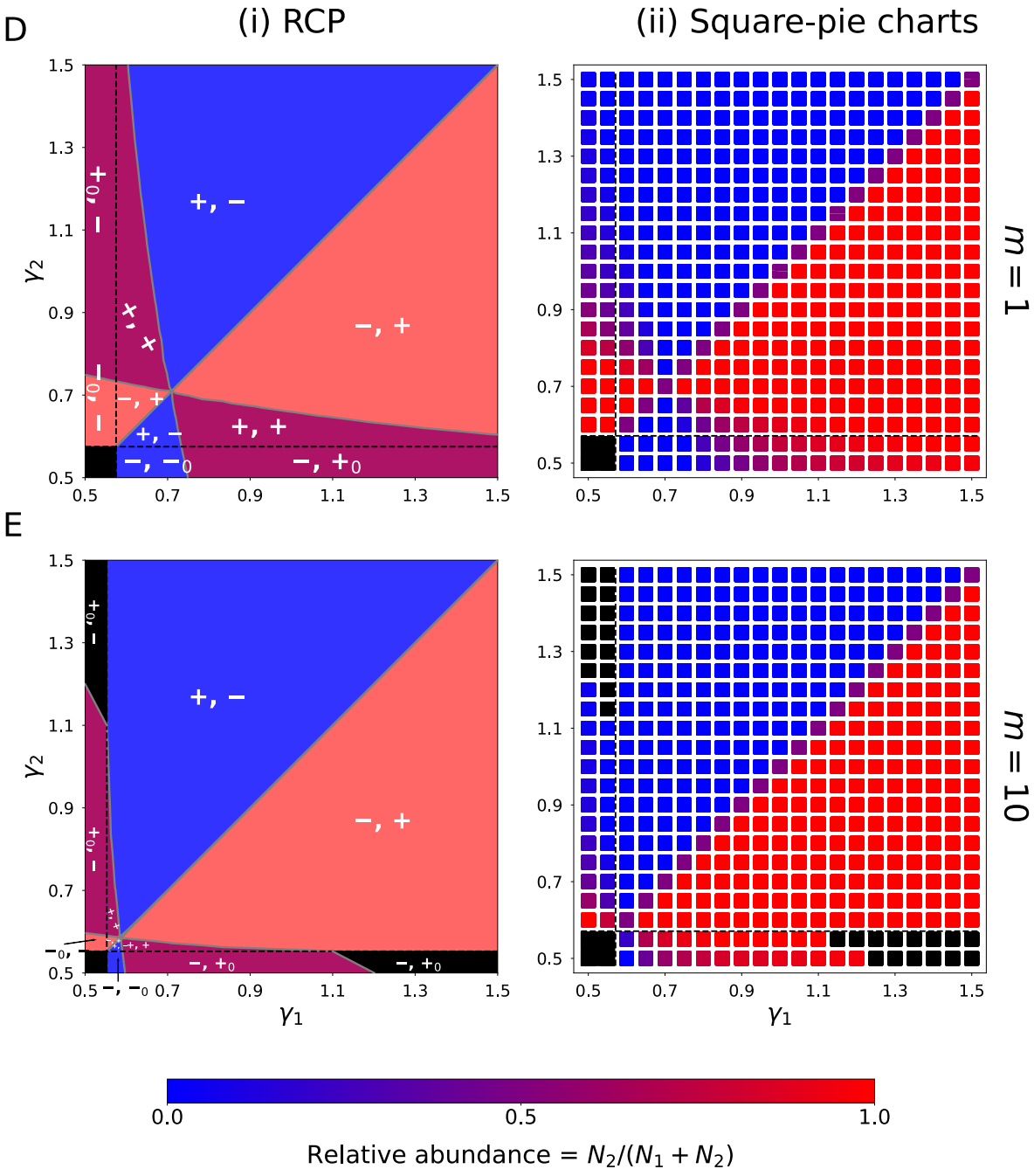

Fig. 4.10. Coexistence of different strategies in cooperation in the metacommunity model. **(i) Regional coexistence plots (RCPs).** The RCPs show whether a stable coexistence equilibrium is present for a given combination of γ_1, γ_2 or not. The colour key is as follows: Purple: Stable coexistence possible. Blue: No stable coexistence. Species 1 has a non-zero stable equilibrium. Red: No stable coexistence. Species 2 has a non-zero stable equilibrium. Black: Extinction of both species is the only stable equilibrium. Among the pairs signs on the figures, the first sign indicates whether species 1 can invade (+) when species 2 is at its carrying capacity (which may be zero) or not (−), and the second sign indicates whether species 2 can invade (+) when species 1 is at its carrying capacity (which may be zero) or not (−). (*The caption continues on the next page*).

Fig. 4.10. (*Continued from the previous page*) When a species has a zero regional carrying capacity ($\gamma < \gamma_{\min}$), the same is indicated with a 0 as the subscript to the corresponding sign. The dashed black line is the persistence boundary, i.e. $\gamma_{\min}$. The dashed white line is the invasion boundary for an unoccupied habitat, i.e., the minimum value of γ needed for invading an empty habitat from a small initial abundance (the sidebars in Fig. 4.3). The resulting meanings of different combinations of signs and colours are given in Table 4.1. **(ii) Square-pie charts**. The square pie charts summarise the equilibrium probability distributions. Each square-pie chart represents a γ_1, γ_2 combination. It is divided into different parts, each of which corresponds to a peak in the equilibrium probability distribution. The colour of each part indicates the relative abundance of species 2 at the peak, i.e., $N_2/(N_1+N_2)$. A bluer colour implies greater N_1, and a redder colour implies a greater N_2 at the peak. An intermediate colour indicates local coexistence. Sinks of species 1 and 2 (peaks where N_1 is small but non-zero and $N_2 = 0$, and vice versa) are shown by lighter shades of blue and red, respectively. The entirely black squares correspond to the γ_1, γ_2 combinations where extinction of both species is the only stable equilibrium. Dispersal rates: **A** $m = 0.001$ **B** $m = 0.01$ **C** $m = 0.1$ **D** $m = 1$ **E** $m = 10$. Parameters: $\rho = 3.5$, $a = 10$, $c = 1$, $\alpha = 0.04$, $b = 0.05$, $\theta = 2$, $X = 0$, $\delta = 1$.

There is a mutual invasibility region and a small conditional coexistence region. The equilibrium coexistence distributions (Column ii) show three peaks, corresponding to the dominance of each species and extinction. Thus, there is no local coexistence. Regional coexistence occurs through a competition-colonisation trade-off.

For $m = 0.01$ (Fig. 4.10 B-i), the mutual invasibility region is relatively reduced compared with $m = 0.001$. The conditional coexistence region is larger. The invasion and persistence lines do not coincide, and we have small region where a morph can exclude another morph, but fails to invade the empty system due to a regional Allee effect. The equilibrium distributions still show a separation of peaks (Fig. 4.10 B-ii), with no local coexistence.

For $m = 0.1$ (Fig. 4.10 C-i), the mutual invasibility region is relatively larger compared with $m = 0.01$. Several different outcomes can be clearly discerned, including exclusion of one species by another ($+, -$ and $-, +$), coexistence with mutual invasibility ($+, +$), conditional coexistence ($+, +_0$ and $+_0, +$), and the exclusion of a defector can't persist on its own, without ($+, -_0$ and $-_0, +$) or with ($-, -_0$ and $-_0, -$) regional Allee effects in the cooperator. We spell out these outcomes perspicuously in Fig. 4.9, where we plot the nullclines and time series for each of these cases. The equilibrium distributions (Fig. 4.10 C-ii) now contain sinks, and two morphs can locally coexist within a sink. Sinks containing only one of the morphs can also occur. The square-pie charts also reveal that even in the cases of mutual invasibility (for $m = 0.1$), one morph often has a higher regional abundance, such that the other morph does not even have a peak corresponding to it. Additionally, conditional coexistence also takes place with sinks containing one or both morphs. Importantly, consider the conditional coexistence where γ_1 is close to 1.5 and $\gamma_2 < \gamma_{\min}$, i.e., morph 1 is a cooperator and morph 2 is a defector that can't persist on its own. Here, the coexistence distributions are dominated by the defectors, and only a small proportion of cooperators exist (the red area is larger compared to the blue area). However, if the cooperators were completely absent, the defectors would have gone extinct. Hence, we observe that a small population of cooperators is able to sustain a large defector population, allowing it to coexist with itself.

For $m = 1$ (Fig. 4.10 D-i), the mutual invasibility region is again relatively smaller compared

to $m = 0.1$. A regional Allee effect exists for all values of γ. Hence, conditional coexistence is now unprotected from extinction, as the cooperator in this situation is unable to invade from rarity. Mass effects now lead to local coexistence (Fig. 4.10 D-ii), where a single peak exists in the probability distribution. Local coexistence also occurs in situations with conditional coexistence. Similar to the previous case, the equilibrium distributions can be dominated by the defectors so that a small cooperator population— now without a corresponding peak— sustains a much larger defector population that wouldn't have existed on its own.

For $m = 10$ (Fig. 4.10 E), the mutual invasibility region is reduced even further because the metacommunity becomes homogeneous (Leibold and Miller, 2004) and approaches the nonspatial model. In addition to conditional coexistence, there are now black regions with the sign combinations $-, +_0$ and $+_0, -$. In this portion, the cooperator (the morph with a higher γ) can persist on its own but cannot invade from rarity. A defector can invade the cooperator, but this invasion takes the entire population to extinction. This phenomenon is similar to evolutionary suicide but occurs through a large rather than a small mutation. Interestingly, this suicide through large mutation takes place if the cooperator cooperates to a sufficiently high extent, whereas conditional coexistence takes place for the same defector strategy if the cooperator cooperates lesser. Thus, to protect itself from a suicidal defector invasion, a cooperator should cooperate to a smaller extent. For the nullclines and invasion time series for such an outcome, see Appendix E, Section E.4.

Here, we saw that patch dynamics promotes the coexistence of cooperators and defectors, even allowing defectors who cannot self-sustain to live off the cooperator population without collapsing them. Regional coexistence happens as a result of local colonisations and extinctions. This is essentially the concept of competition-colonisation trade-off, where two species can coexist due to one of them being better at occupying empty patches and the other being better at competing with the first species. The results presented here reveal a direct connection between the dynamics of cooperation in our model and the competition-colonisation trade-off. In the subsequent section, we discuss a potential extension of this concept to an evolutionary scale and explore how it can explain the evolution of cooperation in a metapopulation.

4.4 Evolution of cooperation: A competition-colonisation trade-off?

As we saw in Section 4.1, defection is the locally dominant strategy in our model. In a given patch, defectors will always have a higher growth rate than cooperators.[2] An inescapable question is what mechanism allows the evolution of cooperation when we switch from a deterministic nonspatial to a stochastic metapopulation model.

One longstanding explanation for the evolution of cooperation in spatially structured populations is that a spatial structure allows cooperators to cluster together and form aggregates where they flourish. These clusters are dynamic, as they are prone to invasion by cheaters. However, cooperators can continue to persist in the long term as they form newer clusters, particularly when dispersal rates are low. If cooperation takes place through a common pool resource, such a spatial structure allows its privatisation within clusters, facilitating coopera-

[2] As previously noted, though we use the terms "cooperators" and "defectors" as if they were binary categories, we imply them in a sense relative to each other. Cooperation in our model exists on a continuum, with its magnitude given by the strategy γ.

tion. Indeed, this is the reason why cooperation evolves in spatially explicit models (Hauert and Doebeli, 2004; Nowak and May, 1992).

At the same time, a closer look exposes that this classic description fails in the case of our model. In our metapopulation model, the population inside each patch is well-mixed, ruling out any possibility of within-patch clustering of individuals. Likewise, all the patches are equally connected to each other, effectively rendering the metapopulation a well-mixed collection of well-mixed patches. Thus, any possibility of inter-patch clustering is also ruled out. Hence, the reason why cooperation evolves may still seem mysterious. Here, drawing upon concepts from metacommunity theory, we present a more elegant explanation that lies behind the phenomena exhibited by our model.

To elucidate this solution, we need to revisit Allee effects and stochasticity. Local populations in our model suffer from a strong Allee effect that emerges as a result of cooperation driving the population dynamics. Further, cooperation also affects the carrying capacity. As Fig. 4.1 shows, the carrying capacity is the maximum for an intermediate value of cooperation, and it decreases both when cooperation is too low or too high. Conversely, the local Allee threshold is the minimum for an intermediate level of cooperation, and it increases when cooperation moves towards either of the extremes. While the local outcomes in a deterministic model depend only on the initial conditions, stochasticity can alter them and cause large populations to collapse and small populations to grow. Particularly, a higher carrying capacity implies a smaller probability of collapse. Conversely, a higher Allee threshold implies a greater probability of collapse.

We quantify the previous statement using the mean first-passage times (MFPTs) in our stochastic open system model (Chapter 2, Section 2.2, Subsection 2.2.2) with only one morph (see Appendix E, Section E.3 for the results). We observe that for an intermediate level of cooperation, the average survival time of the patch is the highest. Similarly, the average time required to colonise an empty patch to reach the local carrying capacity is the highest for an intermediate level of cooperation. Thus, intermediate cooperators are the best colonisers.

Next, we observe that defectors are always better competitors against cooperators. In a given patch, defectors will always have a higher per-capita growth rate than cooperators. We have already seen this in Section 4.1 and explained further in Appendix E, Section E.1. We further substantiate the same using MFPT analysis (see Appendix E, Section E.3).

Powered by these insights, we assert that cooperation evolves in our model as a balance between the strength of cooperators to colonise new patches and the strength of defectors to compete with them. Cooperators are better at colonising empty patches and persisting in them. Defectors are better at taking over the patches where resident cooperators are present but are worse at holding onto them and expanding into empty patches. On an evolutionary scale, the invasion dynamics of mutants result from this trade-off between competition and colonisation. A cooperator can invade a defector metapopulation if it colonises empty patches at a sufficient rate to compensate for the rate at which defectors invade and collapse its patches. A defector can invade a cooperator metapopulation if it can invade and collapse the cooperator patches at a sufficiently high rate to compensate for the rate at which cooperators invade new empty patches. The cooperation trait value where both these tendencies match is the evolutionarily stable strategy.

Further, the baffling ability of certain cooperators to regionally exclude defectors (Fig. 4.4) is likely a consequence of stochasticity. To recap, we have seen in Fig. 4.4 that for low dispersal rates, a defector that successfully invades an empty habitat can fail to invade when a cooperator

is already present. In a deterministic system, an invading defector would have had a positive growth rate in both cooperator patches and empty patches, due to which invasion into an empty habitat would also mean a successful invasion into a cooperator metapopulation. However, because of the stochastic nature of our model, a defector that enters a cooperator patch may fail to invade it. Oppositely, a cooperator may successfully invade a defector patch. Hence, a small defector population attempting to invade a cooperator metapopulation will face resistance from the residents at both local and regional levels. If the defector's competitive ability is not strong enough to counteract this stochastic resistance, it will fail to invade and be excluded by the cooperator.

With an increasing dispersal rate, the CSS decreases because the availability of empty patches decreases, hindering cooperators from invading. Evolutionary suicide may or may not occur at high dispersal rates, depending upon the characteristics of mutants near the extinction boundary. If the mutants with γ slightly above the extinction boundary are sufficiently good colonisers to resist the invasion by defectors below the boundary, evolutionary suicide (with small mutations) will be prevented. If they are not, the population will evolve to extinction.

The results in the presence of catastrophes and dispersal mortality (Appendix E, Section E.2) further support our proposed paradigm about the evolution of cooperation as a competition-colonisation trade-off. These two factors create more empty patches that bolster the ability of cooperators to invade.

To sum up, a metapopulation structure combined with stochasticity can avert the tragedy of the commons, allowing cooperation to evolve despite defectors being locally dominant. Viewing the evolution of cooperation through the lens of a competition-colonisation trade-off offers a simple explanation of our results. The MFPT results (Appendix E, Section E.3) quantify this notion and substantiate our idea. The somewhat counterintuitive effects of catastrophes and dispersal mortality (Appendix E, Section E.2) are a testament to the proposed explanation.

While we studied the subtle effects of dispersal mortality on how cooperation evolves, we assumed dispersal to remain constant during the process. However, populations that pay this mortality cost of dispersal also face selection pressure on their dispersal rates. In the next chapter, we switch our focus to this question and explore the evolution of dispersal in our metapopulation model. Then, we also consider how the two traits might coevolve.

Chapter 5

Evolving dispersal and cooperation

> But this power [...] of ranging widely, though so unexpected, can, I think, in most cases be explained by their having become fitted, in a manner highly useful to them, for short and frequent migrations from pond to pond, or from stream to stream; and liability to wide dispersal would follow from this capacity as an almost necessary consequence.
>
> Charles Darwin (1859)

In the previous chapter, we saw the importance of dispersal rate on the dynamics of cooperation. The dispersal rate determines whether cooperation evolves, and to what extent. It also affects the nature of the coexistence of cooperators and defectors. Being such a fundamental trait, dispersal will also be under selection. What happens when populations with different dispersal rates compete? How does cooperation affect the evolution of dispersal? Though we have seen that low dispersal rates promote cooperation, is it possible for such low dispersal rates to evolve? What happens when cooperation and dispersal evolve together? In this chapter, we deal with these questions and study the evolution of dispersal and its coevolution with cooperation.

5.1 Evolution of dispersal

First, we explore how dispersal evolves when cooperation is constant. To study the evolution of dispersal in our metapopulation model, we take an approach similar to that we took in the case of cooperation. We study pairwise invasibility and construct PIPs for dispersal rate, and we look at how different factors influence the evolution of dispersal. The primary difference here is that, unlike for cooperation, we do not have a local model to compare with. Recall that the cost of dispersal materialises in the immigration term $I_i = \delta m N_{R,i}$ (2.4), where δ gives the

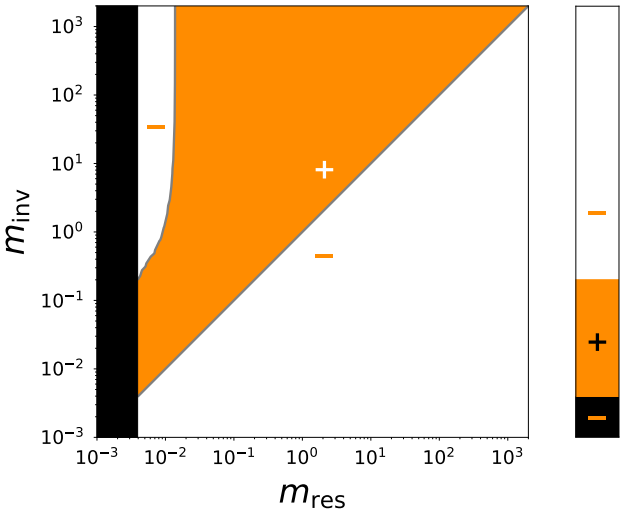

Fig. 5.1. A pairwise invasibility plot (PIP) for dispersal rate (m) in the absence of dispersal mortality ($\delta = 1$). In the square, the coloured ($+$) and white ($-$) portions indicate the resident-invader strategy combinations for which invasion occurs. The black portion shows the strategies for which a resident cannot persist. In the sidebar, the coloured ($+$), white ($-$) and black ($-$) parts indicate the strategy values that can invade an empty system, can persist but cannot invade an empty system and cannot persist, respectively. Parameters: $\gamma = 1$, $\rho = 3.5$, $a = 10$, $c = 1$, $\alpha = 0.04$, $b = 0.05$, $\theta = 2$, $X = 0$.

fraction of dispersing individuals that survive and successfully land on some patch. Thus, the cost affects individuals only when moving from one patch to another.

As a first step, we consider how dispersal evolves in the absence of any dispersal cost. When there is no cost of dispersing, the dispersal rate evolves to infinity (Fig. 5.1). In other words, dispersing more is always beneficial when there is no mortality caused by the process. The reason is straightforward: higher dispersal allows a population to occupy more of the habitat and efficiently recolonise the patches that undergo stochastic local extinctions.

However, faster dispersers need not always successfully invade slower dispersers. Remember that a regional Allee threshold is present for some dispersal rate. In the sidebar in Fig. 5.1, the portion marked with a "+" are the values of the dispersal rate that face no regional Allee effect. If the resident has a low dispersal rate and the invader has a dispersal rate higher than a certain value, the invader cannot invade because it faces a regional Allee effect. However, if the resident has a high enough dispersal rate, the invader with a higher dispersal rate does not face the Allee effect and can invade. Recall that low dispersal rates produce bimodal distributions, whereas high dispersal rates produce unimodal distributions (Chapter 3). If the resident has a low dispersal rate, a large fraction of the patches will remain empty. Consequently, the invader faces an Allee effect. However, for higher dispersal rates, the resident occupies a sufficient proportion of patches for the invader to not face the Allee effect. Nevertheless, Fig. 5.1 reveals that dispersal rates evolve to higher and higher values when there is no cost of dispersing.

On introducing a dispersal cost through mortality, a CSS occurs in dispersal rate (Fig. 5.2). Populations dispersing too fast lose too many individuals during the dispersal process, whereas those dispersing too slowly are unable to sufficiently spread out in the metapopulation. Thus, there is an optimal dispersal rate. In Fig. 5.2, we see another example of evolution to a strategy that cannot invade when rare (see Chapter 4, Section 4.2). The CSS dispersal rate has a regional Allee effect, due to which it will not be able to invade an empty habitat. However, if a resident is already present, it can invade and replace the resident.

Fig. 5.3 further reveals the patterns in the model by showing the CSS dispersal rate (m^*) as a function of cooperation (γ) for different levels of dispersal mortality. Keep in mind that we also have upper and lower limits for γ that also vary with dispersal mortality, due to which the horizontal extents of different curves in Fig. 5.3 are different. In accordance with what one might expect, m^* is lower for higher dispersal mortality (lower fraction of survivors). Further,

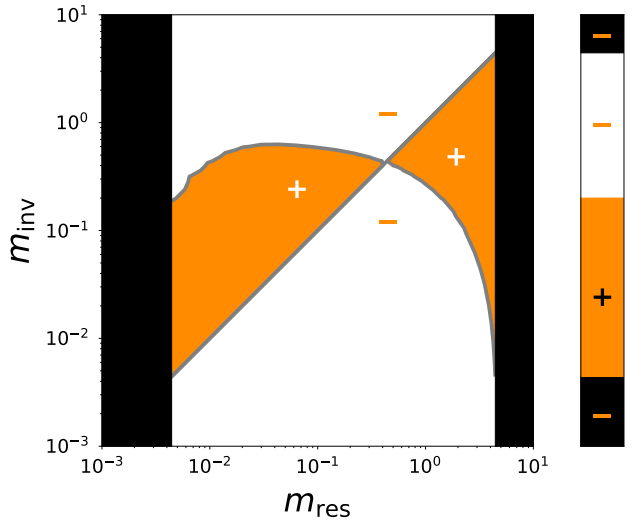

Fig. 5.2. A pairwise invasibility plot (PIP) for dispersal rate (m) dispersal mortality ($\delta = 1$). In the square, the coloured (+) and white (−) portions indicate the resident-invader strategy combinations for which invasion occurs. The black portion shows the strategies for which a resident cannot persist. In the sidebar, the coloured (+), white (−) and black (−) parts indicate the strategy values that can invade an empty system, can persist but cannot invade an empty system and cannot persist, respectively. Parameters: $\gamma = 1$, $\rho = 3.5$, $a = 10$, $c = 1$, $\alpha = 0.04$, $b = 0.05$, $\theta = 2$, $X = 0$, $\delta = 0.9$.

m^* increases with increasing γ, except when γ is close to $\gamma_{\max}$. The increase in m^* is sharp as γ increases from $\gamma_{\min}$, followed by a decrease in the slope. Close to $\gamma_{\max}$, m^* decreases with increasing γ.

The explanation for this pattern lies again in the ecology of the model. It's crucial to note that in the absence of a cost, the dispersal evolves to infinity. Thus, the only incentive for individuals not to disperse is the probability of death during the process. Further, the incentive to disperse is greater when the likelihood of collapse of a patch is greater, as having more colonised patches means a lesser probability of a collapse of all of them.

Near the extremes ($\gamma_{\min}$ and $\gamma_{\max}$), the local carrying capacity K and the local Allee threshold A are close to each other (see Chapter 4, Fig. 4.1). As the equilibrium distributions peak near K, a considerable fraction of the patches will have populations smaller than A, i.e., a negative growth rate. Under such conditions, dispersing more will create sinks that have a smaller likelihood of growing. Additionally, dispersing will enhance the decay of existing high-abundance patches. Thus, dispersing less is beneficial and m^* decreases as we move towards either of the extremes.

Increasing cooperation increases both the birth rate and the death rate (4.1). The effect of increasing the birth (death) rate is two-fold: First, it allows populations to send out more (less) dispersers and colonise more (less) patches despite dispersal mortality. Second, it decreases (increases) the likelihood of the stochastic collapse of a patch, decreasing (increasing) the incentive to disperse and colonise more patches. These two factors oppose each other. As both the birth and the death rate increase when γ increases, we have a total of four effects that interact with each other to produce the trend in m^*. Their combined effect causes the dispersal CSS to increase with increasing cooperation.

We also test the effect of the constant death rate (c) on the evolution of cooperation (see Appendix E, Fig. E.8), which shows that an increased likelihood of collapse promotes greater dispersal. Populations that spread out more by dispersing more are more likely to survive stochastic extinctions than those that are concentrated within a few patches.

Similar is the effect of catastrophes (see Appendix E, Fig. E.9), as increasing catastrophes promote greater dispersal. Since catastrophes hit individual patches, having distributed a greater proportion of patches is more beneficial. However, m^* can also have a maximum when it is varied as a function of the catastrophe rate.

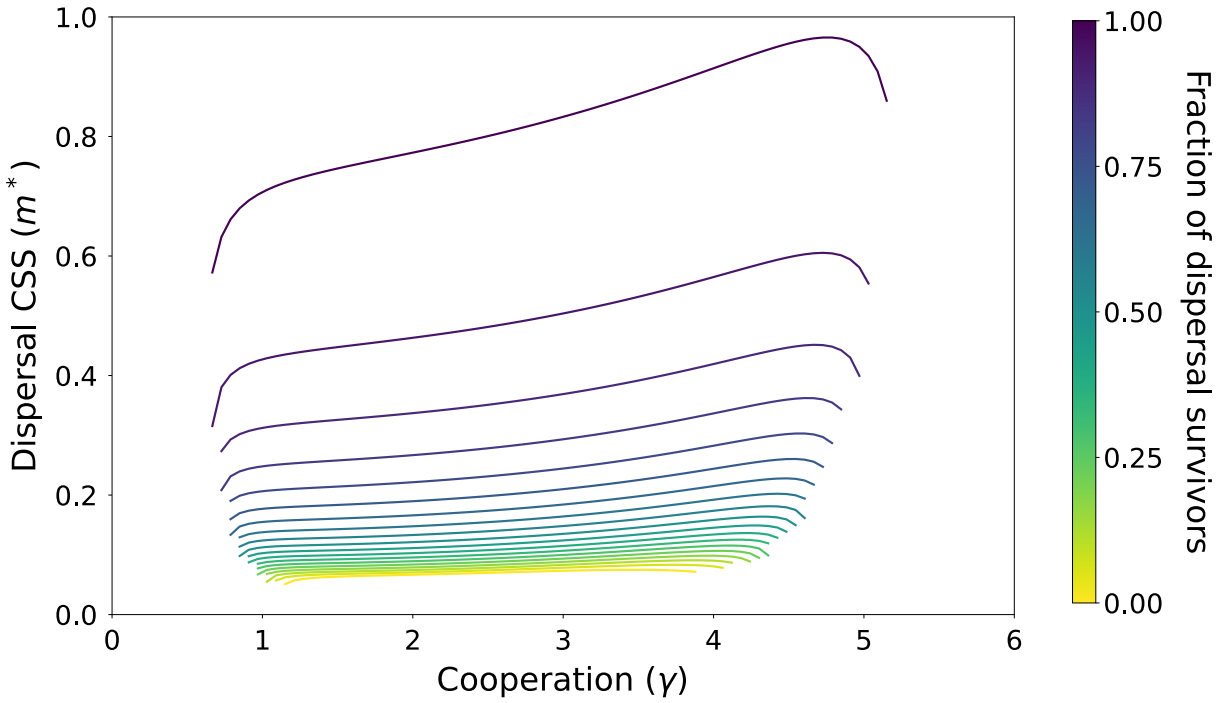

Fig. 5.3. The CSS in dispersal (m^*) as a function of cooperation. Increasing cooperation increases the dispersal CSS, except when cooperation is too high. A higher fraction of dispersal survivors leads to the evolution of a higher dispersal rate. The effect of cooperation is more pronounced when the fraction of dispersal survivors is high, i.e., when the dispersal cost is small. Parameters: $\rho = 3.5$, $a = 10$, $c = 1$, $\alpha = 0.04$, $b = 0.05$, $\theta = 2$, $X = 0$.

We have seen that higher cooperation promotes higher dispersal and also that higher dispersal promotes lower cooperation (Chapter 4). How do these two traits interact when both of them evolve? To study this, we move to the question of coevolution of dispersal and cooperation.

5.2 Coevolution of cooperation and dispersal

To study the situation where both cooperation and dispersal evolve, we make another simplifying assumption. We assume a lack of pleiotropy, i.e., cooperation and dispersal are controlled genes on independent and non-interacting loci. Under such a situation, a coevolutionary CSS (coCSS) is given by the intersection of the curves $\gamma^*(m)$ and $m^*(\gamma)$, where γ^* and m^* are the one-dimensional CSSs in cooperation and dispersal rate, respectively. In all the cases considered, we have observed at most one coCSS.

It may be possible to investigate the coevolution of cooperation and dispersal when the two traits do not evolve independently, but it might require additional assumptions about the genetic correlations between the two traits. We leave this question for the future and focus here on their independent coevolution.

Fig. 5.4 shows the coCSS values as a function of the fraction dispersal survivors. Increasing dispersal mortality leads to the evolution of increasing cooperation and decreasing dispersal. As dispersal rates evolve to smaller values with increased dispersal mortality, and as smaller dispersal rates promote cooperation, we observe that the evolved level of cooperation is high

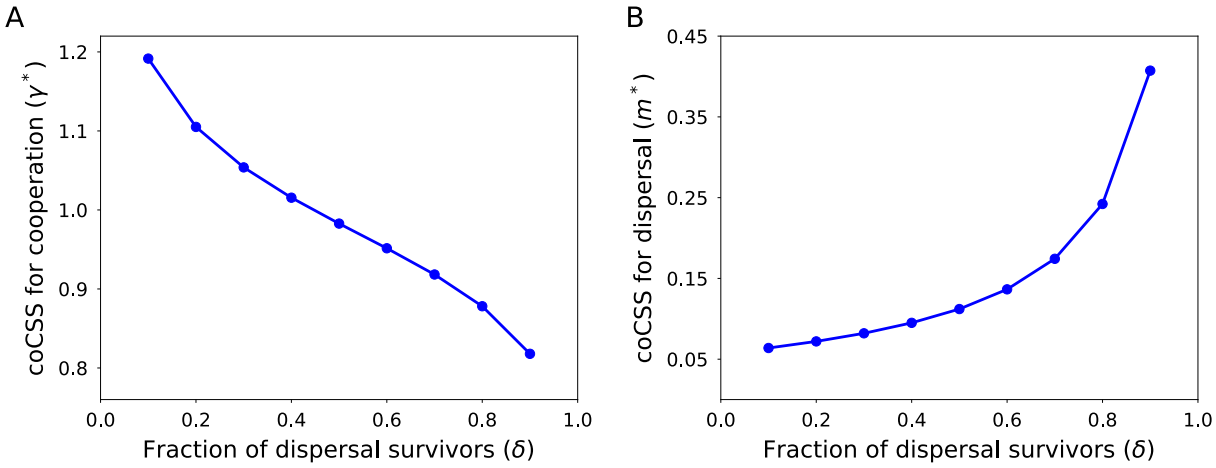

Fig. 5.4. Coevolution of cooperation and dispersal rate. **A** The coCSS in cooperation ($(\gamma^*, m^*)[1]$) as a function of the fraction of dispersal survivors. **B** The coCSS in dispersal ($(\gamma^*, m^*)[2]$) as a function of the fraction of dispersal survivors. Parameters: $\rho = 3.5$, $a = 10$, $c = 1$, $\alpha = 0.04$, $b = 0.05$, $\theta = 2$, $X = 0$.

when dispersal mortality is high.

Thus, there is a negative feedback loop between cooperation and dispersal. Increased cooperation promotes higher dispersal, which in turn promotes lower cooperation. While highly simplistic due to the assumptions of independent mutations, this result on coevolution serves to qualitatively demonstrate the possible outcomes when both dispersal and cooperation evolve.

This was the last of the three chapters that explained the results of our model. Here, we saw how dispersal evolves in populations with local Allee effects, and how cooperation and dispersal coevolve. In the following chapter, we synthesise all these results and discuss their implications and limitations.

Chapter 6

Discussion

> Mountain tops, lakes, individual host plants, a fallen log, a patch of vegetation, a mammalian gut, or, less obviously, a region of optimal temperature or humidity are all islands for the appropriate organisms.
>
> Richard Levins (1970)

We began our quest with the following question: How do cooperators invade and persist despite their ecological and evolutionary fragility that makes them prone to extinction? Knowing that recolonising habitats where the population goes extinct would require immigrants from other spatial locations, we viewed a patch as embedded in a landscape of several patches. To incorporate such a spatial structure, we used a stochastic metapopulation framework. Using this framework, we modelled Allee effects and showed that local Allee effects don't always produce regional Allee effects. Further, we extended the model to evolution and showed that a metapopulation structure favours the evolution of cooperation. Cooperators can be better colonisers and defectors are better competitors. Cooperation can be maintained in a metapopulation due a competition-colonisation trade-off. In this chapter, we synthesise these results together with other related concepts and discuss their applications and limitations.

6.1 Synthesising the ecology and evolution of cooperation

Perhaps the greatest advantage of our modelling framework for studying cooperation is that it is deeply rooted in ecology. Classical frameworks such as the replicator equation (Schuster and Sigmund, 1983) assume constant population sizes and equal growth rates for cooperators and defectors and track the frequencies of cooperators and defectors. These assumptions limit their applicability in biological systems (for example, see Tarnita and Traulsen, 2024). We allow the population sizes to vary as a function of cooperation, enabling us to connect the ecology and evolution of cooperation. Thus, our framework provides a more natural description of the evolution of cooperation by situating it in ecological contexts. Because of the connected nature of our framework, we can also relate the evolution of cooperation with ecological phenomena

like Allee effects and explore the evolution of carrying capacity and Allee thresholds along with their spatial scaling.

The scaling of Allee effects highlights inherent connections between ecological concepts. In ecology, a species is thought to occupy a certain niche if it can overcome the constraints of dispersal limitation, environmental filtering and biotic interactions. In other words, the species has to physically reach the location (dispersal limitation), tolerate the abiotic conditions (environmental filtering) and survive the biotic interactions that take place there. Allee effects materialise through biotic interactions such as cooperation, mate finding or predation or possibly even through environmental filtering. However, the metapopulation-scale strong Allee effects in our model could be interpreted as another scale of dispersal limitation. Here, the limitation is not in the species' ability to reach the habitat but in its ability to spread across the metapopulation to enable its persistence. With an appropriate dispersal rate, the species can exit the extinction regime for the parameter space and invade the habitat. Thus, in addition to the classical dispersal limitation, biotic interactions place additional requirements on a species' dispersal rates for it to persist in a spatial habitat.

With an appropriate dispersal rate, we see how ecological drift propels the invasion of the spatial habitat (Chapter 3, Section 3.5). When the metapopulation is bistable, large abundances are needed to invade and persist. At equilibrium, the local patches remain dynamic, affected by extinctions due to stochasticity and catastrophes and recolonisations due to migration. Therefore, we draw connections between Allee effects and the metacommunity concepts like patch dynamics, mass effects and ecological drift. Illuminated by these insights, we proceed to study the evolution of cooperation in a metapopulation.

While it is well known that spatial structure allows cooperation to evolve, the widely recognised mechanism for that is the spatial clustering of cooperators. As discussed in Chapter 4, there is no possibility of clustering in our model due to its spatially implicit nature. As all patches are well-mixed and equally connected, a cooperator can never surround itself with other cooperators. Instead, we hypothesise that a competition-colonisation trade-off is responsible for the evolution of cooperation in our model. The core idea is that spatial heterogeneity allows cooperators to avoid being exploited by defectors and create enough immigrants that colonise newer patches before their natal patch is taken over by defectors. In principle, this idea is related to Huffaker's (1958) experiments, which concluded that spatial heterogeneity allows prey and predators to coexist.

While we propose a metacommunity theory-based mechanism for the evolution of cooperation, its relationship with other mechanisms merits some discussion. We have already discussed in Chapter 4 how cooperation can arise through clustering in spatially explicit models but not in the implicit model we use. Here, we elaborate on another known mechanism that allows cooperation to evolve, namely, kin selection, and explain how it is distinct from our model yet related (no pun intended) to it. In doing so, we present a scaled interpretation of our results that again draws upon metacommunity theory.

Hamilton (1964a,b) proposed the concept of inclusive fitness, and his eponymous rule (Hamilton, 1963), which states that altruistic behaviours should evolve when the relatedness between individuals is greater than the cost-to-benefit ratio. According to this theory of kin selection, behaviour costly to an individual can evolve if it benefits its relatives, because of shared genes. Since our model doesn't have a notion of relatedness, this concept cannot explain our results. Of course, one may argue that all individuals in our model are equally related to each other, as they are identical in all traits except cooperation. However, this trivial example

of relatedness does not add anything to the explanation.

A similar concept is group selection or multilevel selection, which imagines selection acting on higher levels like groups of individuals rather than individuals themselves. Due to the broader scope of multilevel selection, kin selection can be considered a particular subcase of multilevel selection (Lion and van Baalen, 2008) and Hamilton's rule can be derived from ecological equations in spatial models (Le Galliard *et al.*, 2003; Lion and van Baalen, 2007, 2008; van Baalen and Rand, 1998).

Multilevel selection offers another angle to look at our model. Because defectors are always locally dominant over cooperators, long-term local coexistence requires mass effects that operate through high dispersal rates. Particularly, with low dispersal rates, the interactions within patches occur much faster than the interactions across patches. Under such conditions, the competition-colonisation trade-off in our model can be recast to view patches as individuals. In other words, a patch full of cooperators can be thought of as a cooperator and a patch full of defectors can be thought of as a defector. Then, our model becomes a well-mixed model with a large constant population size and three kinds of patches: cooperator, defector and empty. The rate at which these three interact with each other depends on the dispersal rate. Defector patches are superior competitors against cooperators. Due to local stochasticity, a cooperator patch can also replace a defector patch, and empty patches can replace both cooperator and defector patches. Whether cooperator or defector patches are better off against empty patches depends on the level of cooperation, as those with an intermediate cooperation level are the best colonisers. Thus, a patch becomes an emergent unit of selection, as is seen with several other spatial models (Lion and van Baalen, 2008).

However, note that our model does not formally consider patches as units of selection. Cooperation and competition take place only between individuals, not between patches. All the ecological parameters are defined explicitly for the populations within the patches. The patches are merely spatial containers that restrict individuals within an area. Yet, we observe dynamics where patches seem to act as units of selection. Thus, our work shows that outcomes resembling multilevel selection can occur solely through demographic processes and stochasticity in smaller-scale interactions. Not only does this offer an interpretation of our model, but it also highlights the similarities between the ecological concept of patch dynamics and the evolutionary concept of multilevel selection.

Now, we describe some relations between our work and previous spatial models for the evolution of cooperation. It is known that the scale of cooperation matters in spatially structured systems (Lion and van Baalen, 2008). Kin selection models have shown that when the local abundances are fixed, dispersal has a negligible impact on the evolution of cooperation, while low dispersal promotes cooperation if cooperation increases the local abundance (Lehmann *et al.*, 2006; West *et al.*, 2002). Further, as cooperators are prone to invasion by defectors, cooperators need to be able to disperse to create new colonies (Lion and van Baalen, 2008; Wilson *et al.*, 1992). Despite being based on kin selection, these insights may be applicable more generally due to kin selection being a special case of multilevel selection. Indeed, the variation in population abundance as a function of cooperation is an important factor that creates a competition-colonisation trade-off in our model. The evolutionary suicide we observe with decreasing dispersal rates in some cases (Fig. 4.6; Appendix E, Fig. E.1) could be considered an example of a tragedy of the commons occurring due to the inability of cooperators to "export" individuals and create new cooperator patches (Wilson *et al.*, 1992).

Like most models, we observe that increasing dispersal reduces the level of cooperation

(Akçay, 2020). In an individual-based spatially implicit model, Purcell *et al.* (2012) studied the coevolution of cooperation and dispersal, observing that patch-level extinction leads to the evolution of greater dispersal rates. This result is similar to the effect of catastrophes on the evolution of dispersal in our model. Their model also showed that empty patches promote cooperation, as is the case with our model. Similar results were obtained by Lion and Gandon (2009), though they found the effect of empty space to be nuanced and dependent on the form of cooperation and competition. In an intricate model with a large number of parameters, Lehmann *et al.* (2006) showed that cooperation can evolve when cooperating leads to an increase in the ability to invade new patches and a decrease in the extinction rate of the patches. We obtain similar results using a much simpler model. Overall, our model not only recreates these outcomes of previous studies but also sets a metacommunity frame around them.

Finally, we elaborate on the similarities and differences between our results and those of Lerch *et al.* (2023), on whose framework our model is based. Unlike their Lotka-Volterra competition model, our model does not have the possibility of local coexistence in the deterministic well-mixed case. While they observed that the parameter space allowing coexistence decreased in the spatially structured case, we see the opposite results: spatial structure allows regional and local coexistence, unlike the well-mixed case. They observed that a competition-colonisation trade-off can allow coexistence, and we use the same concept to explain why cooperation evolves in our model. Note that their competition-colonisation trade-off is based on differences in two parameters: the interspecific competition coefficient and the dispersal rates. However, the trade-off in our model emerges from a single parameter, i.e., cooperation, even for equal dispersal rates. This makes more sense if we consider an inclusive definition of colonisation that takes into account not only the ability to enter a patch but also to hold on to it. Another important difference is that Lerch *et al.* (2023) formally define parameters like intrinsic growth rate and local carrying capacity, whereas we assume them to emerge from cooperative interactions. Their approach allowed them to explore the metacommunity archetypes in the model, while ours is more suited towards focusing on the evolution of cooperation.

6.2 Implications for applied ecology

Our model generates several insights that could potentially inform the practices employed in fields such as conservation biology and invasion biology. Needless to say, one must exercise high caution while applying the results from general theoretical work such as this, as these results emerge from several modelling assumptions and without any thought about a specific organism or ecosystem. Examining which of these assumptions are relevant to a system under consideration is essential while deducing practical measures based on such theoretical frameworks. Nevertheless, one can conjecture a few possible applications of our models to real-world metapopulations. We first discuss the relevance of our results to species conservation and then discuss how they could be apposite in managing the spread of invasive species.

Conservation biology aims to protect species from extinction for various reasons, including beliefs in the intrinsic value of diversity (Soulé, 1985). Allee effects are a vital concern in conservation praxis due to the role they play in small or sparse populations that may be close to extinction (Courchamp *et al.*, 2008). The switch in the sign of the growth rate, when the population falls below the Allee threshold, is of particular concern, as recovery becomes difficult and the population heads towards extinction. Allee effects have been detected in a number of species of concern from the point of view of conservation, including several mammal, bird, fish,

arthropod and other species (reviewed in detail in Kramer *et al.*, 2009).

Habitat fragmentation due to human activities has narrowed the ranges of a large number of species and divided their populations into several small groups. These populations cornered into narrow ranges suffer a greater risk of extinction due to Allee effects. One of the measures taken to protect fragmented populations is to connect them via "wildlife corridors", which are areas that link habitat patches separated by anthropogenic activities (Rosenberg *et al.*, 1997). These links can facilitate the dispersal of animals and prevent extinction due to Allee effects and adverse genetic effects like inbreeding depression. Our model indicates that if a patch has a stable population, connecting it to a small-abundance patch can save the latter from extinction. However, if multiple patches have small abundances, taking the magntidue of the Allee effects may be crucial when planning corridor design, as an excessive increase in the dispersal rates can be counterproductive in that case if individuals desert patch while its abundance is growing.

A related question is the single large or several small (SLOSS) debate, which asks whether it is more beneficial to conserve an at-risk population within one large patch or multiple smaller patches. In the context of our model, increasing the dispersal rates is similar to melding all the patches into one, whereas decreasing them could be thought of as having several distinct patches. Once again, the magnitude of the local Allee threshold plays a role, denoting that single large patches may be favourable when the local Allee threshold is high, whereas having intermediate dispersal rates is the most favourable for low local Allee thresholds. Our model thus broadly agrees with that of Zhou and Wang (2006), whose simulations showed that an intermediate size and number of reserves is optimal to enhance metapopulation persistence when Allee effects are present.

Allee effects have concerned conservationists because of their importance in small populations. Our work evinces that along with reduced population sizes, a reduction in dispersal rates can also fuel extinction. Specifically, the transition between the extinction regime and the bistability regime (Figs. 3.4, 3.5 B,C, 3.6) occurs abruptly through a saddle-node bifurcation. Thus, reduced dispersal rates due to habitat loss or fragmentation may cause an entire metapopulation to go extinct without a preceding decline in population size. As the population may not fall to a small size before going extinct, monitoring population sizes may not be able to predict such extinctions. Anticipating these events would require detailed knowledge of the severity of the Allee effect and the rates of movement of individuals across patches. Hence, using well-mixed models can underestimate the extinction risk, and the spatial structure of the habitat should be accounted for while analysing the state of a population. However, observing strong bimodality in the system may possibly indicate the closeness to the critical dispersal rate, as we observe bimodal distributions near the extinction boundary (Figs. 3.6, 3.7).

As humans traverse different parts of the world, they also sometimes carry species from one geographical region to another, intentionally or unintentionally. When these species are introduced into new environments, they have the potential to adversely affect the native species and the interactions among them. The newly introduced species can turn invasive and dominate the new environment. Along with their destructive ecological influence, some invasive species also have negative consequences for human health and the economy. To restore the ecological balance and avoid other harmful effects, it is essential to take steps to eradicate invasive species and control their outbreaks.

While Allee effects may be a bane for conservation, they are a boon for managing the spread of invasive species. Invasive species like gypsy moth, house finch, Eurasian ruffe and

nutria rodents have been shown to face Allee effects (Kramer *et al.*, 2009).

One can bank upon this flipside of Allee effects to curb the growth and spread of invasive populations. Our model hints at some conceptual propositions and conceivable methods for controlling invasive species in spatial habitats, which could be further explored by studies that model specific ecosystems.

It is often observed that invasive species are maintained at small abundances for a long time before their population explodes (Courchamp *et al.*, 2008). This phenomenon has been attributed to weak Allee effects, due to which a population has a small growth rate until it reaches a sufficiently large abundance. Our results suggest that in spatial habitats, this type of pattern can occur due to low dispersal rates. An invasive species with a small abundance may stay close to the extinction boundary with a bimodal distribution, such as it occupies very few patches where its population is large enough to overcome the local Allee effect. Increased dispersal rates due to changes in the environment or repeated introductions due to human activities might enable mass effects and fuel its spread in the region.

Since dispersal rates play a key role in the dynamics, it may be possible to envision eradication strategies that target the dispersal of populations. Modulating dispersal between patches can not only prevent the direct spread of invasive populations but also strengthen the Allee effect, helping restrain its spread.

Additionally, another strategy employed for controlling invasive species is to induce an Allee effect in the population by techniques such as introducing sterile individuals or parasites into the populations (Courchamp *et al.*, 2008). According to our results, in situations where an invasive population occupies the region despite local Allee effects, it can be possible, in principle, to induce a regional Allee effect by performing local eradications. Akin to catastrophes, focusing on the removal of the species from certain parts of the region can raise the regional Allee threshold, making re-invasion more difficult.

Although our model could be suggestive in several ways for applied branches of ecology, as mentioned previously, pragmatically considering which of our assumptions are germane to particular systems is necessary while making practical decisions. Felicitous system-specific models that derive ideas from our framework could potentially serve such purposes. In this regard, one must also be careful about the limitations and core assumptions on which our model is based. We discuss these limitations in depth in the following section and specify some of the ways in which future research could overcome or build upon them.

6.3 Limitations and future directions

Numerous limitations of our model and the results presented ought to be highlighted. Some of these limitations are intrinsic to the assumptions of our framework, rectifying which may require an entire shift in its mathematical structure. On the other hand, relaxing some of the assumptions and overcoming the limitations could form directions for future work.

We begin by discussing the former kind of limitations. First, we assume that the metapopulation consists of infinitely many patches. While such a model may well approximate a system where the number of patches is large, assuming an infinite number of them is an important limitation despite its mathematical advantages. Specifically, this assumption allows us to equate the instantaneous regional probability distribution with the local probability distribution over time, and make use of the black-box function to calculate equilibrium points. In our model, stochasticity plays a role in the demographic processes. However, the regional outcomes are de-

terministic. With a finite number of patches, stochasticity may become important at a regional scale. Thus, assuming a finite number of patches may preclude us from elegantly modelling the probability distributions but may also provide us with more realistic insights about natural systems.

Second, we assume global dispersal, i.e., that all patches are equally connected to each other. Again, this mathematical idealisation serves us in developing a general theory but fails to take distances between the patches into account. Patches in natural habitats are at different distances from each other, due to which dispersal need not take place at equal rates across all patches.

While these assumptions are central to our framework, modifying them may be essential while constructing models applicable to specific systems to pragmatically study the interplay of spatial dynamics with Allee effects and cooperation.

Now, we look at the limitations of our work that can potentially act as stepping stones for future research in the field. These include exploring transient dynamics, the density dependence of dispersal, the role of timescales and the individual payoff dynamics.

First, we impose some assumptions on the role of time in our model. As with several evolutionary models, we assume a clear separation of timescales between ecological and evolutionary processes. Though our framework incorporates ecological factors such as population sizes and Allee effects, our analysis of the evolution of cooperation separates the ecological dynamics from its evolutionary counterpart. Particularly, we assume that mutations are rare so that a dimorphic population reaches its equilibrium before a mutation occurs. Nevertheless, with the growing understanding that evolution can take place at much faster timescales than previously expected (for instance, see Hairston Jr *et al.*, 2005), it is important to also investigate the eco-evolutionary dynamics of cooperation. Additionally, we have shown that two different morphs can coexist with large mutations. Though we expect such coexistence to be transient on the evolutionary timescale, future work could try to confirm this and explore how evolution proceeds when two different morphs co-occur in the metapopulation. However, as the two-morph metacommunity model is already computationally heavy, multi-species theoretical investigations would likely require methodological innovations that can handle stochasticity along with multi-strategy dynamics.

Second, though our model can stand for cooperative interactions mediated by a common good (see Appendix C), the dynamics of the common good are subsumed within the equations for population dynamics. This formulation ignores the timescale of the common good itself, such as its growth, lifespan, and decay. Future studies could explicitly incorporate the common good dynamics into our model, to potentially reveal the feedback between the cooperative strategy and the resource. For instance, differential timescales may lead to oscillatory dynamics between the resource and the consumer (Weitz *et al.*, 2016). It may also influence our results on Allee thresholds, such as reducing the invasion propensity in the metapopulation if the common good is slow to build up. Further, depending on whether the common good is stationary or mobile, different levels of cooperation may be favoured. For example, mobile common goods may favour defection due to the reduced ability of individuals to privatise them.

Third, besides the interactions mediated by common goods, cooperation in nature can take several different forms. How a metapopulation structure affects the evolution of cooperation in these cases remains a standing question that future studies could explore. To illustrate, consider the case of the Hawk-Dove game (Osborne and Rubinstein, 1994). In a well-mixed population playing this game, the evolutionarily stable strategy is a mixed strategy to cooperate or defect

with a certain probability. This result arises because an individual receives the maximum payoff on interacting with an individual with the opposite strategy. Hence, an equilibrium population consists of a mixture of cooperators and defectors. When one considers strategies varying on a continuum, this game can favour either cooperation or defection and produce wonderful phenomena such as evolutionary branching and bistability (Doebeli *et al.*, 2004). Moreover, spatial structure in the Hawk-Dove game can actually hamper the evolution of cooperation, if the cost of cooperation is high (Hauert and Doebeli, 2004). Thus, incorporating different kinds of payoff structures into our metapopulation model can form another line of work. Including explicit game dynamics into our model would require appropriately transforming the payoffs into population growth rates. For example, to convert our model to Hawk-Dove, one might consider including a cost of defection in the per-capita growth rate, that makes competition with the opposite strategy the best outcome. Such analyses for different payoff structures may reveal deeper associations between metacommunity ecology and the evolution of cooperation.

Fourth, our metapopulation model assumes density-independent dispersal. The probability of an individual migrating into a patch and away from that patch is not influenced by the local population on that patch. Though this assumption may be valid for certain organisms, local densities often influence the probability that an individual migrates (Matthysen, 2005). For example, individuals in overcrowded patches may be more likely to migrate. In cognitively complex organisms, if individuals are aware of the benefits of having a threshold abundance level and can sense the population sizes, sparsely occupied patches may attract fewer immigrants. Preferential group sizes can coevolve with cooperation (Powers *et al.*, 2011) or even produce coevolutionary cycles (Avilés, 2002). When dispersal evolves, the cost of dispersal can affect its relationship with population density (Travis *et al.*, 1999). Future work could explore how Allee effects, cooperation, and dispersal evolve under such scenarios of density-dependent dispersal.

6.4 Conclusion

Populations can span multiple spatial scales, where the processes at one scale affect the processes at other scales. This feedback between scales can have consequences for the ecological and evolutionary dynamics of populations, producing distinct patterns on different scales. Thus, how phenomena at one scale manifest at other scales is an important question in ecology and evolution.

In this thesis, we have explored the scaling of cooperation to understand its persistence on ecological and evolutionary timescales. Ecologically, we saw that the interplay of spatial scales can make Allee effects disappear, producing contrasting patterns on different scales: locally, small populations tend to shrink, yet, the population can grow on the regional scale. Evolutionarily, we saw that competition between cooperators and defectors can produce opposite patterns on different scales: although defectors locally outcompete cooperators, cooperators can outcompete defectors on the regional scale. We explain these results using concepts in metacommunity ecology, a field whose heart is the problem of spatial scales.

Thus, the research presented here highlights the significance of scale in ecology and evolution in general, as well as in the particular case of cooperation. By integrating metacommunity ecology and cooperation, we hope to have unveiled new paradigms and perspectives that may inspire future breakthroughs in ecology and evolution.

Appendix A

Analytical proofs and explanations

In this appendix, we provide some analytical and numerical justifications for the model results. Specifically, we prove the outcomes for no dispersal and high dispersal, derive an expression for the regional abundance, use it to calculate the equilibria in the high-dispersal limit and analytically explain the comparison between high-dispersal equilibria and the local equilibria in the nonspatial deterministic model. Finally, we also show that the local deterministic model is recovered in the limit of large abundance and high dispersal.

A.1 Stochastic population collapse in the absence of dispersal

Here, we prove that the only equilibrium in the stochastic open system model and in the metapopulation model in the absence of dispersal is extinction. I.e., if $m = 0$ ($\implies I = E = 0$), then the equilibrium distribution is given by $P_{\text{eq}}(0) = 1, P_{\text{eq}}(N) = 0$ for $N > 0$. We first prove the two base cases of $P(1) = P(2) = 0$ and then use mathematical induction.

Consider the master equation (2.6) with $I = 0$. As $B(0) = 0$ for a population to make sense biologically, the equation for $\frac{d}{dt}P(0,t)$ in the absence of immigration ($I = 0$) is

$$\frac{d}{dt}P(0,t) = [D(1) + E(1)]P(1) - XP(0) + X$$

If $X = 0$, then it is obvious that at equilibrium $P_{\text{eq}}(1) = 0$. If $X > 0$,

$$P_{\text{eq}}(0) = \frac{1}{X}[D(1) + E(1)]P(1) + 1$$

Because probability cannot be greater than 1 and as $D(1) \neq 0, E(1) \neq 0$, $P_{\text{eq}}(1) = 0$. Now, consider the equation for $\frac{d}{dt}P(1,t)$. As $B(0) = 0$, $I = 0$ the equation for $\frac{d}{dt}P(0,t)$ in the absence of immigration is

$$\frac{d}{dt}P(1,t) = [D(2) + E(2)]P(2) - [B(1) + I + D(1) + E(1) + X]P(1)$$

But as $P_{\text{eq}}(1) = 0$ as shown above, $P_{\text{eq}}(2) = 0$. Now consider the general master equation (2.6) again. At equilibrium, if $P_{\text{eq}}(N-1) = P_{\text{eq}}(N) = 0$, it is clear that $P_{\text{eq}}(N+1) = 0$. With the two base cases, $P_{\text{eq}}(1) = P_{\text{eq}}(2) = 0$, the proof that $P_{\text{eq}}(N) = 0$ for $N > 0$ is complete by mathematical induction, implying that $P_{\text{eq}}(0) = 1$ in the absence of dispersal.

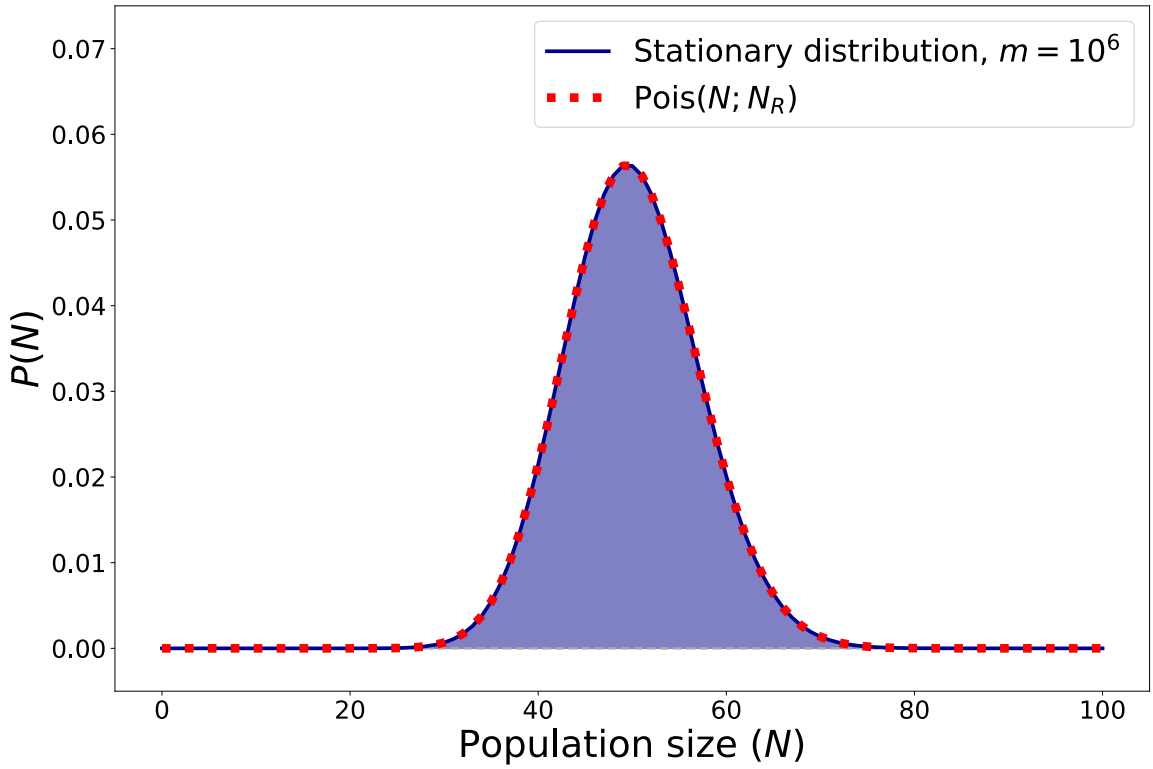

Fig. A.1. The stationary distribution in the stochastic open system model approaches a Poisson distribution for high dispersal rates. Parameters: $r = 1$, $A = 10$, $K = 50$, $a = 10$, $N_R = 50$, $X = 0$.

In the metapopulation model, each local population will go extinct in the absence of dispersal, as proved above. Thus, the metapopulation goes extinct in the absence of dispersal.

Note that extinction in the absence of dispersal is only a long-term outcome, and it may take a long time for the population to go extinct, depending on its abundance. The difficulty in tracking the transient dynamics and evolutionary outcomes in such cases is indeed a drawback of our model.

A.2 Poisson distribution in the high-dispersal limit

Consider the stochastic open system model (Subsection 2.2.2) with a constant regional abundance of N_R and no catastrophes ($X = 0$). At the stationary distribution, $\frac{d}{dt}P(i) = 0 \; \forall \; i$. As $m \to \infty$, locally, the process is driven solely by migration events since the immigration and emigration rates are very large compared to the birth and death rates. We use mathematical induction to prove that the resulting stationary distribution is given by

$$P(n) = \frac{N_R^n}{n!}P(0) \tag{A.1}$$

First, we prove the two base cases $P(0)$ and $P(1)$. For $n = 0$, it is trivial from (A.1) that $P(0) = P(0)$.

From (2.6), we can write that at equilibrium, under the limit $m \to \infty$,

$$P(1) = \frac{I}{E(1)}P(0) = \frac{mN_R}{m}P(0) = N_R P(0)$$

which satisfies (A.1). Now, we assume that the equation applies to $n = k$ and $n = k + 1$ and then prove that it applies to $n = k + 2$. From (2.6), at equilibrium

$$\begin{aligned} P(k+1) &= \frac{(I + E(k))P(k) - IP(k-1)}{E(k+1)} \\ &= \frac{(mN_R + mk)P(k) - mN_R P(k-1)}{k+1} \\ &= \frac{1}{k+1}\left((N_R + k)\frac{N_R^k}{k!}P(0) - N_R\frac{N_R^{k-1}}{(k-1)!}P(0)\right) \\ &= \frac{N_R^{k+1}}{(k+1)!}P(0) \end{aligned}$$

By induction, we have proved equation (A.1). Now, we calculate the value of $P(0)$ by observing that the probability distribution must sum to 1, giving us

$$\sum_i \frac{N_R^i}{i!}P(0) = 1 \implies e^{N_R}P(0) = 1 \implies P(0) = e^{-N_R}$$

Hence, we have proved that

$$P(n) = \frac{N_R^n}{n!}e^{-N_R} \tag{A.2}$$

i.e., the stationary distribution in the stochastic open system is a Poisson distribution with a Poisson parameter N_R. Fig. A.1 compares the stationary distribution for a high dispersal rate ($m = 10^6$) to a Poisson distribution, showing that they are near identical.

A.3 An expression for the regional dynamics

The dynamics of the average local (i.e., regional) abundance $\overline{N}$ in the metapopulation model are given by (2.13). We can derive it as follows:

$$\begin{aligned} \overline{N}(t) &= \sum_{N=0}^{\infty} NP(N,t) = \sum_{N=1}^{\infty} NP(N,t) \\ \implies \frac{d\overline{N}}{dt} &= \sum_{N=1}^{\infty} N\frac{d}{dt}P(N,t) \\ \implies \frac{d\overline{N}}{dt} &= \sum_{N=1}^{\infty} N\{[B(N-1) + I(N-1)]P(N-1,t) \\ &\quad + [D(N+1) + E(N+1)]P(N+1,t) \\ &\quad - [B(N) + I(N) + D(N) + E(N) + X]P(N,t)\} \end{aligned}$$

Splitting the summation over the terms, we have

$$\begin{aligned}\frac{d\overline{N}}{dt} &= \sum_{N=1}^{\infty} N[B(N-1)+I(N-1)]P(N-1,t) \\ &+ \sum_{N=1}^{\infty} N[D(N+1)+E(N+1)]P(N+1,t) \\ &- \sum_{N=1}^{\infty} N[B(N)+I(N)+D(N)+E(N)+X]P(N,t)\end{aligned}$$

Now, we change the variables and put $x = N-1$ and $y = N+1$.

$$\begin{aligned}\frac{d\overline{N}}{dt} &= \sum_{x=0}^{\infty} (x+1)[B(x)+I(x)]P(x,t) \\ &+ \sum_{y=2}^{\infty} (y-1)[D(y)+E(y)]P(y,t) \\ &- \sum_{N=1}^{\infty} N[B(N)+I(N)+D(N)+E(N)+X]P(N,t)\end{aligned}$$

Expanding, we get

$$\begin{aligned}\frac{d\overline{N}}{dt} &= \sum_{x=0}^{\infty} x[B(x)+I(x)]P(x,t) + \sum_{x=0}^{\infty} [B(x)+I(x)]P(x,t) \\ &+ \sum_{y=2}^{\infty} y[D(y)+E(y)]P(y,t) - \sum_{y=2}^{\infty} [D(y)+E(y)]P(y,t) \\ &- \sum_{N=1}^{\infty} N[B(N)+I(N)+D(N)+E(N)+X]P(N,t)\end{aligned}$$

which can be rearranged as

$$\begin{aligned}\implies \frac{d\overline{N}}{dt} &= \sum_{x=1}^{\infty} x[B(x)+I(x)+D(x)+E(x)]P(x,t) \\ &+ \sum_{x=0}^{\infty} [B(x)+I(x)-D(x)-E(x)]P(x,t) \\ &- \sum_{y=0}^{1} y[D(y)+E(y)]P(y,t) + \sum_{y=0}^{1} [D(y)+E(y)]P(y,t) \\ &- \sum_{N=1}^{\infty} N[B(N)+I(N)+D(N)+E(N)+X]P(N,t)\end{aligned}$$

finally giving us

$$\frac{d\overline{N}}{dt} = \sum_{x=0}^{\infty} [B(x)+I(x)-D(x)-E(x)-xX]P(x,t)$$

which we expand further.

$$\frac{d\overline{N}}{dt} = \sum_{x=0}^{\infty}[B(x) - D(x) - xX]P(x,t) + \sum_{x=0}^{\infty}[I(x) - E(x)]P(x,t)$$

Since $I(N) = \delta\overline{N}$ and $E(N) = mN$, we have

$$\sum_{x=0}^{\infty}[I(x) - E(x)]P(x,t) = \delta m\overline{N}\sum_{x=0}^{\infty}P(x,t) - m\sum_{x=0}^{\infty}xP(x,t) = \delta m\overline{N} - m\overline{N} = (\delta - 1)m\overline{N}.$$

Thus, we get

$$\frac{d\overline{N}}{dt} = \sum_{x=0}^{\infty}[B(x) - D(x)]P(x,t) - [X + (1-\delta)m]\overline{N}$$

which is equation (2.13).
In the absence of catastrophes and dispersal mortality,

$$\frac{d\overline{N}}{dt} = \sum_{N=0}^{\infty} f(N)P(N,t) \tag{A.3}$$

A.4 Metapopulation equilibria in the high-dispersal limit

Consider a birth-death function given by the logistic equation (i.e., $f(N) = rN(1 - N/K)$) in the absence of any catastrophes or dispersal mortality. The equilibria in the high dispersal limit can be calculated as follows:

$$\begin{aligned}
&\sum_N f(N)\text{Pois}(N;\overline{N}) = 0 \\
\implies &\sum_N rN\big(1 - \frac{N}{K}\big)\text{Pois}(N;\overline{N}_{\text{eq}}) = 0 \\
\implies &\sum_N rN\text{Pois}(N;\overline{N}_{\text{eq}}) - \sum_N \frac{rN^2}{K}\text{Pois}(N;\overline{N}_{\text{eq}}) = 0 \\
\implies &\overline{N}_{\text{eq}} - \frac{1}{K}(\overline{N}_{\text{eq}} + \overline{N}_{\text{eq}}^2) = 0 \text{ (from the moments of the Poisson distribution)} \\
\implies &\overline{N}_{\text{eq}} = 0 \text{ or } \overline{N}_{\text{eq}} = K - 1
\end{aligned} \tag{A.4}$$

An analytical calculation of this kind is not possible for $f(N)$ given by (3.3). Hence, we apply a numerical root-finding algorithm to (2.14, $f(N)$ given by 3.3) in the absence of dispersal mortality ($\delta = 1$) to calculate the equilibria as $m \to \infty$. We consider the case without dispersal mortality because high dispersal causes extinction when $\delta < 1$. In Fig. A.2, we compare the equilibria obtained from (2.14) to the equilibria obtained from the LMAO function (2.11) for a high value of the dispersal rate ($m = 10^6$). The close match highlights that with high dispersal, the system dynamics indeed approach (2.13).

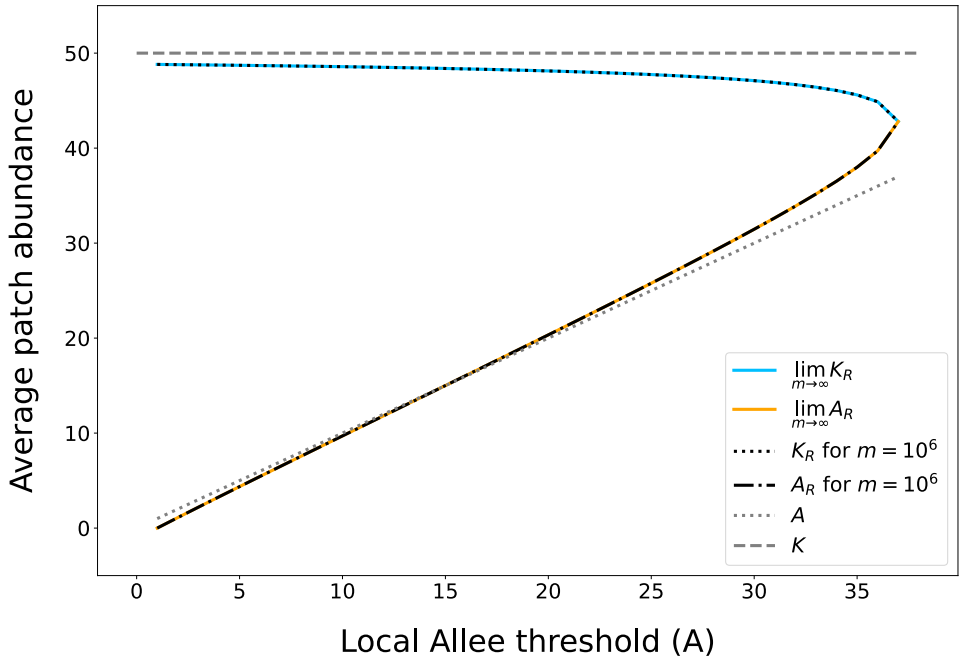

Fig. A.2. The averages of metapopulation equilibria in the high-dispersal limit obtained by solving (2.14) for different local Allee threshold values, and their comparison with the metapopulation equilibria from the LMAO function for $m = 10^6$. The local equilibria are also shown for comparison. Parameters: $r = 1$, $K = 50$, $a = 10$, $X = 0$.

In addition, we also plot alongside the local equilibrium values in Fig. A.2. This comparison demonstrates that as the dispersal rate approaches infinity ($m \to \infty$), the regional carrying capacity (K_R) approaches a value smaller than the local carrying capacity (2.15, Fig. 3.5). The regional quasi-Allee threshold (A_R), on the other hand, approaches a value smaller than its local counterpart (A) if A is small, but a value larger than A if A is large.

A.4.1 Heuristics based on Jensen's inequality

We use Jensen's inequality (Ross, 2010) to explain the mathematical reasons for the behaviour of our model in the limit of high dispersal.

The regional carrying capacity with high dispersal

Here, we illustrate why $\lim_{m\to\infty} K_R < K$. We denote $\lim_{m\to\infty} K_R$ as K_R^∞. Jensen's inequality states that for a convex function ϕ and a random variable X, $\phi(\mathrm{E}[X]) \leq \mathrm{E}[\phi(x)]$. The equality occurs when ϕ is linear or when X is degenerate. For a concave function, the opposite is true, i.e., $\phi(\mathrm{E}[X]) \geq \mathrm{E}[\phi(x)]$.

Take the death rate function in the deterministic nonspatial model, which is given by $D(N) = cN + \alpha N^2$ 3.1. In the overall growth rate $f(N) = B(N) - D(N)$, this function takes a negative sign. The function $-D(N)$ is concave in nature. By Jensen's inequality,

$$-D(\sum_N N\mathrm{Pois}(N; K_R^\infty)) > -\sum_N D(N)\mathrm{Pois}(N; K_R^\infty)$$

Since $\sum_N N\mathrm{Pois}(N; K_R^\infty) = K_R^\infty$,

$$-D(K_R^\infty) > -\sum_N D(N)\mathrm{Pois}(N; K_R^\infty) \tag{A.5}$$

Now, consider the birth rate function $B(N) = \frac{\rho N^2}{N+a}$. This function is convex in nature. However, for high enough N, it is approximately linear. The second derivative is given by

$$B''(N) = \frac{2a^2}{(N+a)^3}$$

For the parameters $a = 10$ and $N = 50$, $B''(N) \approx 0.0009$. The small second derivative shows the approximate linearity. Moreover, assuming that K is sufficiently large and that K_R^∞ is close to K, the distribution $\text{Pois}(N; K_R^\infty)$ provides a negligibly small weight to the highly nonlinear parts of B. So, by Jensen's inequality, we can write

$$B\left(\sum_N N\text{Pois}(N; K_R^\infty)\right) + \varepsilon = \sum_N B(N)\text{Pois}(N; K_R^\infty)$$

where ε is a small positive number.
Thus, we have

$$B(K_R^\infty) \approx \sum_N B(N)\text{Pois}(N; K_R^\infty) \tag{A.6}$$

Adding (A.5) and (A.6), we have

$$B(K_R^\infty) + D(K_R^\infty) > \sum_N (B(N) + D(N))\text{Pois}(N; K_R^\infty)$$

$$\implies f(K_R^\infty) > \sum_N f(N)\text{Pois}(N; K_R^\infty)$$

From (A.3), in the absence of catastrophes, we have

$$\implies f(K_R^\infty) > \frac{d\overline{N}}{dt}(N_R = K_R^\infty)$$

Since K_R^∞ is a regional equilibrium, $\frac{d\overline{N}}{dt}(\overline{N} = K_R^\infty) = 0 \implies f(K_R^\infty) > 0$. Thus, the non-zero stable equilibrium of the metapopulation model occurs when f is positive, i.e., at a smaller value than K. Hence, as Fig. A.2 depicts,

$$\lim_{m\to\infty} K_R < K$$

The regional quasi-Allee threshold with high dispersal

The difference between $\lim_{m\to\infty} A_R$ (henceforth, A_R^∞) and A can be partly explained using Jensen's inequality. The overall growth rate function (3.3) has a convex part and a concave part. They are separated by an inflection point, which some tedious algebra shows to occur at $N_{\text{flex}} = [a(A+a)(K+a)]^{1/3} - a$. The distribution corresponding to A_R^∞ is a Poisson distribution, as we have seen. For $A < N_{\text{flex}}$, A is in the convex part. Assuming that A_R^∞ is close to A and that A is sufficiently small, the probability mass corresponding to the distribution is mostly concentrated in the convex part. By Jensen's inequality,

$$f(A_R^\infty) < \sum_N f(N)\text{Pois}(N; A_R^\infty)$$

Since A_R^∞ is a regional equilibrium,

$$\implies f(A_R^\infty) < 0$$

Thus, the unstable equilibrium of the stochastic closed system occurs when f is negative, i.e., at a smaller value than A. However, as A becomes larger, the probability mass in the concave region of the function keeps growing and cannot be ignored. Beyond a threshold, A_R^∞ exceeds A (Fig. A.2).

A.4.2 Recovering the original model

While we have shown above that the regional carrying capacity (K_R) in the high dispersal limit must always be smaller than the local carrying capacity K, the former approaches the latter as the latter tends to infinity. I.e., $\lim_{m,K\to\infty} K_R = K$. Consider the example of the logistic model (A.4) given at the beginning of Section A.4. Clearly, $\lim_{K\to\infty} K_R = K$ in that case.

Fig. A.3 A shows $\lim_{m\to\infty} \frac{K_R}{K}$ as a function of K for our metapopulation model with Allee effects (Chapter 3, Section 3.4). The parameters A and a are scaled with K. The ratio $\frac{K_R}{K}$ approaches 1 with increasing K.

Similarly, the regional quasi-Allee threshold (A_R) also approaches the local Allee threshold (A) if both A and K tend to infinity. In Fig. A.3 B, we scale A with K and plot $\lim_{m\to\infty} \frac{A_R}{A}$ against increasing K to depict that $\lim_{\substack{m,K\to\infty,\\ A=\kappa K}} A_R = A$ where $\kappa \in [0, 1)$ is a constant. Interestingly, the A_R approaches A only if we scale A with K. If A is kept constant as K increases, $\lim_{m,K\to\infty} A_R \neq A$.

In other words, for large population sizes, stochastic fluctuations— the source of the difference between the deterministic and average stochastic equilibria— become irrelevant, and we recover the original deterministic model for high dispersal rates.

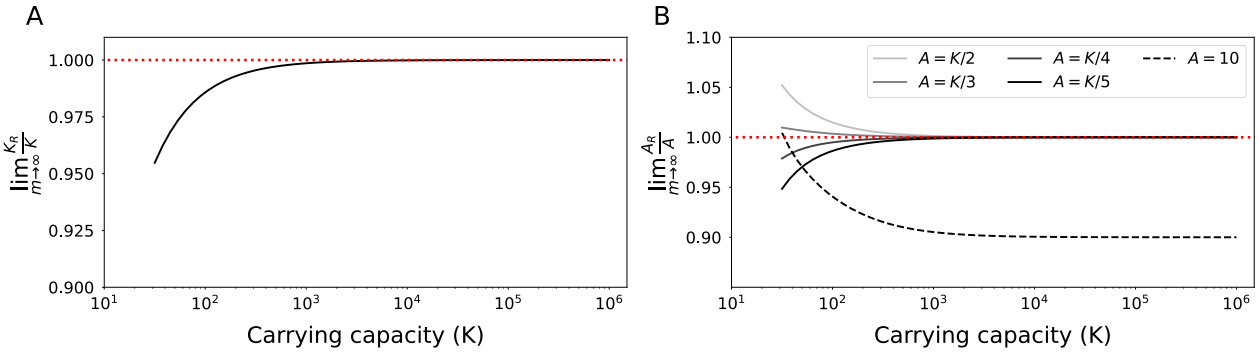

Fig. A.3. The averages of the metapopulation equilibria for high dispersal rates approach the local equilibria with increasing carrying capacity. **A** The ratio of regional carrying capacity and local carrying capacity (K_R/K) as a function of the local carrying capacity (K) for $m \to \infty$. $A = K/5$. **B** The ratio of regional quasi-Allee threshold and local Allee threshold (A_R/A) as a function of the local carrying capacity (K) for $m \to \infty$ for different constant A/K ratios. Parameters: $r = 1$, $a = K/5$, $X = 0$.

Appendix B

Jacobian calculations in the metapopulation model

In this appendix, we derive the Jacobian matrix for the metapopulation model (Chapter 2, Section 2.2, Subsection 2.2.3), i.e., the Jacobian matrix of (2.7) in conjunction with (2.9). The eigenvalues of this matrix can be used to assess the stability of a fixed point. Additionally, we use its eigenvalues to measure a "rate of invasion" for the parameter combinations where a regional Allee effect does not exist (Chapter 3, Section 3.4, Figs. 3.5, 3.6).

Since the probability distribution must sum to 1, we have an additional condition on our $N_{\max}+1$ variables $P(N)$, which renders one of the dimensions redundant. Hence, the Jacobian of the entire master equation necessarily has a zero eigenvalue. Thus, we ignore $P(0)$ and focus on the $N_{\max}$ variables from $P(1)$ to $P(N_{\max})$. We write $P(N)$ as P_N for short, and $\frac{dP(N)}{dt}$ as ϕ_N.

Partially differentiating the master equation (2.7, 2.9) we get

$$\frac{\partial \phi_1}{\partial P_j} = \begin{cases} mj(P_0 - P_1) - 2I - B(1) - D(1) - E(1) & \text{for } j = 1 \\ mj(P_0 - P_1) + D(2) + E(2) - I & \text{for } j = 2 \\ mj(P_0 - P_1) - I & \text{for } j \neq 1, 2 \end{cases} \tag{B.1}$$

$$\frac{\partial \phi_i}{\partial P_j} = \begin{cases} mj(P_{i-1} - P_i) + B(i-1) + I & \text{for } j = i-1 \\ mj(P_{i-1} - P_i) - B(i) - I - D(i) - E(i) & \text{for } j = i \\ mj(P_{i-1} - P_i) + D(i+1) + E(i+1) & \text{for } j = i+1 \\ mj(P_{i-1} - P_i) & \text{for } j \neq i-1, i, i+1 \end{cases} \tag{B.2}$$

$$\frac{\partial \phi_{N_{\max}}}{\partial P_j} = \begin{cases} mjP_{N_{\max}-1} + B(N_{\max}-1) + I & \text{for } j = N_{\max}-1 \\ mjP_{N_{\max}-1} - D(N_{\max}) - E(N_{\max}) & \text{for } j = N_{\max} \\ mjP_{N_{\max}-1} & \text{for } j \neq N_{\max}-1, N_{\max} \end{cases} \tag{B.3}$$

The term in the i^{th} row and the j^{th} column of the Jacobian matrix is given by $\frac{\partial \phi_i}{\partial P_j}$.

Further, for the combinations of m and A for which $A_R = 0$ (Fig. 3.6), we calculate the eigenvalues at the zero equilibrium ($P(0) = 1, P(N) = 0, N > 0$). The eigenvalue with the largest real part provides a measure of how rapidly a population invades this empty habitat.

For a given Allee threshold, this rate of invasion is the maximum at an intermediate dispersal rate, signifying that intermediate dispersal rates are optimal when a population faces local but not regional strong Allee effects (Fig. B.1).

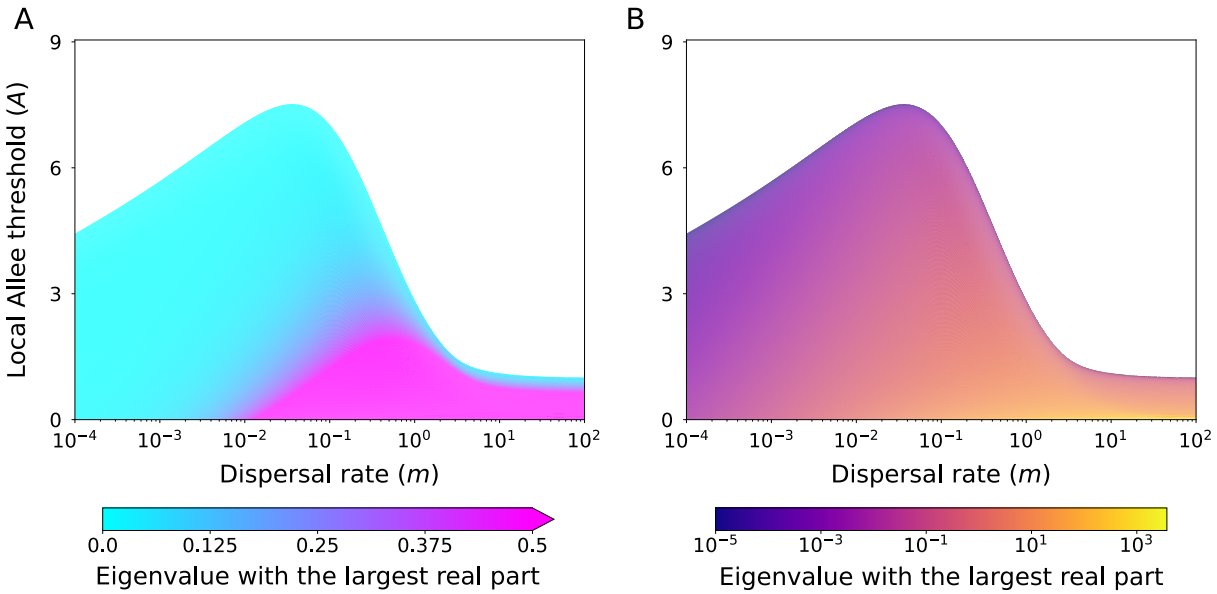

Fig. B.1. The eigenvalue with the largest real part for the combinations of dispersal rate (m) and local Allee threshold (A) where there is no regional Allee threshold. The white-coloured parts possess a non-zero regional Allee threshold. The eigenvalue acts as a proxy for the rate of invasion of a small population, which is the maximum for an intermediate dispersal rate. Both panels show the same values but on different colour scales to highlight different factors. **A** Linear colour scale clamped above at 0.5, to show that invasion rate is the maximum for an intermediate value of the dispersal rate. **B** Logarithmic colour scale, to show that there is no abrupt transition, unlike the illusion panel A creates. Parameters: $r = 1$, $K = 50$, $a = 10$, $X = 0$.

Appendix C

Derivation based on a more mechanistic model

In this appendix, we begin with a more mechanistic consumer-resource model and show that we can arrive at (4.3) through quasi-steady state assumptions. Note that these derivations are only illustrative, and there may be other ways to obtain the same equation starting with other models. The aim is to show that our model can be obtained based on cooperation for a common good or a public good. We also explain how one rewrites the model in terms of its equilibria.

Derivation for two morphs

We assume there are two strategies γ_1 and γ_2 present, which may represent either different morphs within the same species or two different species. These morphs are the consumers, whose abundances are denoted by N_1 and N_2. There are two resources, whose abundances are represented by R_1 and R_2. In the absence of any consumer resource 1 grows logistically. it is harvested by the consumers at certain rates. On the other hand, resource 2 is a common good. It does not grow by itself but requires some investment from the consumers. This investment is measured by the strategy γ, for which the consumers also pay a cost. It decays at a constant rate. Both these resources promote the growth of the consumers. Resource 1 affects the growth linearly, but resource 2 has a saturating effect. Thus, we can express this model with the following equations:

$$\begin{aligned}
\frac{dN_1}{dt} &= (\beta_1 R_1 + \frac{\beta_2 R_2}{h + R_2} - c' - b\gamma_1^\theta)N_1 \\
\frac{dN_2}{dt} &= (\beta_1 R_1 + \frac{\beta_2 R_2}{h + R_2} - c' - b\gamma_2^\theta)N_2 \\
\varepsilon\frac{dR_1}{dt} &= (r_1 - \alpha_1 R_1)R_1 - q\beta_1 R_1 N_1 - q\beta_1 R_1 N_2 \\
\varepsilon\frac{dR_2}{dt} &= \gamma_1 N_1 + \gamma_2 N_2 - d_2 R_2
\end{aligned} \tag{C.1}$$

Here, β_1 is the per-capita growth rate of the consumers per unit resource 1 and β_2 is the maximum per-capita growth rate of the consumers due to resource 2. h is the resource 2 abundance at which the per-capita growth rate of the consumer is $\beta_2/2$. c' is the constant

death rate, and $b\gamma_i^\theta$ is the cost paid by consumer i.r_1 and α_1 are the intrinsic growth rate and the intraspecific competition coefficient of resource 1, respectively. q is a conversion coefficient. d_2 is the per-capita decay rate of resource 2 (which may be considered an intrinsic decay rate in the case of a public good, or a decay due to consumption by individuals in the case of a common good). Additionally, $\varepsilon << 1$. The terms like β_1,, β_2, h, c', b, q could in principle have different values for different consumers. However, for simplicity, we assume here that they are the same for both consumers.

The ε terms indicate the assumption that the resource timescales are much faster than the consumer timescales so that each resource is present at its quasi-steady state. The quasi-steady states of these resources are given by

$$\begin{aligned}\tilde{R}_1 &= \frac{1}{\alpha_1}(r_1 - q\beta_1 N_1 - q\beta_1 N_2)\\ \tilde{R}_2 &= \frac{1}{d_2}(\gamma_1 N_1 + \gamma_2 N_2)\end{aligned} \tag{C.2}$$

Putting these back into the equations for N_1 and N_2, we get

$$\begin{aligned}\frac{dN_1}{dt} &= (\frac{\beta_1}{\alpha_1}(r_1 - q\beta_1 N_1 - q\beta_1 N_2) + \frac{\frac{\beta_2}{d_2}(\gamma_1 N_1 + \gamma_2 N_2)}{h + \frac{1}{d_2}(\gamma_1 N_1 + \gamma_2 N_2)} - c' - b\gamma_1^\theta)N_1\\ \frac{dN_2}{dt} &= (\frac{\beta_1}{\alpha_1}(r_1 - q\beta_1 N_1 - q\beta_1 N_2) + \frac{\frac{\beta_2}{d_2}(\gamma_1 N_1 + \gamma_2 N_2)}{h + \frac{1}{d_2}(\gamma_1 N_1 + \gamma_2 N_2)} - c' - b\gamma_2^\theta)N_2\end{aligned} \tag{C.3}$$

Rearranging the terms, we get

$$\begin{aligned}\frac{dN_1}{dt} &= \left[\frac{\beta_2(\gamma_1 N_1 + \gamma_2 N_2)}{hd_2 + \gamma_1 N_1 + \gamma_2 N_2} + (\frac{\beta_1}{\alpha_1}r_1 - c') - \frac{\beta_1^2 q}{\alpha_1}(N_1 + N_2) - b\gamma_1^\theta\right]N_1\\ \frac{dN_2}{dt} &= \left[\frac{\beta_2(\gamma_1 N_1 + \gamma_2 N_2)}{hd_2 + \gamma_1 N_1 + \gamma_2 N_2} + (\frac{\beta_1}{\alpha_1}r_1 - c') - \frac{\beta_1^2 q}{\alpha_1}(N_1 + N_2) - b\gamma_2^\theta\right]N_2\end{aligned} \tag{C.4}$$

Thus, we have obtained a saturating birth rate that arose from resource 2. From resource 1, we got a constant birth rate $\frac{\beta_1}{\alpha_1}r_1$ and the competition term $\frac{\beta_1^2 q}{\alpha_1}(N_1 + N_2)$ We assume that the constant birth rate is smaller than the already existing constant death rate, i.e., $\frac{\beta_1}{\alpha_1}r_1 < c$, which gives us strong Allee effects. We define

$$\begin{aligned}\rho &= \beta_2\\ a &= hd_2\\ c &= \frac{\beta_1}{\alpha_1}r_1 - c'\\ \alpha &= \frac{\beta_1^2 q}{\alpha_1}\end{aligned} \tag{C.5}$$

with which we get

$$\begin{aligned}\frac{dN_1}{dt} &= \left[\frac{\rho(\gamma_1 N_1 + \gamma_2 N_2)}{a + \gamma_1 N_1 + \gamma_2 N_2} - c - \alpha(N_1 + N_2) - b\gamma_1^\theta\right]N_1\\ \frac{dN_2}{dt} &= \left[\frac{\rho(\gamma_1 N_1 + \gamma_2 N_2)}{a + \gamma_1 N_1 + \gamma_2 N_2} - c - \alpha(N_1 + N_2) - b\gamma_2^\theta\right]N_2\end{aligned} \tag{C.6}$$

which is (4.3). Combining different terms (like the constant birth and constant death terms) has no consequences in the deterministic model. However, when we convert this into a stochastic model, the choice of transition rates determines the magnitude of fluctuations.

Restricting to one morph and rewriting in terms of the equilibria

If only one strategy is present, we can put $N_2 = 0$ to get the equation from morph 1 as

$$\frac{dN_1}{dt} = \left[\frac{\rho(\gamma_1 N_1)}{a + \gamma_1 N_1} - c - \alpha(N_1) - b\gamma_1^{\theta}\right] N_1 \tag{C.7}$$

Putting $\gamma_1 = 1$, $b = 0$ and writing $N_1 = N$, we get

$$\frac{dN}{dt} = \left(\frac{\rho N}{a + N} - c - \alpha N\right) N \tag{C.8}$$

which is (3.3).

Equations (3.3) and (3.4) are related by the following expressions:

$$\begin{aligned}
\rho &= r + \frac{ra^2}{AK} + \frac{ra(A+K)}{AK} \\
\alpha &= \frac{ra}{AK} \\
c &= r
\end{aligned}$$

Putting these into (C.8, i.e., 3.3) after rearranging it, we get

$$\begin{aligned}
&\frac{N+a}{N}\frac{dN}{dt} = \rho N - ca - cN - \alpha a N - \alpha N^2 \\
\implies &\frac{N+a}{N}\frac{dN}{dt} = \left(r + \frac{ra^2}{AK} + \frac{ra(A+K)}{AK}\right) N - ra - rN - \frac{ra}{AK} aN - \frac{ra}{AK} N^2 \\
\implies &\frac{N+a}{rN}\frac{dN}{dt} = \left(1 + \frac{a^2}{AK} + \frac{a(A+K)}{AK}\right) N - a - N - \frac{a^2}{AK} N - \frac{a}{AK} N^2 \\
\implies &\frac{N+a}{rN}\frac{dN}{dt} = \left(\frac{a(A+K)}{AK}\right) N - a - \frac{a}{AK} N^2 \\
\implies &\frac{N+a}{raN}\frac{dN}{dt} = \frac{N}{K} + \frac{N}{A} - 1 - \frac{N^2}{AK} \\
\implies &\frac{N+a}{raN}\frac{dN}{dt} = \left(1 - \frac{N}{K}\right)\left(\frac{N}{A} - 1\right) \\
&\implies \frac{dN}{dt} = \frac{raN}{N+a}\left(1 - \frac{N}{K}\right)\left(\frac{N}{A} - 1\right) \\
&\implies \frac{dN}{dt} = \frac{rN}{\frac{N}{a}+1}\left(1 - \frac{N}{K}\right)\left(\frac{N}{A} - 1\right)
\end{aligned} \tag{C.9}$$

which is (3.4).

Appendix D

Supporting results: Spatial Allee effects

In this appendix, we provide supporting results for Chapter 3. We compare the three models studied in Chapter 3, explain the significance of the term "quasi" in the name "regional quasi-Allee threshold", and describe the effects of catastrophes and dispersal mortality on metapopulation-scale Allee effects.

D.1 Mainland-island vs metapopulation

In the deterministic open system model (3.5), the upper stable equilibrium approaches the regional abundance with increasing dispersal rates. This is simply because

$$\lim_{m\to\infty}\frac{dN}{dt}=\lim_{m\to\infty}\left(\frac{rN}{\frac{N}{a}+1}\left(1-\frac{N}{K}\right)\left(\frac{N}{A}-1\right)+m(N_R-N)\right)=m(N_R-N) \tag{D.1}$$

whose equilibrium point is at $N = N_R$. It is trivial to show that this equilibrium is stable. Fig. D.1 shows an example of this.

Now, we compare the three different models in Chapter 3: the two open system (i.e., mainland-island) models (deterministic and stochastic), which we use as steps towards our metapopulation model, and the metapopulation model. When we compare the deterministic (Fig. D.2 A) and the stochastic (Fig. D.2 B) mainland-island models, we observe that the bimodality parameter space in the stochastic model is larger than the bistability parameter space in its deterministic counterpart. As previously discussed in Chapter 3, Section 3.3, this is because, in the deterministic model, a large population can never collapse. However, it can collapse in the stochastic model. Thus, a greater dispersal rate is required to overcome the Allee effect in the stochastic (getting rid of bimodality) than in the deterministic model (getting rid of bistability).

When we compare the mainland-island models (Fig. D.2 A,B) and the metapopulation model, we observe that the main difference is that the former models do not have an extinction regime, while the latter does. Clearly, this occurs because the mainland-island models have fixed regional abundances, whereas it is a function of the local probability distributions in the metapopulation model. Further, note that the invasion/unimodality and bistability/bimodality regimes of the mainland-island models are not exactly the same as the invasion and bistability regimes of the metapopulation model. In the mainland-island models, we are concerned with the local dynamics, where the regional abundance is constant. The invasion regime, here,

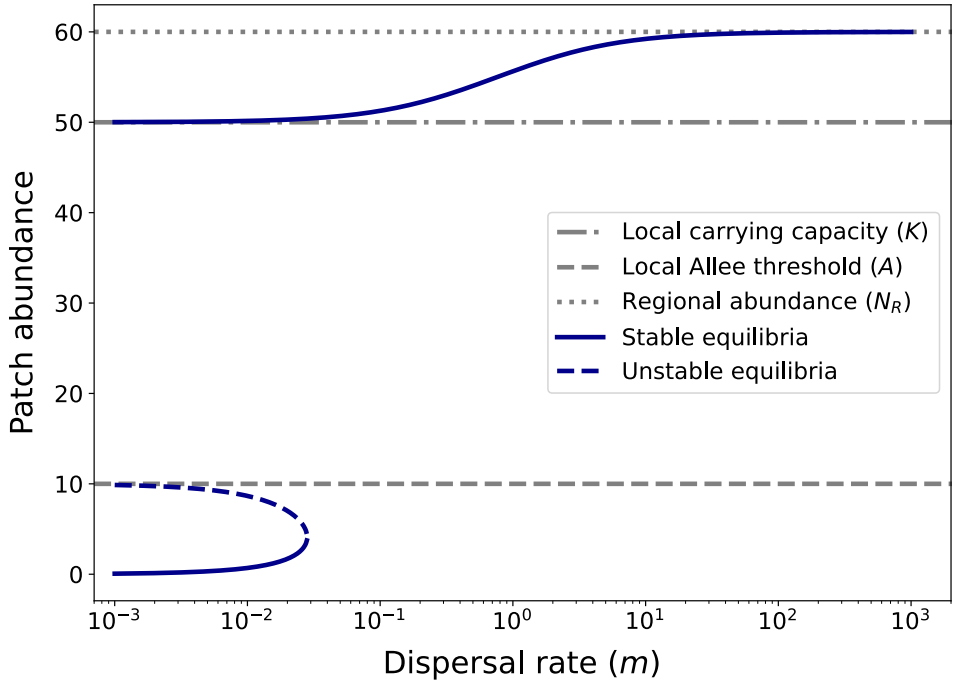

Fig. D.1. The upper stable equilibrium in the deterministic open system model approaches the regional abundance with high dispersal rates. Parameters: $A = 10$, $r = 1$, $K = 50$, $a = 10$, $X = 0$, $N_R = 60$.

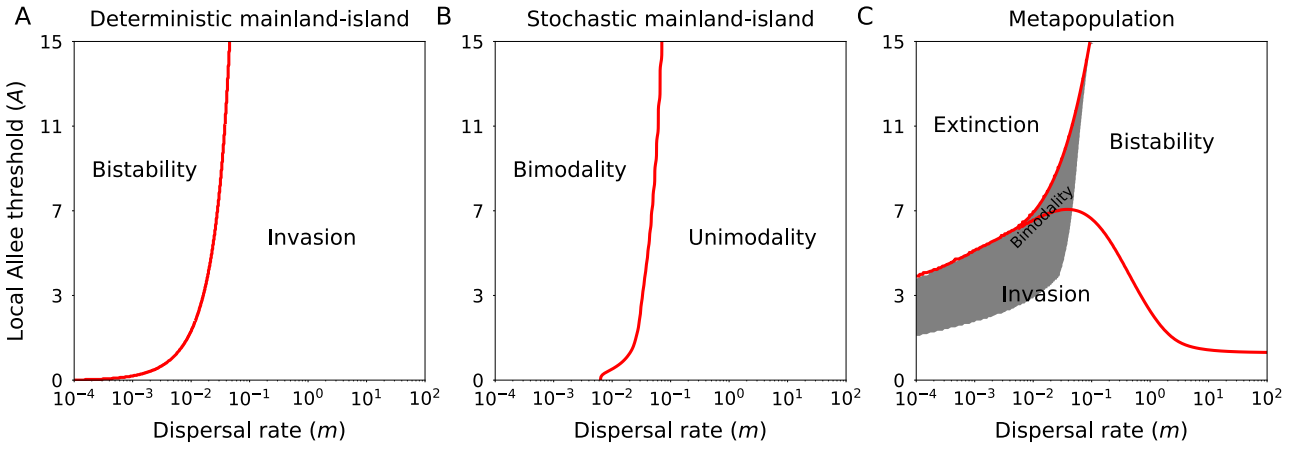

Fig. D.2. Comparison among the three models in Chapter 3. **A** Deterministic mainland-island model. **B** Stochastic mainland-island model. **C** Metapopulation model. The parts of the parameters space corresponding to different regimes are marked accordingly. The grey shaded area in panel C is where the metapopulation model has a bimodal equilibrium distribution. Parameters:$r = 1$, $K = 50$, $a = 10$, $X = 0$; **A**, **B** $N_R = 50$.

corresponds to invasion in a single patch. The bistability is the initial abundance dependence for invading a single patch. Similarly, the bimodality and unimodality regimes refer to the modality in the local probability distribution. This situation corresponds to the equilibria in the metapopulation model.

On the other hand, the extinction, invasion and bistability regimes in the metapopulation model refer to the properties of the entire metapopulation. The metapopulation equilibrium distribution can be bimodal, which happens close to the boundary of the extinction regime (Fig. D.2 C). Hence, the mainland-island models can be interpreted as the local dynamics when the metapopulation is at equilibrium. Thus, bistability appears in the metapopulation model with increasing dispersal rates, whereas bistability/bimodality disappears in the mainland-island models with increasing dispersal rates. This difference highlights the separation of spatial scales and the distinction between the equilibria at different spatial scales.

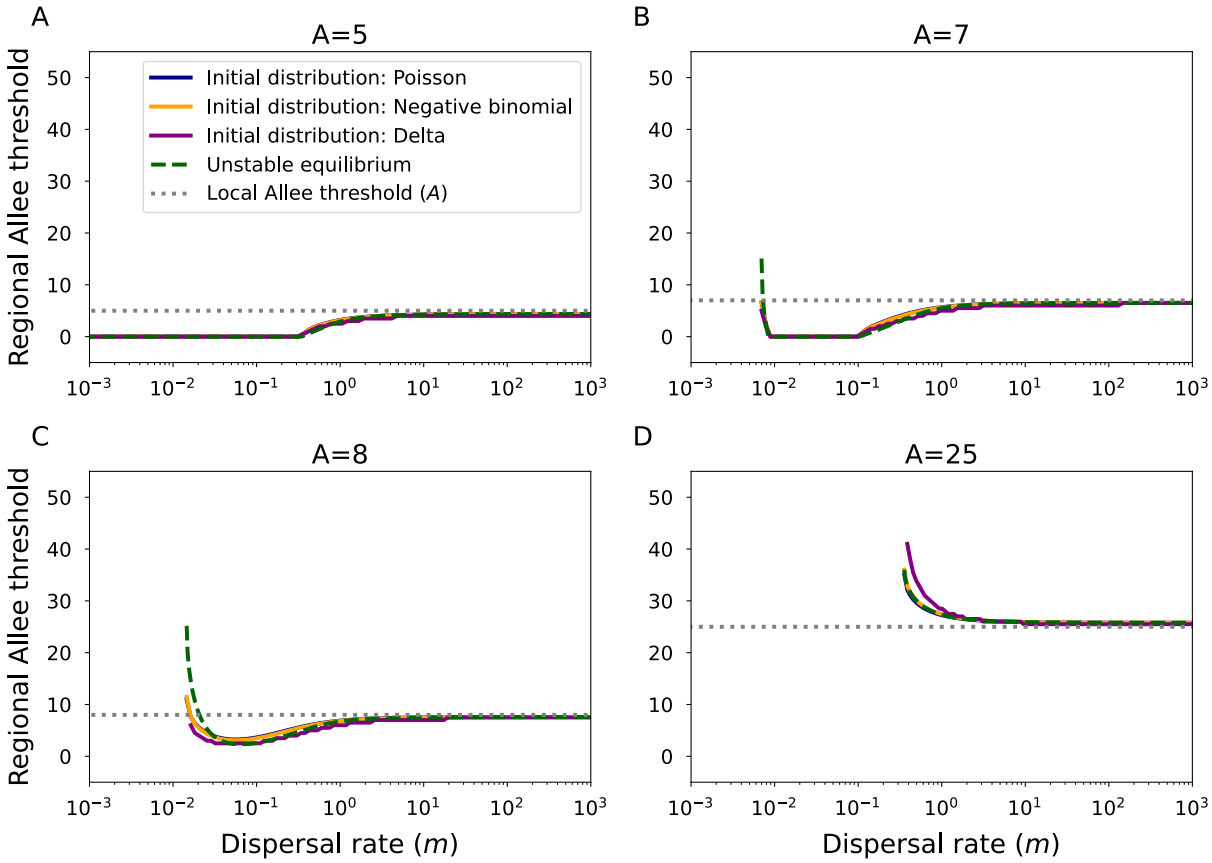

Fig. D.3. The minimum average population required for persistence for different types of initial distributions and the average of the unstable equilibrium point for different local Allee threshold values: **A** A=5, **B** A=7, **C** A=8, **D** A=25. The initial distributions assumed are: (i) Poisson distribution; (ii) Negative binomial distribution: $P(n) = {}^{n+k-1}\mathrm{C}_n(p^k)(1-p)^n, k = 10$; (iii) Delta distribution: $P(0) = 0.5, P(\mathrm{ceil}(2\overline{N})) = 0.5, P(n) = 0$ for $n \neq 0, 2\overline{N}$. Parameters: $r = 1$, $K = 50$, $a = 10$, $X = 0$.

D.2 Why is the regional Allee threshold "quasi"?

In our metapopulation model with Allee effects, we found that there can be an unstable equilibrium point, which we call the "regional quasi-Allee threshold", denoted by A_R (Chapter 3, Section 3.4). We could have very well called it a "regional Allee threshold", but we chose to include the prefix "quasi" in the name. Here, we explain our choice of the name.

As described in Chapter 2, the equilibrium points in the metapopulation model are located in a high-dimensional space in which the N^{th} dimension corresponds to the value of $P(N)$. Each point in this high-dimensional space is related to a distribution. Since A_R is only an average of the unstable equilibrium point, it cannot completely characterise the ecological fate of a population. Basically, whether a population can invade or not depends not only on its average initial abundance but also on its initial distribution in space. This is why the term "quasi" is included in the name "regional quasi-Allee threshold". However, we analyse the average initial population sizes required for invasion for multiple types of distributions and find that they are often close A_R (Fig. D.3), indicating that A_R may still hold some value and be an informative measure. Additionally, when $A_R = 0$, the population can invade from any positive initial population size irrespective of the initial distribution.

In Fig. D.3, we show the results for three different kinds of distributions:

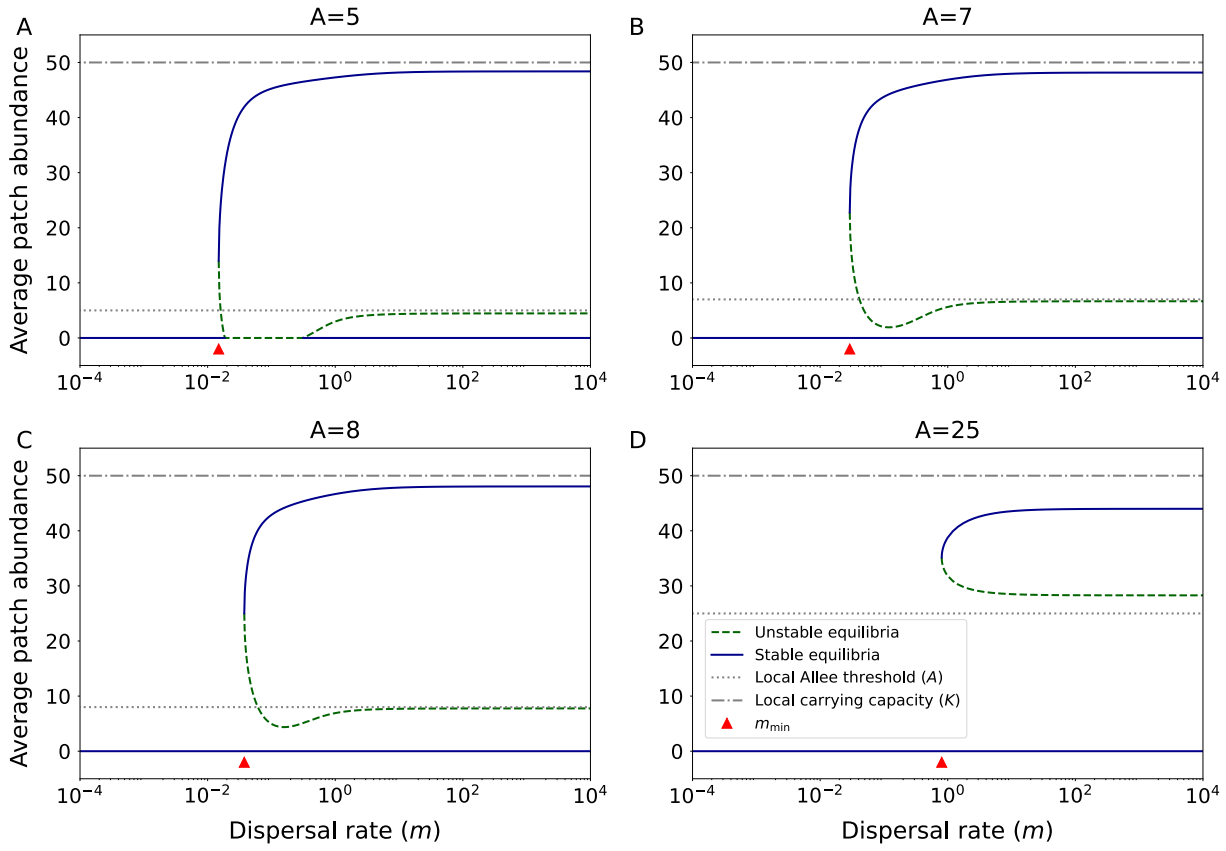

Fig. D.4. Metapopulation model bifurcation diagrams with catastrophes. Catastrophes alter the bifurcation scenario in a similar way to increasing the local Allee threshold. Parameters: $r = 1$, $K = 50$, $a = 10$, $X = 0.01$.

- Poisson distribution: $P(n) = \frac{\overline{N}^n}{n!}e^{-\overline{N}}$
- Negative binomial distribution: $P(n) =^{n+k-1} \mathrm{C}_n(p^k)(1-p)^n$
- Delta distribution: $P(0) = 0.5, P(\mathrm{ceil}(2\overline{N})) = 0.5, P(n) = 0$

For each of these distributions, we compute the minimum average value $\overline{N}$ needed for invasion, and call it the regional Allee threshold for that particular distribution. Comparing these values with the unstable equilibrium shows that all of them lie close to each other.

D.3 Catastrophes, dispersal mortality and metapopulation-level Allee effects

We explore how catastrophes affect the regional equilibria by taking them into account as a stochastic process taking place at the rate X (Chapter 2, Section 2.2, Subsection 2.2.2). Catastrophes modify the way bifurcations take place in the model (Fig. D.4). They lower the regional carrying capacity and increase the minimum dispersal rate required for persistence. Concerning the regional quasi-Allee threshold (A_R), the effect of catastrophes is similar to increasing the local Allee threshold A. For example, the pattern for $A = 5$ with catastrophes

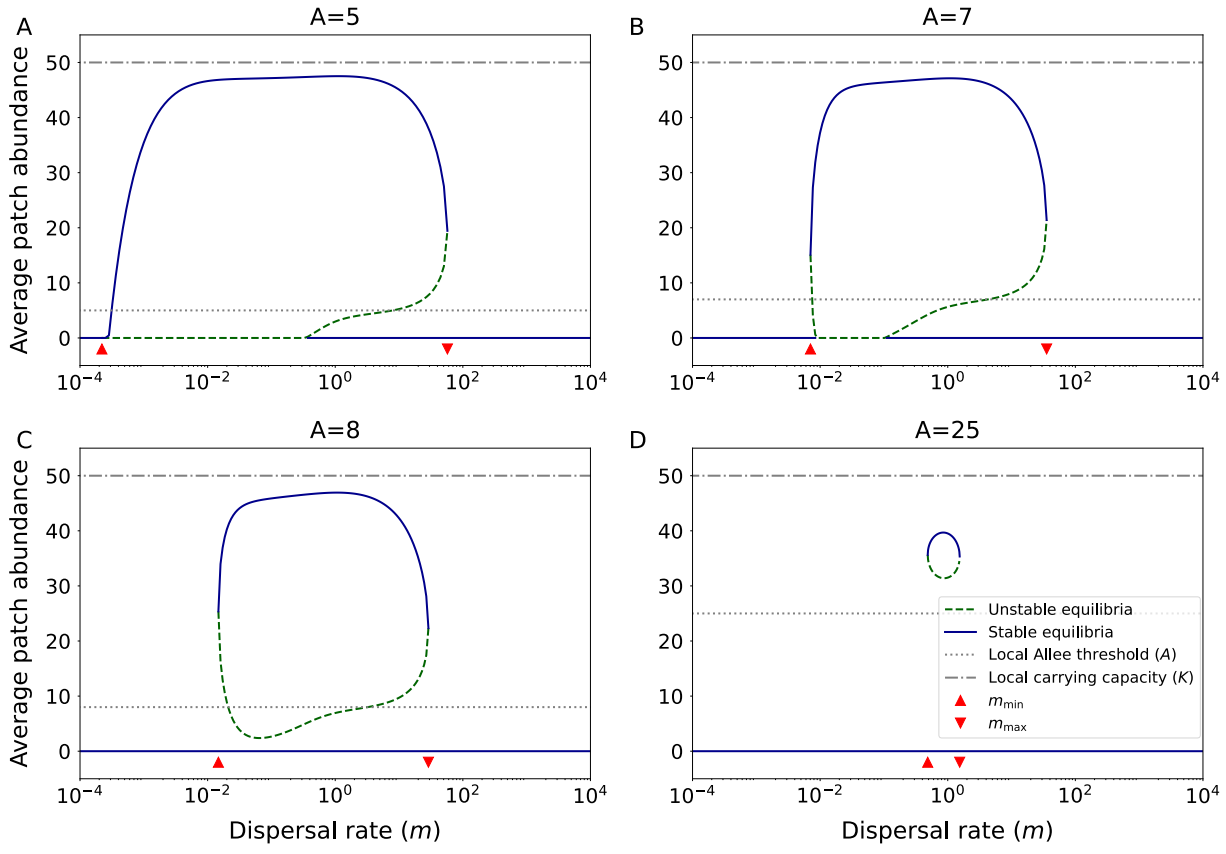

Fig. D.5. Metapopulation model bifurcation diagrams with dispersal mortality. High dispersal causes an additional bifurcation, producing an upper limit dispersal rate ($m_{\max}$) for persistence. Parameters: $r = 1$, $K = 50$, $a = 10$, $X = 0.0$, $\delta = 0.99$.

(Fig. D.4 A; compare with Fig. 3.5 A) is similar to that seen for $A = 7$ without catastrophes (Fig. 3.5 B). The pattern for $A = 7$ with catastrophes (Fig. D.4 B; compare with Fig. 3.5 B) is similar to that seen for $A = 8$ without catastrophes (Fig. 3.5 C).

We incorporate dispersal mortality in our model to study its influence on metapopulation equilibria (2.4). Since only a fraction of dispersers survive, the process comes at the cost of lowering the abundance. Consequently, high dispersal becomes detrimental (Fig. D.5). K_R increases with increasing dispersal rate when the latter is small but decreases when the dispersal rate is too high. A_R behaves similarly to the model without dispersal mortality for low dispersal rates but increases for high dispersal rates, ultimately merging with K_R. We call the dispersal rate at the point where these two equilibria merge as $m_{\max}$. At $m = m_{\max}$, another bifurcation occurs such that extinction is the only equilibrium for higher dispersal rates.

Appendix E

Supporting results: Evolution of cooperation and dispersal

In this appendix, we provide supporting results for the findings in Chapter 4 and Chapter 5. We derive the invasion fitness and selection gradient for the deterministic model of a well-mixed population (Chapter 4, Section 4.1), and show that evolutionary suicide occurs in the model. We show how catastrophes, dispersal mortality and cost functions affect the evolution of cooperation in our metapopulation model. We also provide the data on mean first-passage times (MFPT) in the metapopulation model. Additionally, we explore the coexistence of cooperators and defectors in further detail. We distinguish between protected and unprotected conditional coexistence, explain how a suicidal invasion with large mutations occurs using projected nullclines and also elaborate on how these nullclines are obtained. We conclude with supporting figures for the evolution of dispersal.

E.1 Invasion fitness and selection gradient for the evolution cooperation

Suppose morph 1 with strategy γ_1 is the resident in the well-mixed population at its carrying capacity given by $K_1(\gamma_1)$. Now, assume that morph 2 having a strategy γ_2 with a small population ε_2 invdes the resident population. From (4.3), its per-capita growth rate is given by

$$\frac{1}{N_2}\frac{dN_2}{dt} = \frac{\rho(\gamma_1 K_1 + \gamma_2\varepsilon_2)}{a + \gamma_1 K_1 + \gamma_2\varepsilon_2} - c - \alpha(K_1 + \varepsilon_2) - b\gamma_2^\theta \tag{E.1}$$

where Assuming that ε_2 is small, we can neglect its effect on the per-capita growth rate of morph 2. Thus, the per-capita growth rate is

$$\frac{1}{N_2}\frac{dN_2}{dt} = \frac{\rho(\gamma_1 K_1)}{a + \gamma_1 K_1} - c - \alpha K_1 - b\gamma_2^\theta \tag{E.2}$$

As we can see, the trait value γ_2 appears only in the cost term. This per-capita growth rate of a rare morph is called invasion fitness. Observe from (4.1) that the carrying capacity of morph 1 is given by

$$\frac{\rho(\gamma_1 K_1)}{a + \gamma_1 K_1} - c - \alpha(K_1) - b\gamma_1^\theta = 0 \tag{E.3}$$

From (E.2) and (E.3), the invasion fitness is given by

$$b(\gamma_1^\theta - \gamma_2^\theta) \tag{E.4}$$

Thus, invasion is always successful when $\gamma_2 < \gamma_1$. Hence, a defector can always a cooperator population. If the defector strategy is not viable ($\gamma_2 < \gamma_{\min}$), the invasion leads to extinction of both the morphs (Fig. 4.2).

The evolutionary trajectory with small and rare mutations is given by the selection gradient (Chapter 2, Section 2.3, Subsection 2.3.1), which is the derivative of the invasion fitness w.r.t the mutant strategy, evaluated where the mutant strategy equals the resident strategy. Here, the selection gradient is

$$\frac{d}{d\gamma_2}\left(\frac{1}{N_2}\frac{dN_2}{dt}\right)\Bigg|_{\gamma_2=\gamma_1} = -b\theta\gamma_1^{\theta-1} < 0 \tag{E.5}$$

Evidently, the selection gradient is always negative. A negative selection gradient implies that the trait γ evolves to lower and lower values. With small and rare mutations, the process continues, decreasing the level of cooperation in the population. As γ decreases with evolution, it eventually crosses the persistence boundary and falls below $\gamma_{\min}$. Then, the population cannot persist and goes extinct. Evolutionary suicide occurs.

While the concept selection gradient is applicable only in the small mutation limit, note that the result in Fig. 4.2 is stronger: it does not require the assumption of small mutations. Even with large mutations, the population will evolve to extinction.

In the metapopulation model (Chapter 4, Section 4.2), we use numerical methods to determine whether the invasion is successful. Specifically, a proxy for the invasion fitness is obtained using the LMAO function. The details are given in Chapter 2, Section 2.3, Subsection 2.3.2.

E.2 Evolution of cooperation: Effect of various factors

Here, we illustrate how catastrophes, dispersal mortality and cost functions affect the evolution of cooperation. These results support our idea of the evolution of cooperation as a competition-colonisation tradeoff (Chapter 4, Section 4.4).

Catastrophes and evolution of cooperation

Perhaps the most surprising result of our model is the effect of local catastrophes, whereby they enhance the evolution of cooperation in a seemingly counterintuitive fashion. These catastrophes wipe out entire patches and make persistence harder on an ecological scale. As discussed in Chapter 3 and Appendix D, catastrophes lower the regional carrying capacity and increase the regional quasi-Allee threshold. However, despite being detrimental on an ecological scale, they seem to promote the evolution of cooperation.

Fig. E.1 shows the CSS (γ^*) as a function of dispersal rate (m) for different catastrophe rates (X). In these figures, the point where γ^* falls below $\gamma_{\min}$, causing evolutionary suicide, is marked with a dot. Note that changing the catastrophe rate changes the limits $\gamma_{\min}$ and $\gamma_{\max}$, as well the minimum dispersal rate required for persistence. However, we do not show the trends in $\gamma_{\min}$ and $\gamma_{\max}$ to avoid cluttering the figure. The inset shows γ^* as a function of X for a fixed dispersal rate. γ^* increases with increasing X.

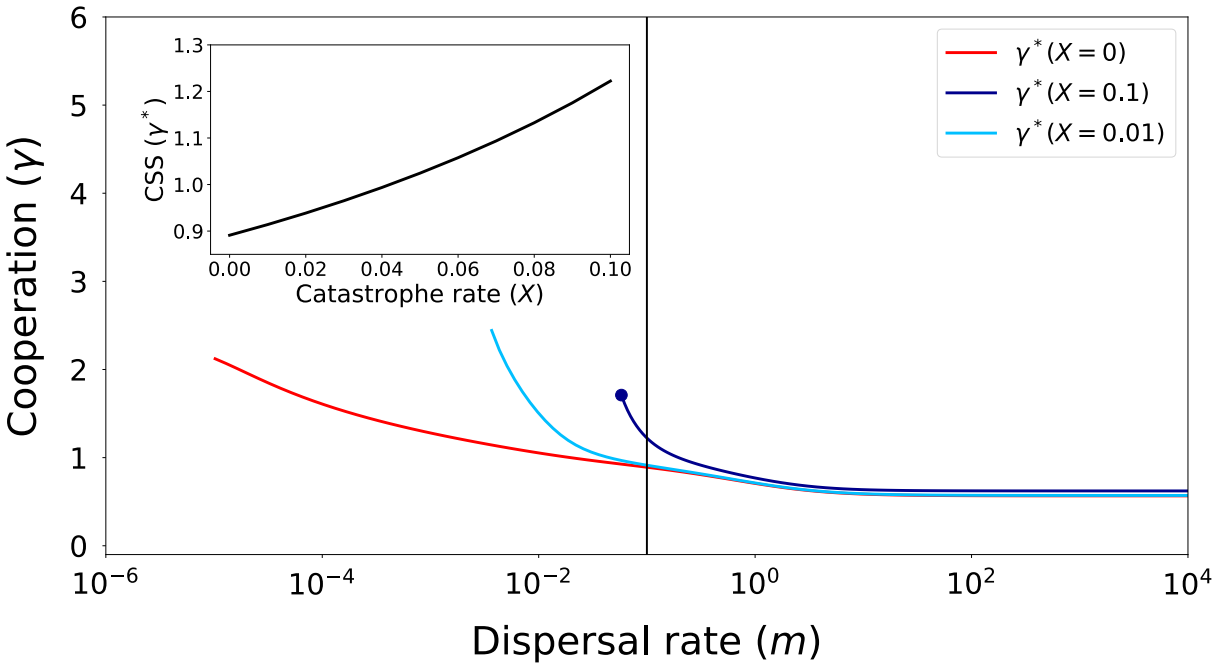

Fig. E.1. Catastrophes favour the evolution of cooperation. Main plot: CSS for cooperation (γ^*) as a function of dispersal rate (m) for different values of the catastrophe rate (X). The grey vertical line marks the dispersal rate in the inset. The terminal dots indicate evolutionary suicide. Inset: CSS for cooperation (γ^*) as a function of the catastrophe rate (X) for $m = 0.1$. Parameters: $\rho = 3.5$, $a = 10$, $c = 1$, $\alpha = 0.04$, $b = 0.05$, $\theta = 2$, $\delta = 1$.

For $X = 0.01$, γ^* is higher than for $X = 0.0$ for all values of m. For $X = 0.1$, evolutionary suicide takes place when the dispersal rates are low. However, in the range where a γ^* exists, it is higher than in the case with no catastrophes. A hint for this perplexing phenomenon lies in the creation of more empty patches by catastrophes, which we discuss in Chapter 4, Section 4.4.

Dispersal mortality and evolution of cooperation

In addition to catastrophes, a greater proportion of unoccupied patches can arise via mortality during dispersal. As a result, dispersal mortality also has a positive effect on the evolution of cooperation (Fig. E.2). For all dispersal rates, γ^* is higher when the fraction of dispersal survivors is smaller. With increasing dispersal rates, evolutionary suicide takes place due to increasing $\gamma_{\min}$. However, prior to evolutionary suicide, γ^* increases with increasing m. The inset shows the CSS as a function of the fraction of dispersal survivors (δ), depicting that γ^* decreases with increasing δ (decreasing dispersal mortality). Hence, when dispersal is costly, greater cooperation evolves.

Effect of cost functions

Besides observing the effect of the cost of dispersal, it is also important to investigate how the form of the cost of cooperation affects its evolution. As we see in Fig. E.3, for low dispersal rates, a higher cost of cooperation promotes cooperation, whereas it hampers the evolution of cooperation at higher dispersal rates. γ^* is smaller for a quadratic cost ($\theta = 2$) than for a linear

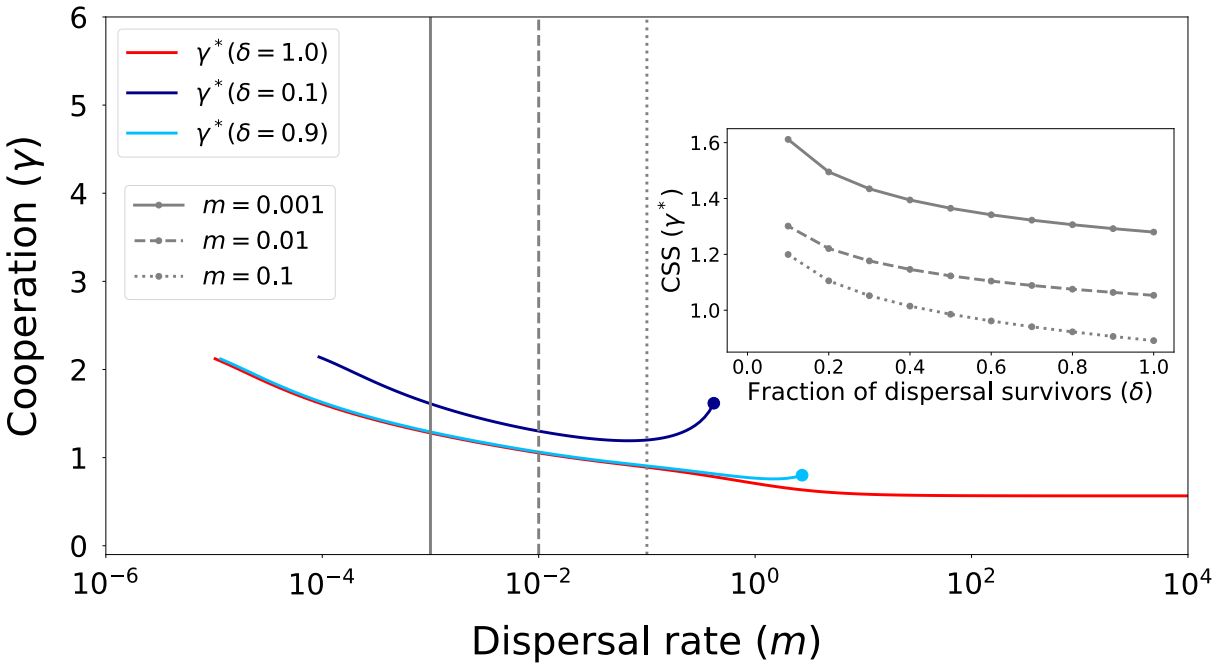

Fig. E.2. Dispersal mortality favours the evolution of cooperation. Main plot: CSS for cooperation (γ^*) as a function of dispersal rate (m) for different values of the fraction of dispersal survivors (δ). The grey vertical line marks the dispersal rates in the inset. The terminal dots indicate evolutionary suicide. Inset: CSS for cooperation (γ^*) as a function of the fraction of dispersal survivors (δ) for specific dispersal rates. Parameters: $\rho = 3.5$, $a = 10$, $c = 1$, $\alpha = 0.04$, $b = 0.05$, $\theta = 2$, $X = 0$.

cost ($\theta = 1$), except at low dispersal rates. Further, γ^* is smaller when the coefficient b in the cost function $b\gamma^\theta$ is larger, except as small dispersal rates. Thus, if individuals disperse less, a greater cost of cooperating enhances cooperation on an evolutionary scale.

We believe that this counterintuitive result is again due to the creation of more empty patches. With a higher cost, the probability of stochastic collapse is greater. Thus, at low dispersal rates, a higher cost promotes the evolution of cooperation. However, when the dispersal rate is high, these empty patches will be colonised again more rapidly, reducing the effect of the stochastic collapse due to greater cost. This trade-off results in the pattern depicted in Fig. E.3.

E.3 Mean first-passage times

In this section, we calculate mean first-passage times, specifically, the average survival time of a patch, the average time to colonise a patch and the average time to replace a resident for different levels of cooperation. These results quantify the notion of competition-colonisation trade-off in our model. Note that MFPTs are calculated for the stochastic open system models with one and two morphs (2.7, 2.19) because the metapopulation model is nonlinear in the probabilities. However, as we will see, using the stochastic open system model also allows us to dissect the effect of dispersal and regional abundance.

In order to disentangle the role of dispersal, we first look at the case with no dispersal ($m =$

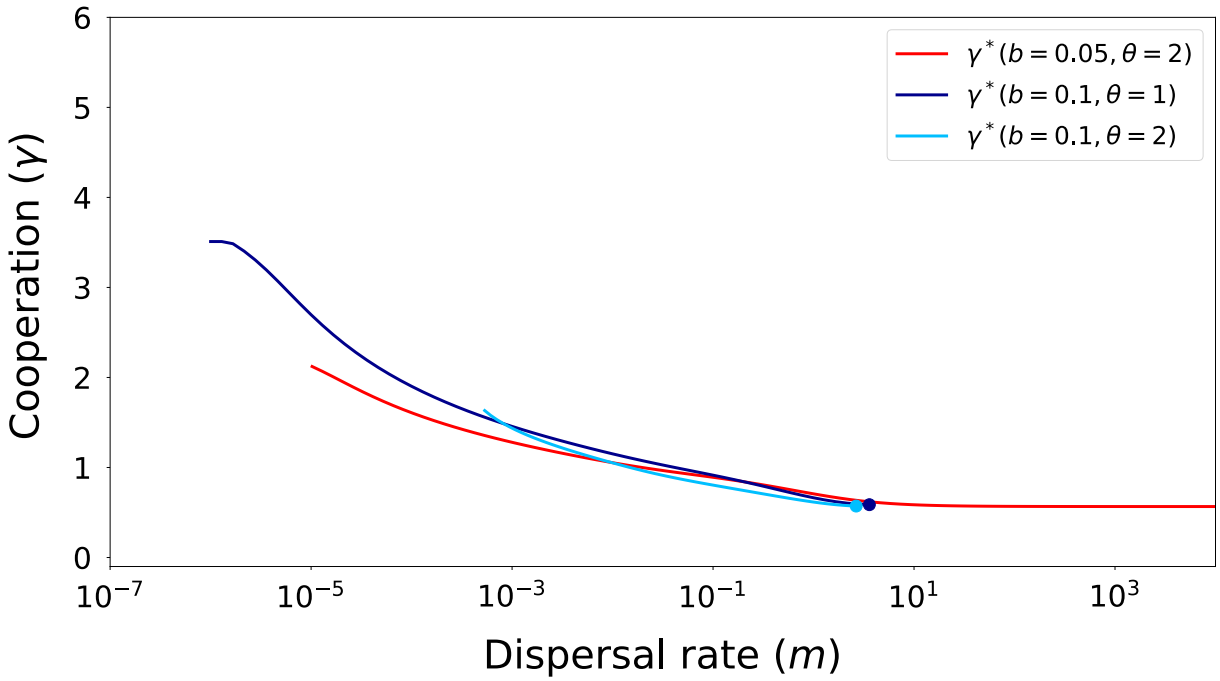

Fig. E.3. Effect of cost functions on the CSS for cooperation (γ^*). The terminal dots indicate evolutionary suicide. Parameters: $\rho = 3.5$, $a = 10$, $c = 1$, $\alpha = 0.04$, $X = 0$, $\delta = 1$.

0). Such a population will eventually collapse due to stochastic fluctuations (see Appendix A, Section A.1). The MFPT measures the average time taken for transition from one state to another. Fig. E.4 A shows the MFPT from $N = \lfloor K(\gamma) \rceil$ to $N = 0$. The MFPT is the largest for intermediate values of γ and peaks around $\gamma \approx 2.0$. Thus, when left on its own without any dispersal, a morph with an intermediate level of cooperation can survive for the longest duration.

Next, we consider the time it takes for a morph to colonise an empty patch and reach its local carrying capacity. Fig. E.4 B shows the MFPT from $N = 0$ to $N = \lfloor K(\gamma) \rceil$. Here, we also take dispersal into account and show the MFPT for different dispersal rates. To disentangle the effect of dispersal, we assume that the regional abundance is equal for all values γ. The MFPT is the minimum for an intermediate value of *gamma*. Thus, a morph with an intermediate value level of cooperation is the quickest in colonising an empty patch and reaching its carrying capacity.

As Figs. E.4 A,B highlight, populations with an intermediate level of cooperation are the least prone to collapse and the most predisposed to rise from small local abundances. In other words, the ability to colonise new patches and retain them is the best for an intermediate γ. Populations that cooperate either too less or too much are worse colonisers.

Now, we shift our attention to competition between different morphs. As shown in Section E.1, defectors always have a higher growth rate than cooperators on a local scale. In other words, defectors are the better competitors. Again, we can use MFPTs in the stochastic open system model to further characterise this notion. To separate the effect of dispersal, we consider a case where two morphs have equal dispersal rates and equal regional abundances and then calculate the MFPT for transition from the attractor of one population to another. Fig. E.4 C shows the MFPT for transition from the state $(K(\gamma_1 = 2.5), 0)$ to $(0, K(\gamma_2))$ as function of γ.

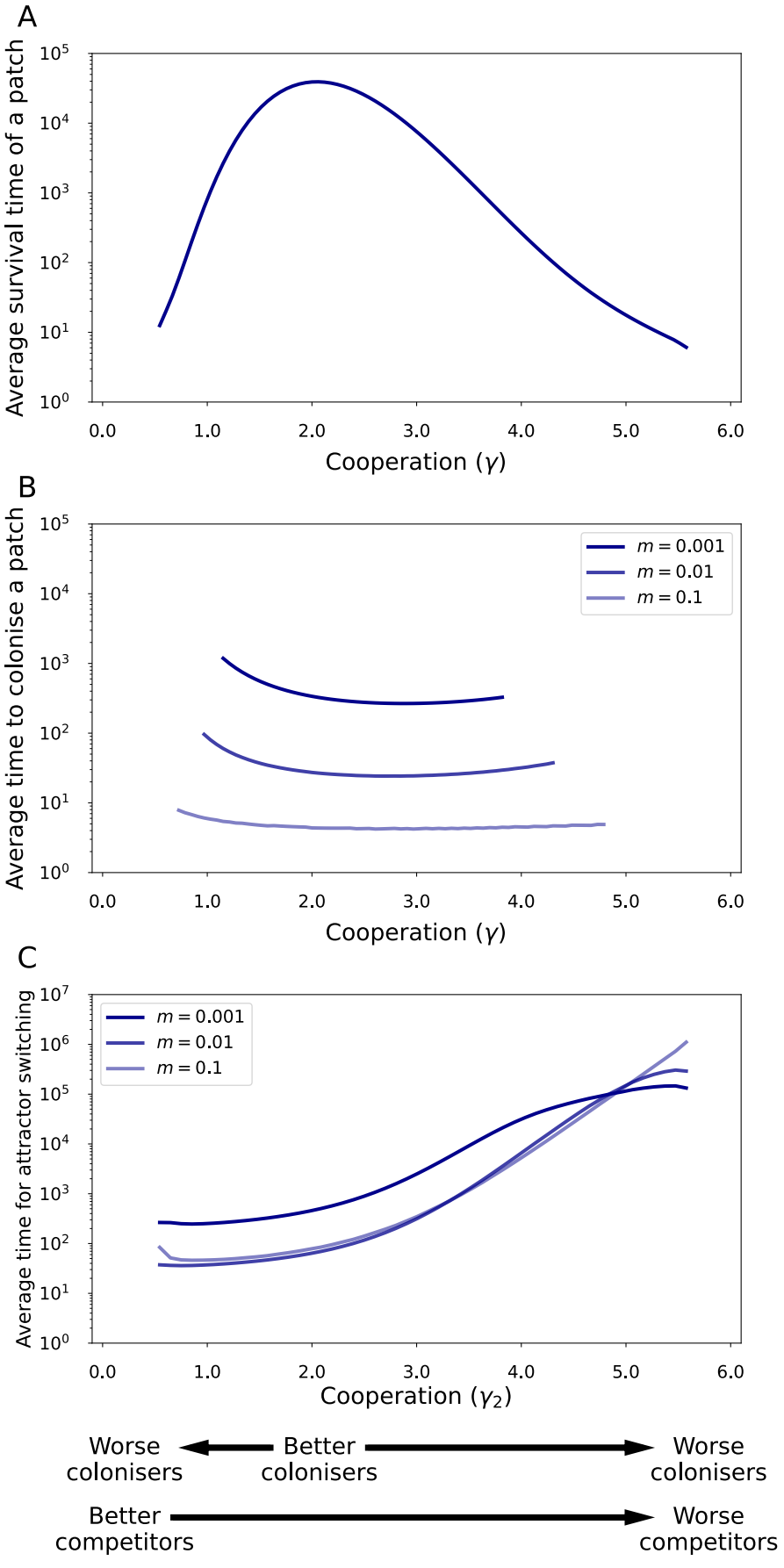

Fig. E.4. Mean first-passage times (MFPTs) in the stochastic open system model. **A** MFPT for the collapse of a monomorphic population, i.e. the MFPT to reach the state 0 from an initial local abundance of $\lfloor K(\gamma) \rceil$. **B** MFPT for the establishment of a monomorphic population, i.e. the MFPT to reach the state $\lfloor K(\gamma) \rceil$ from an initial local abundance of 0. **C** MFPT for morph 2 to take over a patch occupied by morph 1, i.e., the MFPT to reach the state $(0, \lfloor K_2(\gamma_2) \rceil)$ from an initial state of $(\lfloor K_1(\gamma_1) \rceil, 0)$. $\lfloor . \rceil$ denotes the nearest integer function. Panels A and B show that cooperators with an intermediate level of cooperation are the best colonisers since their patches take the longest to go extinct and the shortest to be colonised. Panel C shows that defectors are always the superior competitors since they take the shortest time to take over the patch from another morph. Cooperation evolves in our model due to this trade-off between competition and colonisation. Parameters: $\rho = 3.5$, $a = 10$, $c = 1$, $\alpha = 0.04$, $X = 0$, $\delta = 1$. **A** $m = 0$, $N_R = 0$. **B** $N_R = 50$. **C** $\gamma_1 = 2.5$, $N_{R1} = 50$, $N_{R2} = 50$.

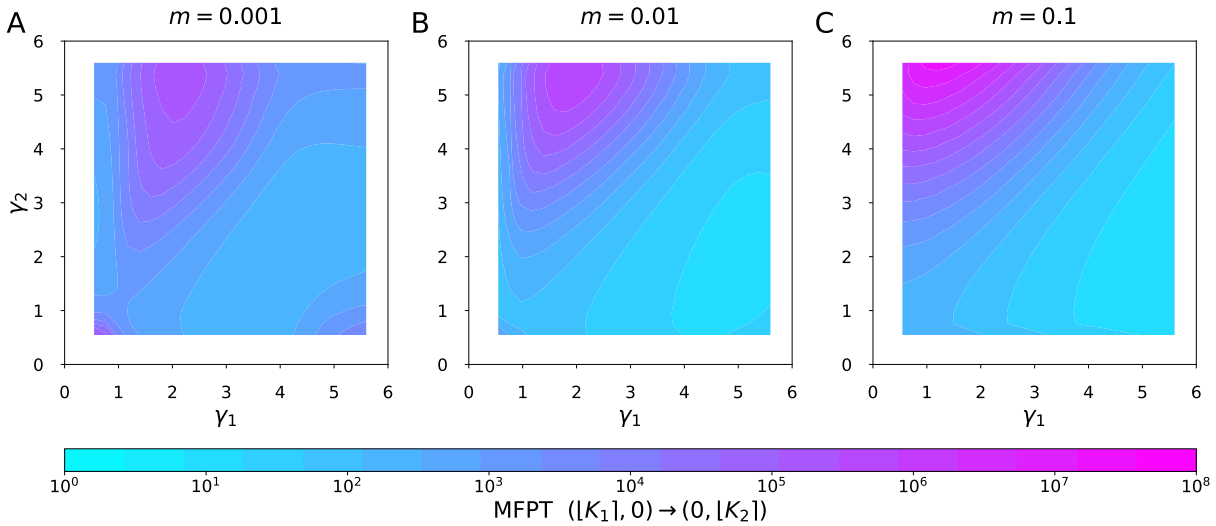

Fig. E.5. Mean first-passage times (MFPTs) in the stochastic open system model for the transition to $(0, \lfloor K_2(\gamma_2) \rceil)$ from an initial state of $(\lfloor K_1(\gamma_1) \rceil, 0)$ **A** $m = 0.001$. **B** $m = 0.01$. **C** $m = 0.1$. $\lfloor . \rceil$ denotes the nearest integer function. Parameters: $\rho = 3.5$, $a = 10$, $c = 1$, $\alpha = 0.04$, $X = 0$, $\delta = 1$. **A** $m = 0$, $N_R = 0$. **B** $N_R = 50$. **C** $\gamma_1 = 2.5$, $N_{R1} = 50$, $N_{R2} = 50$.

Evidently, morphs with a smaller value of γ require a shorter amount of time to take over a patch occupied by a morph with $\gamma = 2.5$. Hence, defectors are the better competitors.

Fig. E.5 shows the MFPT for a transition from $(K(\gamma_1), 0)$ to $(0, K(\gamma_2))$. Again, we see that a defector is always a better competitor than a cooperator. For given γ_1, the transition takes the least time when γ_2 is the smallest (except near the extremities of the trait space). However, for a given γ_2, the transition takes the longest for an intermediate value of γ_1. This reflects the same phenomenon shown in Fig. E.4 A, as the MFPT for a transition also takes into account the probability that morph 1 collapses on its own.

E.4 Further exploring coexistence

In this section, we further describe the coexistence of cooperators and defectors in our model. Thus, this section supplements Chapter 4, Section 4.3. We explain how the projected nullclines in Fig. 4.9 and the figures in this section were obtained, distinguish between protected and unprotected conditional coexistence and show an example of extinction caused by large mutations[1].

E.4.1 Obtaining projected nullclines

The nullclines in Fig. 4.9 are the projections of the actual high-dimensional nullclines in the space of probabilities $P(N_1, N_2)$ onto the two-dimensional space spanned by the two vectors $\sum_{(N_1,N_2)} N_1 P(N_1, N_2)$ and $\sum_{(N_1,N_2)} N_2 P(N_1, N_2)$. To obtain these projected nullclines, we use the LMAO function (2.22).

[1]The time series figures in this section were obtained using a modified version code originally written by Dr. Jonas Wickman.

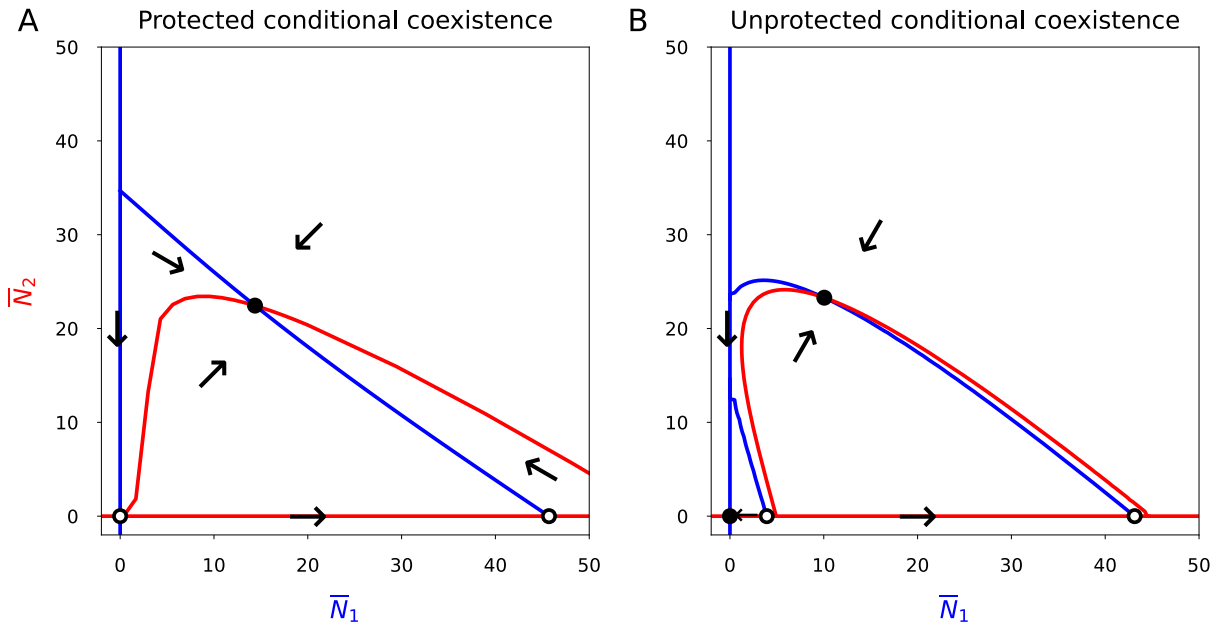

Fig. E.6. Examples of **A** Protected and **B** unprotected conditional coexistence. In panel A, the coexistence is protected from extinction since the morph 1 has no regional Allee effect. In panel B, morph 1 has an Allee effect, due to which the coexistence is unprotected. Parameters: $\rho = 3.5$, $a = 10$, $c = 1$, $\alpha = 0.04$, $X = 0$, $\delta = 1$. **A** $m = 0.1$, $\gamma_1 = 1.3$, $\gamma_2 = 0.65$. **B** $m = 1.0$, $\gamma_1 = 1.0$, $\gamma_2 = 0.55$.

Multiple possible methods to obtain the nullclines exist. One way is to calculate the LMAO function keeping $N_{R,2}$ constant and solving for $\mathbf{f}_{\text{LMAO}}(N_{R,1}, \kappa)[1] = 0$, which gives the morph 1 regional abundance where the growth rate of morph 1 is 0, where κ is a constant and [1] is the first component of the vector. Solving it for several κ values gives the morph nullcline. Similarly, solving $\mathbf{f}_{\text{LMAO}}(\kappa, N_{R,2})[2] = 0$ for different values gives the morph 2 nullcline. Alternatively, one can solve $\mathbf{f}_{\text{LMAO}}(\kappa, N_{R,2})[1] = 0$ $\mathbf{f}_{\text{LMAO}}(N_{R,1}, \kappa)[2] = 0$ for different κ values to obtain the two nullclines.

Another way is to compute $\mathbf{f}_{\text{LMAO}}(N_{R,1}, N_{R,2})[1]$ $\mathbf{f}_{\text{LMAO}}(N_{R,1}, N_{R,2})[2]$ for a grid of $N_{R,1}$ and $N_{R,2}$ values and to draw the contours where each of them equals 0, thus obtaining the respective nullclines for morphs 1 and 2.

E.4.2 Conditional coexistence: Protected vs unprotected

In Chapter 4, Section 4.3, we described a type of coexistence which we call *conditional coexistence*. In this situation, a resident is present at its metapopulation equilibrium. An invader with an inviable strategy invades. This invader cannot persist on its own. However, when it invades the resident metapopulation, it coexists with the resident. In Fig. 4.9, we showed an example of conditional coexistence. In this example, the coexistence was protected, as the resident did not have a regional Allee effect. If the resident becomes rare, it can invade back. However, it is possible to have a scenario where the conditional coexistence is unprotected. If the resident has a regional Allee effect, both the morphs go extinct if the resident becomes rare. Here, we show an example of such a scenario (Fig E.6).

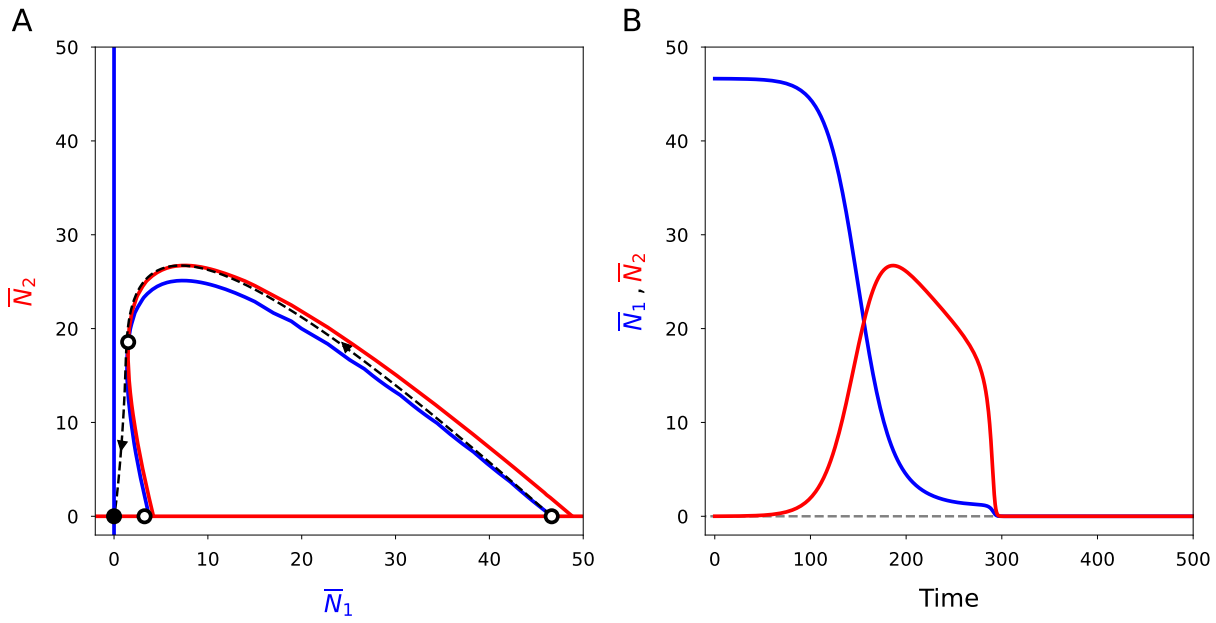

Fig. E.7. An example of invasion leading to the extinction of both the morphs. **A** Projected nullclines. The black line with the arrow shows the time series. **B** Time series of invasion. Parameters: $\gamma_1 = 1.0$, $\gamma_2 = 0.55$, $m = 10$, $\rho = 3.5$, $a = 10$, $c = 1$, $\alpha = 0.04$, $X = 0$, $\delta = 1$.

E.4.3 Suicidal invasion with large mutations

We also saw in Chapter 4, Section 4.3 that an invasion by an inviable mutant need not lead to conditional coexistence. For one, it is possible that invasion by such a mutant fails (Fig. 4.9). If the invasion is successful, it may lead either to conditional coexistence or to the extinction of both morphs. A clear example is seen in Fig. 4.10 E (the black area marked with $-, +_0$ and $+_0, -$). Here, we show the projected nullclines and the time series for such a suicidal invasion.

As seen in Fig. E.7 A, the morphs do have a coexistence equilibrium, similar to the situation with conditional coexistence. However, this coexistence equilibrium is unstable. Thus, extinction is the only stable equilibrium. The defector initially increases in abundance slowly, followed by a rapid increase. Simultaneously, the cooperator abundance decreases. The defector abundance reaches a maximum and then falls rapidly, following which both the morphs go extinct.

E.5 Evolution of dispersal: Effect of various factors

Here, we provide supporting results for the evolution of dispersal. We show how dispersal evolution is affected by the constant death rate c and catastrophes.

Effect of the constant death rate

Increasing c increases the chances that a patch collapses due to stochastic fluctuations. Thus, for higher c, having spread more widely in the spatial habitat should be beneficial, due to which a higher dispersal rate should evolve. Indeed, we observe that m^* increases when c increases, except when γ is close to $\gamma_{\min}$ or $\gamma_{\max}$ (Fig. E.8). Changing c also changes the limits $\gamma_{\min}$ and

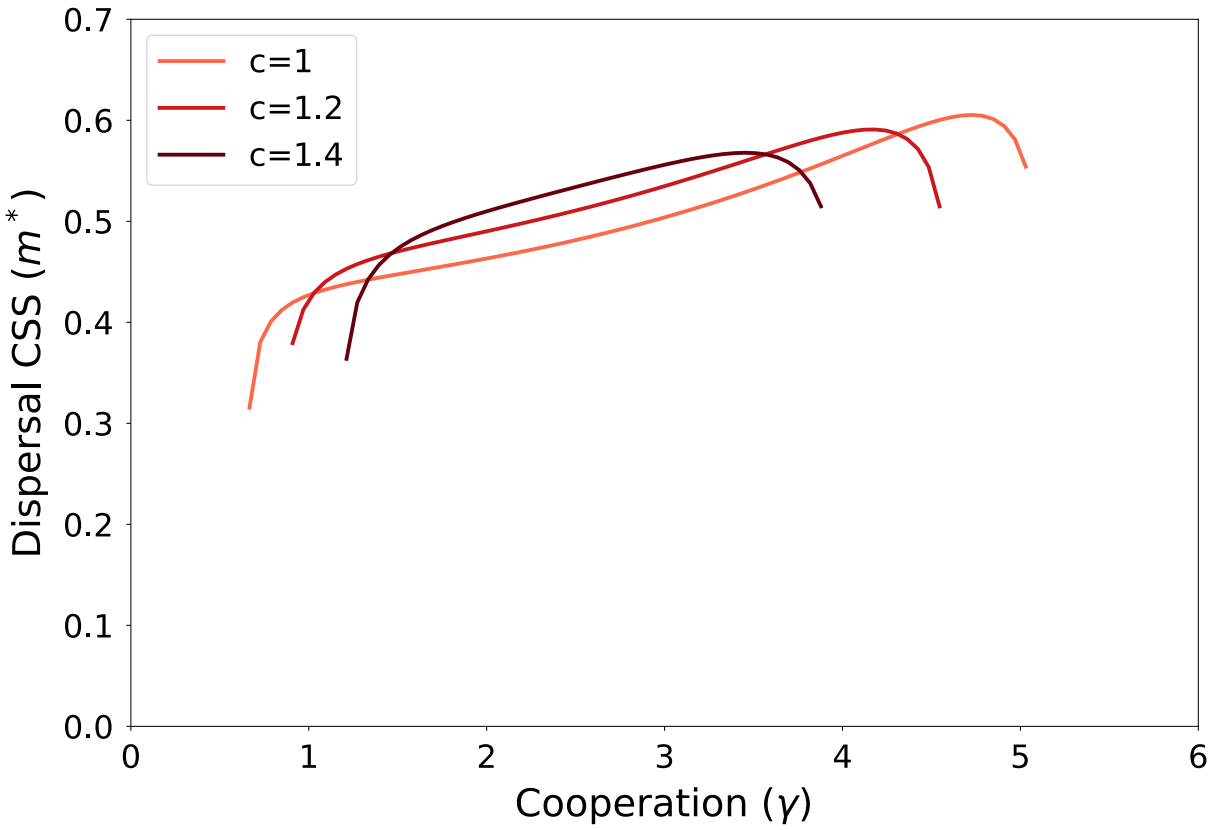

Fig. E.8. The CSS in dispersal (m^*) as a function of cooperation for different values of the constant death rate c. A higher constant death rate leads to the evolution of a higher dispersal rate, but its effect can be non-monotonic when cooperation is close to its extreme possible values. Parameters: $\rho = 3.5$, $a = 10$, $\alpha = 0.04$, $b = 0.05$, $\theta = 2$, $X = 0$, $\delta = 0.9$.

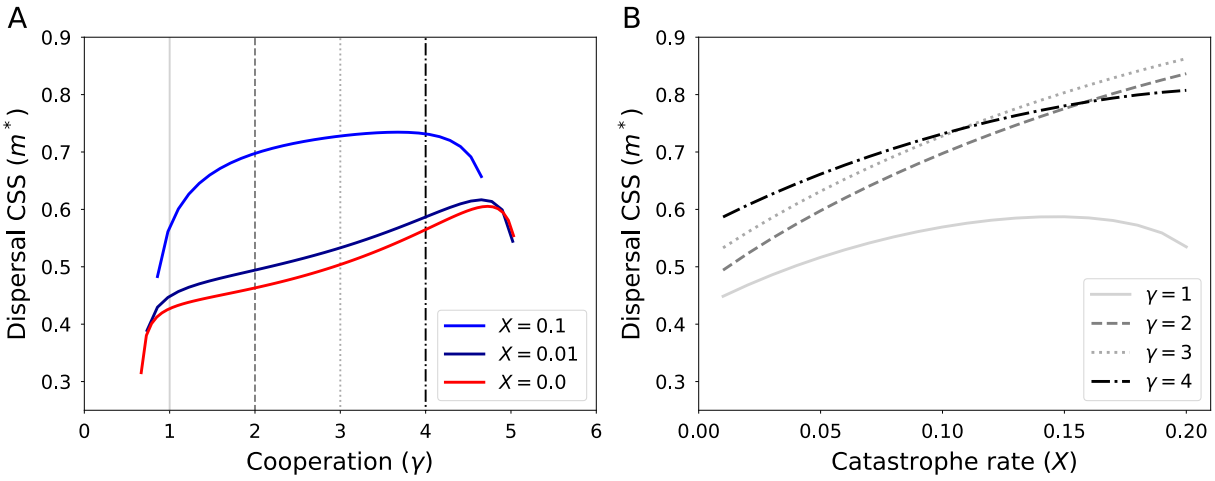

Fig. E.9. Evolution of dispersal in the presence of catastrophes. **A** The CSS in dispersal (m^*) as a function of cooperation for different values of the catastrophe rate (X). **B** The CSS in dispersal (m^*) as a function of the catastrophe rate (X) for different values of cooperation. Parameters: $\rho = 3.5$, $a = 10$, $c = 1$, $\alpha = 0.04$, $b = 0.05$, $\theta = 2$, $\delta = 0.9$.

$\gamma_{\max}$, due to which the horizontal extent of different curves is different in Fig. E.8.

Catastrophes and the evolution of dispersal

Adding catastrophes directly enhances the collapse of patches by causing sporadic local extinctions. Having spread across more patches should be beneficial in the presence of catastrophes, as it reduces the chances of extinction due to all individuals lying in the same patch. In accordance with our expectations, catastrophes generally increase m^* (Fig. E.9). However, the slope of m^* w.r.t. the catastrophe rate (X) decreases with increasing X. A maximum in m^* may also occur with increasing X (Fig. E.9).

Appendix F

Numerical analysis and code

All numerical analyses were performed in Python, except in the time series figures in Chapter 4 and Appendix E. The code is available in a GitHub repository. As of the date of the submission of the thesis, the GitHub repository is private, since the contents of the thesis are being processed for publication in scientific journals. After their publication, the repository will be made public and should be accessible at https://github.com/pentathis/kaustubh-ms-thesis-code.

Constructing PIPs

The PIPs for the metapopulation model were calculated using the LMAO function (2.22). Specifically, for a grid of strategy values γ_1 and γ_2, we computed $\frac{1}{\varepsilon} f_{\text{LMAO}}(\overline{N}_1(\gamma_1), \varepsilon(\gamma_2))$, where $\overline{N}_1$ is the equilibrium regional (average local) abundance of morph 1 with the strategy γ_1, and ε is a small number. Using these values for the entire grid, the invasion boundary was obtained by drawing a contour where $\frac{1}{\varepsilon} f_{\text{LMAO}}(\overline{N}_1(\gamma_1), \varepsilon) = 1$.

CSS calculations

The CSS calculations for cooperation were also performed using the LMAO function. We constructed a wrapper function

$$\frac{1}{\varepsilon} f_{\text{LMAO}}(\overline{N}_1(\gamma_1), \varepsilon(\gamma_1 + \varepsilon')) - \frac{1}{\varepsilon} f_{\text{LMAO}}(\overline{N}_1(\gamma_1), \varepsilon(\gamma_1 - \varepsilon'))$$

where ε and ε' are small positive numbers. This function was solved numerically using the bisection method.

For dispersal we used the wrapper function given by

$$\frac{1}{\varepsilon} f_{\text{LMAO}}(\overline{N}_1(m_1), \varepsilon(m_1(1 + \varepsilon'))) - \frac{1}{\varepsilon} f_{\text{LMAO}}(\overline{N}_1(\gamma_1), \varepsilon(m_1(1 - \varepsilon')))$$

and solved it using the bisection method. For the coCSS, we used a combinations of these two functions.

References

Ackleh AS, Allen LJS, Carter J (2007). Establishing a beachhead: A stochastic population model with an Allee effect applied to species invasion. Theoretical Population Biology 71(3), 290–300.

Akçay E (2020). Deconstructing Evolutionary Game Theory: Coevolution of Social Behaviors with Their Evolutionary Setting. The American Naturalist 195(2), 315–330.

Allen LJS, Fagan JF, Högnäs G, Fagerholm H (2005). Population extinction in discrete-time stochastic population models with an Allee effect. Journal of Difference Equations and Applications 11(4-5), 273–293.

Amarasekare P (1998a). Allee Effects in Metapopulation Dynamics. The American Naturalist 152(2), 298–302.

Amarasekare P (1998b). Interactions between Local Dynamics and Dispersal: Insights from Single Species Models. Theoretical Population Biology 53(1), 44–59.

Avilés L (2002). Solving the freeloaders paradox: Genetic associations and frequency-dependent selection in the evolution of cooperation among nonrelatives. Proceedings of the National Academy of Sciences 99(22), 14268–14273.

Brännström Å, Johansson J, Von Festenberg N (2013). The Hitchhiker's Guide to Adaptive Dynamics. Games 4(3), 304–328.

Casagrandi R, Gatto M (2002). A Persistence Criterion for Metapopulations. Theoretical Population Biology 61(2), 115–125.

Chesson P (1991). Stochastic Population Models. In J Kolasa, STA Pickett, editors, Ecological Heterogeneity, 123–143. Springer, New York, NY.

Chesson PL (1981). Models for spatially distributed populations: The effect of within-patch variability. Theoretical Population Biology 19(3), 288–325.

Courchamp F, Berec L, Gascoigne J (2008). Allee Effects in Ecology and Conservation. OUP Oxford.

Crespo-Miguel R, Jarillo J, Cao-García FJ (2022). Dispersal-induced resilience to stochastic environmental fluctuations in populations with Allee effect. Physical Review E 105(1), 014413.

Darwin C (1859). On the Origin of Species by Means of Natural Selection, Or, The Preservation of Favoured Races in the Struggle for Life. J. Murray.

DeAngelis DL, Yurek S (2017). Spatially Explicit Modeling in Ecology: A Review. Ecosystems 20(2), 284–300.

Dennis B (1989). Allee Effects: Population Growth, Critical Density, and the Chance of Extinction. Natural Resource Modeling 3, 481–538.

Dennis B (2002). Allee effects in stochastic populations. Oikos 96(3), 389–401.

Dennis B, Assas L, Elaydi S, Kwessi E, Livadiotis G (2016). Allee effects and resilience in stochastic populations. Theoretical Ecology 9(3), 323–335.

Dieckmann U, Law R (1996). The dynamical theory of coevolution: a derivation from stochastic ecological processes. Journal of Mathematical Biology 34(5), 579–612.

Diekmann O, *et al.* (2004). A beginner's guide to adaptive dynamics. Banach Center Publications 63, 47–86.

Doebeli M, Hauert C, Killingback T (2004). The Evolutionary Origin of Cooperators and Defectors. Science 306(5697), 859–862.

Doebeli M, Knowlton N (1998). The evolution of interspecific mutualisms. Proceedings of the National Academy of Sciences 95(15), 8676–8680.

Drechsler M, Wissel C (1997). Separability of Local and Regional Dynamics in Metapopulations. Theoretical Population Biology 51(1), 9–21.

Dudley SA (2015). Plant cooperation. AoB PLANTS 7, plv113.

Dugatkin LA (1997). Cooperation Among Animals: An Evolutionary Perspective. Oxford University Press.

Ferdy JB, Molofsky J (2002). Allee Effect, Spatial Structure and Species Coexistence. Journal of Theoretical Biology 217(4), 413–424.

Gaines MS, McClenaghan LR (1980). Dispersal in Small Mammals. Annual Review of Ecology and Systematics 11, 163–196.

Geritz S, Gyllenberg M, Jacobs F, Parvinen K (2002). Invasion dynamics and attractor inheritance. Journal of Mathematical Biology 44(6), 548–560.

Geritz SAH (2005). Resident-invader dynamics and the coexistence of similar strategies. Journal of Mathematical Biology 50(1), 67–82.

Geritz SAH, Éva K, Meszéna G, Metz J (1998). Evolutionarily singular strategies and the adaptive growth and branching of the evolutionary tree. Evolutionary Ecology 12(1), 35–57.

Geritz SAH, Metz JAJ, Kisdi É, Meszéa G (1997). Dynamics of Adaptation and Evolutionary Branching. Physical Review Letters 78(10), 2024–2027.

Gillespie DT (1977). Exact stochastic simulation of coupled chemical reactions. The Journal of Physical Chemistry 81(25), 2340–2361.

Greenwood PJ, Harvey PH (1982). The Natal and Breeding Dispersal of Birds. Annual Review of Ecology and Systematics 13, 1–21.

Greig D, Travisano M (2004). The Prisoner's Dilemma and polymorphism in yeast SUC genes. Proceedings of the Royal Society of London Series B: Biological Sciences 271(suppl_3), S25–S26.

Gruntfest Y, Arditi R, Dombrovsky Y (1997). A Fragmented Population in a Varying Environment. Journal of Theoretical Biology 185(4), 539–547.

Guillemin F, Simonian A (1995). Transient characteristics of an M/M/∞ system. Advances in Applied Probability 27(3), 862–888.

Gyllenberg M, Hemminki J, Tammaru T (1999). Allee Effects Can Both Conserve and Create Spatial Heterogeneity in Population Densities. Theoretical Population Biology 56(3), 231–242.

Gyllenberg M, Parvinen K, Dieckmann U (2002). Evolutionary suicide and evolution of dispersal in structured metapopulations. Journal of Mathematical Biology 45(2), 79–105.

Hairston Jr NG, Ellner SP, Geber MA, Yoshida T, Fox JA (2005). Rapid evolution and the convergence of ecological and evolutionary time. Ecology Letters 8(10), 1114–1127.

Hamilton WD (1963). The Evolution of Altruistic Behavior. The American Naturalist 97(896), 354–356.

Hamilton WD (1964a). The genetical evolution of social behaviour. I. Journal of Theoretical Biology 7(1), 1–16.

Hamilton WD (1964b). The genetical evolution of social behaviour. II. Journal of Theoretical Biology 7(1), 17–52.

Hanski I, Gyllenberg M (1993). Two General Metapopulation Models and the Core-Satellite Species Hypothesis. The American Naturalist 142(1), 17–41.

Hardin G (1968). The Tragedy of the Commons. Science 162(3859), 1243–1248.

Hauert C, Doebeli M (2004). Spatial structure often inhibits the evolution of cooperation in the snowdrift game. Nature 428(6983), 643–646.

Hofbauer J, Sigmund K (1990). Adaptive dynamics and evolutionary stability. Applied Mathematics Letters 3(4), 75–79.

Hogeweg P (1988). Cellular automata as a paradigm for ecological modeling. Applied Mathematics and Computation 27(1), 81–100.

Huffaker C (1958). Experimental studies on predation: Dispersion factors and predator-prey oscillations. Hilgardia 27(14), 343–383.

Hui C, Li Z (2004). Distribution patterns of metapopulation determined by Allee effects. Population Ecology 46(1), 55–63.

Jacobs J (1984). Cooperation, optimal density and low density thresholds: yet another modification of the logistic model. Oecologia 64(3), 389–395.

Jorge DCP, Martinez-Garcia R (2024). Demographic effects of aggregation in the presence of a component Allee effect. Journal of The Royal Society Interface 21(215), 20240042.

Kanarek AR, Webb CT (2010). Allee effects, adaptive evolution, and invasion success. Evolutionary Applications 3(2), 122–135.

Kanarek AR, Webb CT, Barfield M, Holt RD (2013). Allee effects, aggregation, and invasion success. Theoretical Ecology 6(2), 153–164.

Kang Y, Lanchier N (2011). Expansion or extinction: deterministic and stochastic two-patch models with Allee effects. Journal of Mathematical Biology 62(6), 925–973.

Kang Y, Yakubu AA (2011). Weak Allee effects and species coexistence. Nonlinear Analysis: Real World Applications 12(6), 3329–3345.

Karlin S (2014). A First Course in Stochastic Processes. Academic Press.

Keizer J (1972). On the solutions and the steady states of a master equation. Journal of Statistical Physics 6(2), 67–72.

Kierstead H, Slobodkin L (1953). The size of water masses containing plankton blooms. Journal of Marine Research 12(1).

Killingback T, Doebeli M (2002). The Continuous Prisoner's Dilemma and the Evolution of Cooperation through Reciprocal Altruism with Variable Investment. The American Naturalist 160(4), 421–438.

Kisdi V, Meszena G (1995). Life Histories with Lottery Competition in a Stochastic Environment: ESSs which Do Not Prevail. Theoretical Population Biology 47(2), 191–211.

Klausmeier CA, Kremer CT, Koffel T (2020). Trait-based ecological and eco-evolutionary theory. In Theoretical Ecology, 161–194. Oxford University Press.

Klok C, De Roos AM (1998). Effects of habitat size and quality on equilibrium density and extinction time of Sorex araneus populations. Journal of Animal Ecology 67(2), 195–209.

Koffel T, Boudsocq S, Loeuille N, Daufresne T (2018). Facilitation- vs. competition-driven succession: the key role of resource-ratio. Ecology Letters 21(7), 1010–1021.

Kramer AM, Dennis B, Liebhold AM, Drake JM (2009). The evidence for Allee effects. Population Ecology 51(3), 341–354.

Kramer J, Özkaya Ö, Kümmerli R (2020). Bacterial siderophores in community and host interactions. Nature Reviews Microbiology 18(3), 152–163.

Lawton JH (1999). Are There General Laws in Ecology? Oikos 84(2), 177–192.

Le Galliard JF, Ferriére R, Dieckmann U (2003). The adaptive dynamics of altruism in spatially heterogeneous populations. Evolution 57(1), 1–17.

Lehmann L (2008). The adaptive dynamics of niche constructing traits in spatially subdivided populations: Evolving posthumous extended phenotypes. Evolution 62(3), 549–566.

Lehmann L, Perrin N, Rousset F (2006). Population Demography and the Evolution of Helping Behaviors. Evolution 60(6), 1137–1151.

Leibold MA, Chase JM (2017). Metacommunity Ecology. Princeton University Press.

Leibold MA, Holyoak M, Mouquet N, Amarasekare P, Chase JM, Hoopes MF, Holt RD, Shurin JB, Law R, Tilman D, Loreau M, Gonzalez A (2004). The metacommunity concept: a framework for multi-scale community ecology. Ecology Letters 7(7), 601–613.

Leibold MA, Miller TE (2004). 6 - From Metapopulations to Metacommunities. In I Hanski, OE Gaggiotti, editors, Ecology, Genetics and Evolution of Metapopulations, 133–150. Academic Press, Burlington.

Lerch BA, Nolting BC, Abbott KC (2018). Why are demographic Allee effects so rarely seen in social animals? Journal of Animal Ecology 87(6), 1547–1559.

Lerch BA, Rudrapatna A, Rabi N, Wickman J, Koffel T, Klausmeier CA (2023). Connecting local and regional scales with stochastic metacommunity models: Competition, ecological drift, and dispersal. Ecological Monographs 93(4), e1591.

Levin SA (1992). The Problem of Pattern and Scale in Ecology: The Robert H. MacArthur Award Lecture. Ecology 73(6), 1943–1967.

Levins R (1966). The Strategy of Model Building in Population Biology. American Scientist 54(4), 421–431.

Levins R (1969). Some Demographic and Genetic Consequences of Environmental Heterogeneity for Biological Control1. Bulletin of the Entomological Society of America 15(3), 237–240.

Levins R (1970). Extinction. In M Gerstenhaber, editor, Some Mathematical Questions in Biology: Lecture Notes on Mathematics in the Life Sciences, 75–107. The American Mathematical Society, Providence, RI.

Lewis MA, Kareiva P (1993). Allee Dynamics and the Spread of Invading Organisms. Theoretical Population Biology 43(2), 141–158.

Liebhold A, Bascompte J (2003). The Allee effect, stochastic dynamics and the eradication of alien species. Ecology Letters 6(2), 133–140.

Lion S, Gandon S (2009). Habitat saturation and the spatial evolutionary ecology of altruism. Journal of Evolutionary Biology 22(7), 1487–1502.

Lion S, Gandon S (2010). Life history, habitat saturation and the evolution of fecundity and survival altruism. Evolution 64(6), 1594–1606.

Lion S, van Baalen M (2007). From Infanticide to Parental Care: Why Spatial Structure Can Help Adults Be Good Parents. The American Naturalist 170(2), E26–E46.

Lion S, van Baalen M (2008). Self-structuring in spatial evolutionary ecology. Ecology Letters 11(3), 277–295.

Loreau M, Mouquet N (1999). Immigration and the Maintenance of Local Species Diversity. The American Naturalist 154(4), 427–440.

Lotka AJ (1932). The growth of mixed populations: Two species competing for a common food supply. Journal of the Washington Academy of Sciences 22(16/17), 461–469.

Lucas JR, Waser PM, Creel SR (1994). Death and disappearance: estimating mortality risks associated with philopatry and dispersal. Behavioral Ecology 5(2), 135–141.

MacArthur RH, Wilson EO (1967). The Theory of Island Biogeography. Princeton University Press, Princeton, NJ.

Mallet J (2012). The struggle for existence: how the notion of carrying capacity, K, obscures the links between demography, Darwinian evolution, and speciation. Evolutionary Ecology Research 14, 627–665.

Massol F, Calcagno V, Massol J (2009). The metapopulation fitness criterion: Proof and perspectives. Theoretical Population Biology 75(2), 183–200.

Matthysen E (2005). Density-dependent dispersal in birds and mammals. Ecography 28(3), 403–416.

Maynard Smith J (1976). Group Selection. The Quarterly Review of Biology 51(2), 277–283.

Maynard Smith JM, Price GR (1973). The Logic of Animal Conflict. Nature 246(5427), 15–18. Publisher: Nature Publishing Group.

Meszéna G, Gyllenberg M, Pásztor L, Metz JAJ (2006). Competitive exclusion and limiting similarity: A unified theory. Theoretical Population Biology 69(1), 68–87.

Metz JAJ, Geritz SAH, Meszena G, Jacobs FJA, van Heerwaarden JS (1995). Adaptive Dynamics: A Geometrical Study of the Consequences of Nearly Faithful Reproduction. IIASA Working Paper, International Institute for Applied Systems Analysis, IIASA. Laxenburg, Austria.

Metz JAJ, Gyllenberg M (2001). How should we define fitness in structured metapopulation models? Including an application to the calculation of evolutionarily stable dispersal strategies. Proceedings of the Royal Society of London Series B: Biological Sciences 268(1466), 499–508.

Metz JAJ, Nisbet RM, Geritz SAH (1992). How should we define 'fitness' for general ecological scenarios? Trends in Ecology & Evolution 7(6), 198–202.

Molles Jr MC, Sher A (2019). Ecology: Concepts & Applications. McGraw-Hill Education.

Méléard S, Villemonais D (2012). Quasi-stationary distributions and population processes. Probability Surveys 9, 340–410.

Nachman G (2000). Effects of demographic parameters on metapopulation size and persistence: an analytical stochastic model. Oikos 91(1), 51–65.

Nowak M (1990). An evolutionarily stable strategy may be inaccessible. Journal of Theoretical Biology 142(2), 237–241.

Nowak MA (2006). Five Rules for the Evolution of Cooperation. Science 314(5805), 1560–1563.

Nowak MA, May RM (1992). Evolutionary games and spatial chaos. Nature 359(6398), 826–829.

Nowak MA, Sigmund K (1998). Evolution of indirect reciprocity by image scoring. Nature 393(6685), 573–577.

Odum HT, Allee WC (1954). A Note on the Stable Point of Populations Showing Both Intraspecific Cooperation and Disoperation. Ecology 35(1), 95–97.

Osborne MJ, Rubinstein A (1994). A Course in Game Theory. MIT Press.

Parvinen K (2005). Evolutionary suicide. Acta Biotheoretica 53(3), 241–264.

Parvinen K (2011). Adaptive Dynamics of Altruistic Cooperation in a Metapopulation: Evolutionary Emergence of Cooperators and Defectors or Evolutionary Suicide? Bulletin of Mathematical Biology 73(11), 2605–2626.

Parvinen K (2013). Joint evolution of altruistic cooperation and dispersal in a metapopulation of small local populations. Theoretical Population Biology 85, 12–19.

Poulsen ET (1979). A model for population regulation with density- and frequency-dependent selection. Journal of Mathematical Biology 8(4), 325–343.

Powers ST, Penn AS, Watson RA (2011). The concurrent evolution of cooperation and the population structures that support it. Evolution 65(6), 1527–1543.

Prout T (1968). Sufficient Conditions for Multiple Niche Polymorphism. The American Naturalist 102(928), 493–496.

Purcell J, Brelsford A, Avilés L (2012). Co-evolution between sociality and dispersal: The role of synergistic cooperative benefits. Journal of Theoretical Biology 312, 44–54.

Rankin DJ, Bargum K, Kokko H (2007). The tragedy of the commons in evolutionary biology. Trends in Ecology & Evolution 22(12), 643–651. Publisher: Elsevier.

Richter-Dyn N, Goel NS (1972). On the extinction of a colonizing species. Theoretical Population Biology 3(4), 406–433.

Rosenberg DK, Noon BR, Meslow EC (1997). Biological corridors: Form, function, and efficacy. BioScience 47(10), 677–687.

Ross SM (2010). A First Course in Probability. Pearson Prentice Hall.

Roughgarden J (2018). 13. Production Functions from Ecological Populations: A Survey with Emphasis on Spatially Implicit Models. In D Tilman, P Kareiva, editors, Spatial Ecology: The Role of Space in Population Dynamics and Interspecific Interactions (MPB-30), 296–317. Princeton University Press.

Sato K (2009). Allee threshold and extinction threshold for spatially explicit metapopulation dynamics with Allee effects. Population Ecology 51(3), 411–418.

Schuster P, Sigmund K (1983). Replicator dynamics. Journal of Theoretical Biology 100(3), 533–538.

Shmida A, Ellner S (1984). Coexistence of plant species with similar niches. Vegetatio 58(1), 29–55.

Shmida A, Whittaker RH (1981). Pattern and Biological Microsite Effects in Two Shrub Communities, Southern California. Ecology 62(1), 234–251.

Shmida A, Wilson MV (1985). Biological Determinants of Species Diversity. Journal of Biogeography 12(1), 1–20.

Skellam JG (1951). Random Dispersal in Theoretical Populations. Biometrika 38(1/2), 196–218.

Soulé ME (1985). What Is Conservation Biology? BioScience 35(11), 727–734.

South AB, Kenward RE (2001). Mate finding, dispersal distances and population growth in invading species: a spatially explicit model. Oikos 95(1), 53–58.

Stephens PA, Sutherland WJ, Freckleton RP (1999). What Is the Allee Effect? Oikos 87(1), 185–190.

Strogatz SH (2018). Nonlinear Dynamics and Chaos with Student Solutions Manual: With Applications to Physics, Biology, Chemistry, and Engineering, Second Edition. CRC Press, Boca Raton, 2 edition.

Surendran A, Plank MJ, Simpson MJ (2020). Population dynamics with spatial structure and an Allee effect. Proceedings of the Royal Society A: Mathematical, Physical and Engineering Sciences 476(2242), 20200501.

Tarnita CE, Traulsen A (2024). Reconciling ecology and evolutionary game theory or 'When not to think cooperation'.

Tilman D (1982). Resource Competition and Community Structure. Princeton University Press.

Tilman D, Lehman CL, Kareiva P (1998). 1. Population Dynamics in Spatial Habitats. In D Tilman, P Kareiva, editors, Spatial Ecology: The Role of Space in Population Dynamics and Interspecific Interactions (MPB-30), 3–20. Princeton University Press.

Travis JMJ, Murrell DJ, Dytham C (1999). The evolution of density–dependent dispersal. Proceedings of the Royal Society of London Series B: Biological Sciences 266(1431), 1837–1842.

Trivers RL (1971). The Evolution of Reciprocal Altruism. The Quarterly Review of Biology 46(1), 35–57.

van Baalen M, Rand DA (1998). The Unit of Selection in Viscous Populations and the Evolution of Altruism. Journal of Theoretical Biology 193(4), 631–648.

Vellend M (2010). Conceptual Synthesis in Community Ecology. The Quarterly Review of Biology 85(2), 183–206.

Verhulst PF (1838). Notice sur la loi que la population suit dans son accroissement. Correspondence mathematique et physique 10, 113–129.

Volterra V (1926). Variazioni e fluttuazioni del numero d'individui in specie animali conviventi. Memoria della Reale Accademia Nazionale dei Lincei 6, 31–113.

Vortkamp I, Schreiber SJ, Hastings A, Hilker FM (2020). Multiple Attractors and Long Transients in Spatially Structured Populations with an Allee Effect. Bulletin of Mathematical Biology 82(6), 82.

Wahl LM, Nowak MA (1999). The Continuous Prisoner's Dilemma: I. Linear Reactive Strategies. Journal of Theoretical Biology 200(3), 307–321.

Webb C (2003). A Complete Classification of Darwinian Extinction in Ecological Interactions. The American Naturalist 161(2), 181–205.

Weitz JS, Eksin C, Paarporn K, Brown SP, Ratcliff WC (2016). An oscillating tragedy of the commons in replicator dynamics with game-environment feedback. Proceedings of the National Academy of Sciences 113(47), E7518–E7525.

West SA, Pen I, Griffin AS (2002). Cooperation and Competition Between Relatives. Science 296(5565), 72–75.

Wilson DS, Pollock GB, Dugatkin LA (1992). Can altruism evolve in purely viscous populations? Evolutionary Ecology 6(4), 331–341.

Yoder JM, Marschall EA, Swanson DA (2004). The cost of dispersal: predation as a function of movement and site familiarity in ruffed grouse. Behavioral Ecology 15(3), 469–476.

Zhou SR, Wang G (2006). One large, several medium, or many small? Ecological Modelling 191(3), 513–520.